International Committee for Future Accelerators

Sponsored by the Particles and Fields Commission of IUPAP

Beam Dynamics Newsletter

No. 55

Issue Editor:
M. A. Palmer

Editor in Chief:
W. Chou

August 2011

Contents

1   Foreword

1.1   From the Chairman

Weiren Chou, Fermilab
Mail to: chou@fnal.gov

The International Committee for Future Accelerators (ICFA) met on August 24, 2011 at the Tata Institute of Fundamental Research (TIFR) in Mumbai, India during LP2011. Atsuto Suzuki, Director General of KEK and Chair of ICFA, chaired this meeting.

Jonathan Bagger, Chair of the ILCSC, presented a summary report of the ILCSC meeting, which had taken place earlier on the same day. ILC accelerator and detector activities are progressing well and the GDE and Research Director mandate will be extended to 31 December 2013. A new structure for linear collider activities after 2012, which will include both ILC and CLIC, was discussed, and will be presented at the February 2012 ILCSC meeting. It is envisaged that the new structure representing a unified linear collider field will last 3-6 years. At the end of this interim period, it should become clear which collider – the ILC or CLIC – to choose. The selection will be based on results from LHC. ICFA will set up a panel to compare the readiness of the available technologies (similar to the 2004 panel that compared superconducting versus room temperature rf systems for the ILC).

A draft document entitled "*Beacons of Discovery*" was presented by Pier Oddone, Fermilab Director. It conveys the excitement of particle physics; and explains how we will be able to answer some of the major science questions in the future. The document also shows the numerous spin-offs from the field of particle physics. The final document will be available at the October 2011 ICFA Seminar at CERN.

Since the present ICFA Chair's term will expire at the end of this year, ICFA unanimously approved Pier Oddone as its next Chair from 1 January 2012 to 31 December 2014.

I gave a presentation at the ICFA meeting on behalf of the Beam Dynamics Panel. ICFA approved two new panel members – Elias Metral from CERN and John Byrd from LBNL – replacing two present members: Alessandra Lombardi and Miguel Furman. Alessandra and Miguel have served on the panel for a number of years and made valuable contributions, including organizing ICFA workshops and editing ICFA BD panel newsletters. On behalf of the panel, I want to thank them for their excellent service. I also welcome Elias and John on board and look forward to working with them in the future.

The BD panel had its biennial meeting on 7 September 2011 in San Sebastian, Spain during IPAC11. It was a joint meeting with the ICFA Advanced and Novel Accelerators (ANA) Panel. The meeting minutes can be found in Section 5.3.

The student selection for *The Sixth International Accelerator School for Linear Colliders*, which will be held from 6 – 17 November 2011 at the Asilomar Conference

Center, Pacific Grove, California, USA, is complete. Details can be found in Section 4.1. The school web address is http://www.linearcollider.org/school/2011/.

The editor of this issue is Dr. Mark Palmer, a panel member and an accelerator scientist at Cornell University, USA. Mark selected the theme of "*Muon Collider and Neutrino Factory*" and collected a number of well-written articles on this theme. These articles give a comprehensive overview of this rapidly developing new accelerator field and the required challenging accelerator technologies. In this issue there are also two workshop reports (SRF2011, TIPP2011) and three workshop announcements (COOL2011, DLA2011, LOWεRING2011). I thank Mark for editing and producing a newsletter of great value to our accelerator community.

1.2   From the Editor

Mark Palmer, Cornell University
Mail to: mark.palmer@cornell.edu

Earlier this year, while considering potential topics for the theme of this Newsletter, anticipation was building towards the summer release of new results from the LHC along with updates from the Tevatron Run II. Over the course of the next year or so, we expect that these datasets will provide our first panoramic view of the physics landscape at the Terascale. With that picture in hand, the high energy physics community can begin the process of specifying the energy reach necessary for a lepton collider which can explore this territory with greater precision. At present, the most developed concepts for the lepton collider are the electron-positron linear collider designs of the International Linear Collider (ILC) Global Design Effort and the Compact Linear Collider (CLIC) Design Study. The superconducting main linac technology of the ILC should provide an energy reach to about 1 TeV while the CLIC warm linac technology is targeted at reaching as high as ~3 TeV. A third lepton collider concept, a ring-based Muon Collider (MC), is also under development and could provide access to still higher energies. Past issues of this Newsletter have provided focused overviews of R&D and design work being carried out for the electron-positron machines. Thus this issue seemed an ideal opportunity to provide a similar overview of the Muon Collider concept and the R&D program that is presently underway to assess its feasibility.

The fundamental accelerator technologies needed for a Muon Collider are also those required for construction of a Neutrino Factory (NF) with the most notable difference being in the final muon storage ring, which provides decay regions for neutrino beam production in the NF and interaction regions for detectors in the case of the MC. In fact, initial design and construction of a Neutrino Factory offers a logical step along the path towards the ultimate realization of a Muon Collider. A rich accelerator R&D program is presently underway to assess the feasibility of both of these concepts. The International Design Study for a Neutrino Factory (IDS-NF) is targeting a Reference Design Report on the 2013 timescale. In the U.S., the Muon Accelerator Program (MAP) was approved by the U.S. Department of Energy last year with the goal of completing the R&D necessary to validate the Muon Collider concept on a 5-7 year timescale.

The contributions associated with the theme of this issue are divided into two sections. The first (Sec. 2) contains a nice overview of the physics motivations for the Neutrino Factory and a multi-TeV collider by Estia Eichten followed by a very readable

end-to-end description of the Muon Collider complex by Bob Palmer and Richard Fernow. The second section (Sec. 3) focuses in greater detail on the design and R&D efforts and includes articles on the IDS-NF, the MAP and the major technical efforts currently underway. I've found all of the articles to be quite informative and would like to express my appreciation to each of the authors for their time and effort spent to make this issue possible. A special thanks goes to the co-directors of the MAP, Mike Zisman and Steve Geer, who were kind enough to help organize the contributions. In particular, Mike Zisman generously took time out of a very busy schedule to provide editorial support as this issue was taking final form.

This issue contains reports from SRF2011 and the accelerator-related sessions of TIPP2011. Announcements for three upcoming workshops are also included:

- COOL`11 – Workshop on beam cooling systems and related techniques in Alushta, Ukraine
- DLA-2011 – Workshop on dielectric laser accelerators at SLAC National Accelerator Laboratory
- LOWεRING - Workshop on the beam dynamics and technology challenges for producing and controlling low emittance beams in Heraklion, Crete.

As this issue nears completion, I would like to take a moment to comment on experimental progress that has been reported while it was in preparation. As of mid-summer, the delivered luminosities from the LHC and the Tevatron Run II have surpassed 2 fb^{-1} and 11 fb^{-1}, respectively, with expectations that the LHC dataset will double by year's end. The list of possible hiding places for the Higgs boson is rapidly shrinking and numerous studies looking for new physics at the Terascale are being reported. While still more data is needed to clarify the overall picture, we expect the physics results that will determine the parameters of an energy frontier lepton collider are only a short wait away. In the neutrino physics arena, this summer has also seen important updates, such as new results from the T2K collaboration on the $\sin^2(2\theta_{13})$ mixing angle and improved Δm^2 comparisons for neutrinos and antineutrinos from the MINOS collaboration. Thus it seems an appropriate time to review the status of the design program for a Neutrino Factory and Muon Collider. Enjoy!

2 Muon Collider and Neutrino Factory Overview

2.1 Towards a Muon Collider

E. Eichten
Theory Group, Fermilab, P.O. Box 500, Batavia IL 60510
Mail to: eichten@fnal.gov

2.1.1 Physics Landscape

The Standard Model (SM) has been a spectacular success. For more than thirty years all new observations have fit naturally into this framework. But basic questions remain: (1) There is as of now no direct evidence for the Higgs boson or its interactions. Is this the correct mechanism of electroweak symmetry breaking? (2) How do the fermion masses and flavor mixings arise? Furthermore, the Standard Model is incomplete. It does not explain dark matter; neutrino masses and mixings require new particles or interactions; and the observed baryon asymmetry in the universe requires additional sources of CP violation. From a theoretical viewpoint there are also problems with the SM. It has been argued by G. 't Hooft that the SM is not natural at any energy scale Λ much above the Terascale (~1 TeV) because the small dimensionless parameter $\xi(\Lambda) = (m_H/\Lambda)^2$ is not associated with any symmetry in the limit $\xi = 0$ [1]. This is the naturalness problem of the SM. If the SM is valid all the way up to the Planck scale Λ_{Pl} (~ 10^{19} GeV), then the SM has to be fine tuned to a precision of one part in $(m_H/\Lambda_{Pl})^{-2}$! In this decade, the physics of the Terascale will be explored at the LHC. Planned experiments studying neutrino oscillations, quark/lepton flavor physics, and rare processes may also provide insight into new physics at the Terascale and beyond.

Discoveries made at the LHC will elucidate the origin of electroweak symmetry breaking. Is that mechanism the SM Higgs scalars or does it involve new physics? New physics might be new gauge bosons, additional fermion generations or fundamental scalars. It might be SUSY or new dynamics or even extra dimensions. Significant theoretical questions will likely remain even after the full exploitation of the LHC. Most notably, the origin of fermion (quark and lepton) masses, mixings and CP violation; the character of dark matter and detailed questions about spectrum, dynamics, and symmetries of any observed new physics. Thus, it is hard to imagine a scenario in which a multi-TeV lepton collider would not be required to fully explore the new physics.

To prepare for the energy frontier in the post-LHC era, research and development is being pursued on a variety of lepton colliders: A low energy ($E_{c.m.} < 1$ TeV) linear electron-positron collider (ILC), a second design (CLIC) capable of higher energies ($E_{c.m.} = 3$ TeV), and a multi-TeV Muon Collider.

A multi-TeV Muon Collider provides a very attractive possibility for studying the details of Terascale physics after the LHC. Presently physics and detector studies are

under way to understand the required Muon Collider parameters (in particular luminosity and energy) and map out, as a function of these parameters, the associated physics potential. The physics studies will set benchmarks for various new physics scenarios (e.g., SUSY, Extra Dimensions, New Strong Dynamics) as well as Standard Model processes.

2.1.2   Neutrino Factory

The SM has three generations of quarks and leptons. The flavor eigenstates for the left-handed neutrinos are denoted ν_e, ν_μ and ν_τ and the mass eigenstates by ν_i (i =1,2,3). In the simpler case of two flavors the probability (P) of flavor (a,b) mixing over a distance (L) for neutrino energy (E) is given by $P_{(a \to b)} = \sin^2 2\theta \sin^2(\Delta m^2 L/4E)$ where Δm^2 is the mass squared difference of the two mass eigenstates. Flavor mixing implies masses for neutrinos. Flavor mixing has been observed for solar neutrinos and atmospheric neutrinos with very different scales of mass difference, Δm^2 (solar) $<< \Delta m^2$ (atmospheric).

In the SM, the mixing is represented by a 3×3 mixing matrix, the Pontecorvo-Maki-Nakagawa-Sakata (PMNS) matrix. This matrix has three angles θ_{12}, θ_{23}, θ_{13} and one phase δ. If there are right-handed neutrinos (sterile under the SM interactions) this is the whole story. If there are no right-handed neutrinos then the mass terms are Majorana, lepton number is broken, and two additional phases appear. There are four important questions about the neutrino sector:

1)   Are the neutrinos Majorana or Dirac?
2)   Is the mass hierarchy normal (smaller splitting between the two lightest neutrinos) or inverted (the two most massive neutrinos have smaller splitting)?
3)   What is the value of θ_{13}? The other two angles are already measured and large.
4)   Is there CP violation, i.e., is δ not equal to 0 (mod π)?

The first question can be addressed in neutrinoless double β decay experiments. The remaining three questions will be addressed with neutrino beams. A Neutrino Factory (NF) has been proposed that uses a muon storage ring at an energy of 25 GeV with long straight sections to produce beams of neutrinos from the muon decays. This approach requires high intensity muon beams as it assumes 10^{21} muon decays per year. It is very likely that a Neutrino Factory will be needed to provide detailed measurements of θ_{13}, the mass hierarchy, and the CP violating phase δ.

The comparison of a Neutrino Factory with other neutrino beam facilities is shown in Fig. 1. As can be seen, the approach with the greatest reach is a Neutrino Factory (NF). This and many other details of the neutrino physics facilities can be found in the reports of the ISS Physics Working Group [2].

One advantage of the Muon Collider is that it lends itself to a staged program with physics at each stage of producing and cooling the muons. An important physics opportunity is the possibility of a Neutrino Factory as a step to a Muon Collider.

14
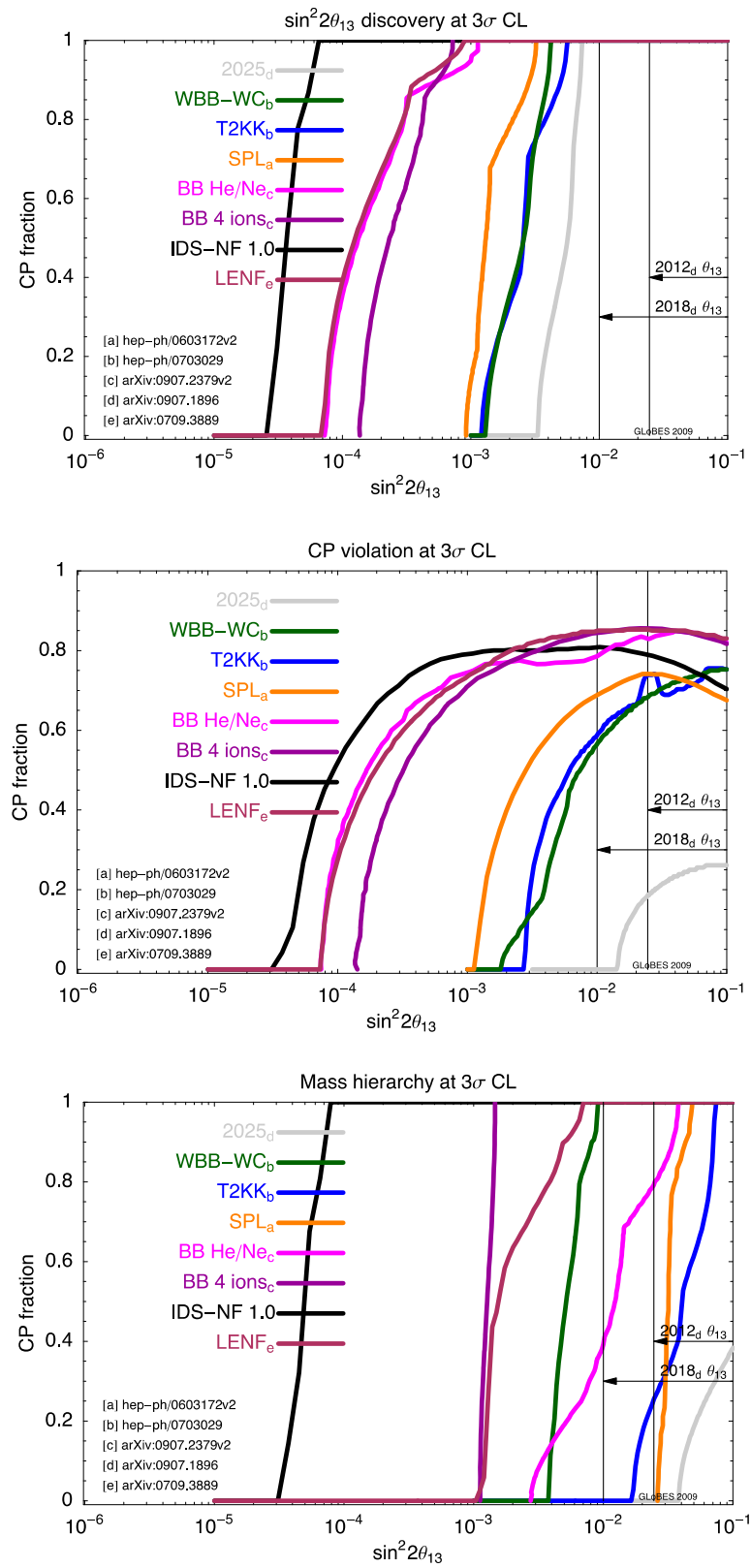
Figure 1: Comparison of physics reach of NF with other potential neutrino facilities [2].

2.1.3 Muon Collider Physics

The Muon Collider is an energy frontier machine. It offers both discovery as well as precision measurement capabilities. The physics goals of a Muon Collider (MC) are for the most part the same as a linear electron collider (CLIC) [3] at the same energy. The main advantages of a MC are the ability of studying the direct (s-channel) production of scalar resonances, a much better energy resolution (because of the lack of significant beamstrahlung), and the possibility of extending operations to very high energies. At CLIC, however, significantly greater polarization of the initial beams is possible [3].

2.1.3.1 *Basics*

There are basically three kinds of channels of interest for a lepton collider: (1) open pair production, (2) *s*-channel resonance production and (3) fusion processes.

2.1.3.1.1 Pair Production

The kinematic thresholds for pair production of standard model particles ($X + \bar{X}$) are well below $E_{\text{c.m.}} = 500$ GeV. For standard model particles at $E_{\text{c.m.}} > 1$ TeV the typical open channel pair production process is well above its kinematic threshold and the cross section becomes nearly flat in

$$R \equiv \frac{\sigma(\mu^+\mu^- \to X + \bar{X})}{\sigma_{QED}(\mu^+\mu^- \to e^+e^-)} \qquad . \tag{1}$$

For the MC a forward/backward angular cut (e.g., 10°) is imposed on the outgoing pair. Closer to the beam direction, a shielding wedge is needed to suppress detector backgrounds arising from the effects of muon decay in the beam.

For a process whose rate is one unit of R, an integrated luminosity of 100 fb^{-1} at $E_{\text{c.m.}} = 3$ TeV yields ~1000 events. As an example, the rate of top quark pair production at 3 TeV is only 1.86 units of R. This clearly demonstrates the need for high luminosity in a multi-TeV lepton collider.

2.1.3.1.2 Resonances

Many models beyond the SM predict resonances that may be produced directly in the s-channel at a Muon Collider. Here, the narrow beam energy spread of a Muon Collider, $\Delta E/E \sim 10^{-3}$, could be an important advantage. The cross section for the production of an s-channel resonance, X, with spin J, mass M and width Γ is given by:

$$\sigma_{\mu^+\mu^- \to X} = \frac{\pi}{4k^2}(2J+1)\frac{\Gamma^2}{(E-M)^2 + \Gamma^2/4}B_{\mu^+\mu^-}B_{visible} \tag{2}$$

where k is the momentum of the incoming muon and E is the total energy of the initial system ($E_{c.m.}$). $B_{\mu^+\mu^-}\Gamma$ is the partial width of $X \to \mu^+ \mu^-$ and $B_{visible}\Gamma$ is the visible decay width of X. At the peak of the resonance with negligible beam energy spread:

$$R_{peak} = 3(2J+1)\frac{B(\mu^+\mu^-)B(visible)}{\alpha_{EM}^2} \qquad (3)$$

For a sequential standard model Z' gauge boson, the value of R_{peak} is strikingly large, typically $R_{peak} \sim 10^4$. The luminosity, L, for $1.5 < M_{Z'} < 5.0$ TeV required to produce 1000 events on the Z' peak is only 0.5–5.0×10^{30} cm^{-2} s^{-1}. Hence, a comprehensive first-order study of the properties of a narrow resonance, such as a Z', in the few-TeV mass range, can be carried out with a low luminosity, $L \sim 10^{30}$ cm^{-2} s^{-1}, Muon Collider.

2.1.3.1.3 Fusion Processes

A typical fusion process $\mu^+ \mu^- \to W^+ W^- \nu_\mu \bar{\nu}_\mu \to X \nu_\mu \bar{\nu}_\mu$ is shown in Fig. 2. For $E_{c.m.} \gg M_X$ the cross section is typically large and grows logarithmically with $s = E_{c.m.}^2$, while the usual pair-production processes are constant in R and thus dropping like $1/s$. Thus, for asymptotically high energies fusion processes dominate. For lepton colliders, this crossover occurs in the few-TeV region in standard model processes, as shown in Fig. 3. A variety of processes are shown including WW and ZZ inclusive production. The large rates for WW, WZ and ZZ fusion processes imply that the multi-TeV Muon Collider is also effectively an electroweak-boson collider.

$$\sigma(s) = C\ln(\frac{s}{M_X^2}) + ...$$
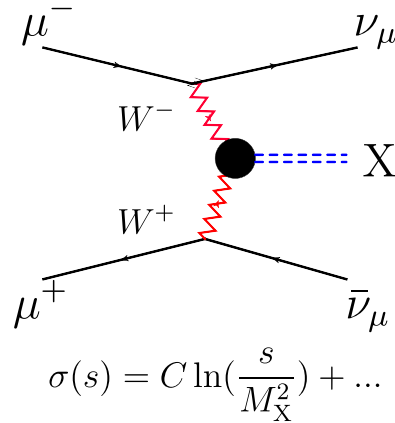
Figure 2: Typical fusion process.

CLIC (or MC e<->μ)
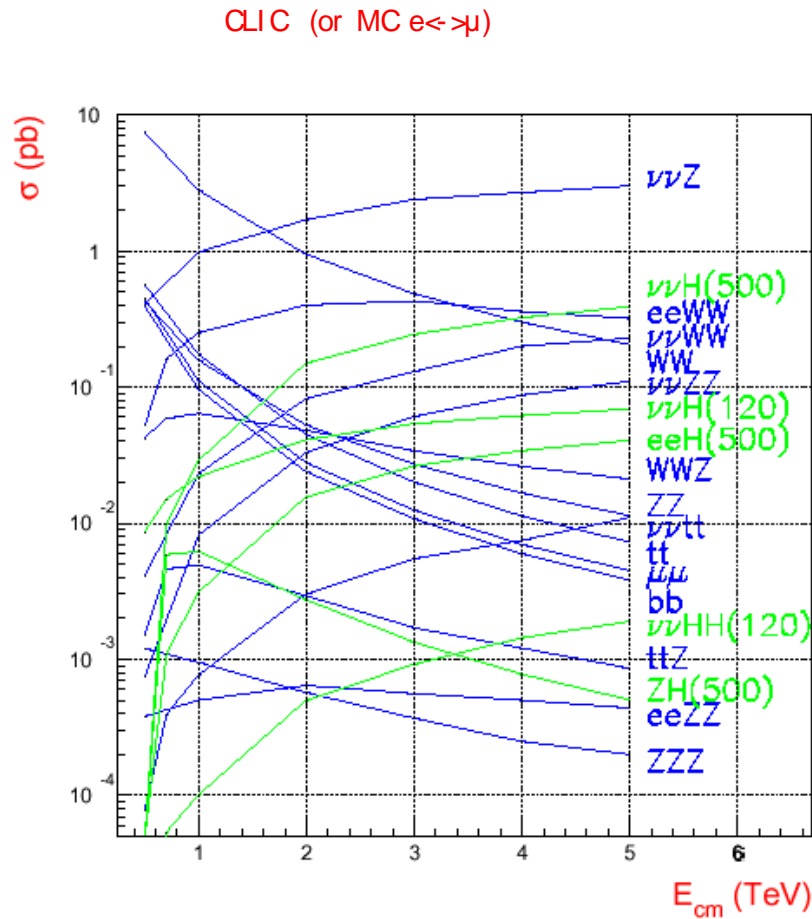
Figure 3: Fusion cross sections versus $\sqrt{s}$ at a lepton collider.

Physics studies of fusion processes such as $\mu^+\mu^- \rightarrow Z^0\,Z^0$ $\mu^+\mu^- \rightarrow X\,\mu^+\mu^-$ benefit greatly by the tagging of the outgoing $\mu^{\pm}$ and hence will be sensitive to the required 10° angular cut.

2.1.3.2 *Standard Model Higgs Bosons*

Studies of the feasibility of direct production of the SM Higgs boson were carried out over a decade ago [4] for a low-energy, high-luminosity MC. It was found that very precise control of the beam energy and energy spread are required.

Higgs bosons can be studied in a number of other ways at a multi-TeV Muon Collider.

1. Associated production: $\mu^+\mu^- \rightarrow Z^* \rightarrow Z^0 + h^0$ has $R \sim 0.12$. We can measure the b-quark Higgs-Yukawa coupling and look for invisible decay modes of the Higgs boson.

2. Higgsstrahlung: $\mu^+\mu^- \rightarrow t\bar{t}\ h^0$ has $R \sim 0.01$ (so such a study requires ~ 5 ab^{-1}). This could provide a direct measurement of the top quark Higgs-Yukawa coupling.

3. W*W* fusion into $\nu_\mu\,\bar{\nu}_\mu\ h^0$ has R ~ 1.1 s ln(s) (for m_h = 120 GeV). It allows the study of Higgs self-coupling and certain rare decay modes.

2.1.3.3 *Extended Higgs Sector*

In the two Higgs-doublet scenario there are five scalars: Two charged scalars $H^\pm$, two neutral CP-even scalars h, H^0, and a CP-odd neutral A. For the supersymmetric MSSM models, as the mass of the A is increased, the h becomes closer to the SM Higgs couplings and the other four Higgs become nearly degenerate in mass, as shown in Fig. 4. This makes resolving the two neutral-CP states difficult without the good energy resolution of a Muon Collider.
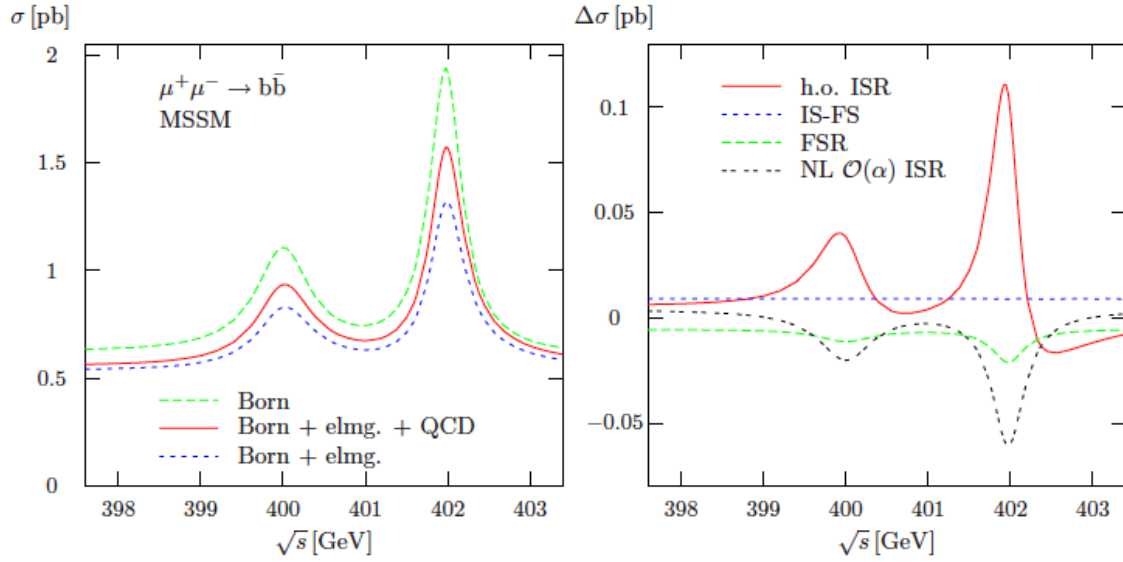
Figure 4: MSSM cross section $\mu^+\mu^- \to b\bar{b}$ near the H and A resonances (with M_A = 400 GeV and tan β = 5 (left), and with some contributions to the radiative corrections (right). From Ref. [5].

2.1.3.4 *Supersymmetry*

Supersymmetry (SUSY) provides a solution to the naturalness problem of the SM. It is a symmetry that connects scalars with fermions, ordinary particles with superpartners—a symmetry that is missing in the SM.

The simplest SUSY model is the MSSM, with only five parameters determining the masses of all the superpartners. It is now highly constrained by direct limits on the Higgs, mainly from LEP, CDF and DZero. Z-pole studies have provided constraints from electroweak precision measurements, and we have no indication of SUSY from flavor physics so far [6]. Recently the LHC has produced strong lower bounds on the masses of squarks and gluinos [7,8]. All this, taken together, makes it almost certain that direct coverage of the remaining MSSM parameter space requires a multi-TeV scale lepton collider such as CLIC or a Muon Collider.

2.1.3.5 *New Strong Dynamics*

Strong dynamical models of electroweak symmetry breaking have no elementary scalars and thus avoid the naturalness problem of the SM. Chiral symmetry breaking (à la QCD) in the technicolor sector produces technipions that give the proper masses to the W and Z bosons. For details and a discussion of various new strong dynamics models see the review of Hill and Simmons [9].

The "minimal Technicolor model" contains an isospin triplet techni-rho (ρ_T) and singlet techni-omega (ω_T) vector mesons, which can be produced in the *s*-channel in lepton colliders. In addition, it contains a techni-eta' (η_T') which would be produced in association with *Z* bosons in analogy to the Higgs boson.

In less minimal schemes, there are residual techni-pions, $\pi_T^\pm$ and π_T^0, that can be produced in lepton colliders. The techni-rho is typically broad if the two–techni-pion channel is open but, as in QCD, the techni-omega is nearly degenerate and narrow. In low-scale Technicolor models, some techni-rho (ρ_T) can be light (~250 GeV) as well as nearly degenerate in mass with a techni-omega, and these can be studied in great detail at a Muon Collider with the appropriate energy [10]. For techni-rho and techni-omega masses in the TeV range, a CLIC study has been done to determine its resolving power. The results for a Muon Collider are essentially the same as the CLIC curve before including the beamstrahlung and ISR effects. For this physics, the Muon Coliider has a distinct advantage over CLIC. The comparison is shown in Fig. 5.

There are other approaches to new strong dynamics: Topcolor, TC2, and Light Higgs models [9]. All of these would provide a rich spectrum of states that can be observed at a multi-TeV Muon Collider.
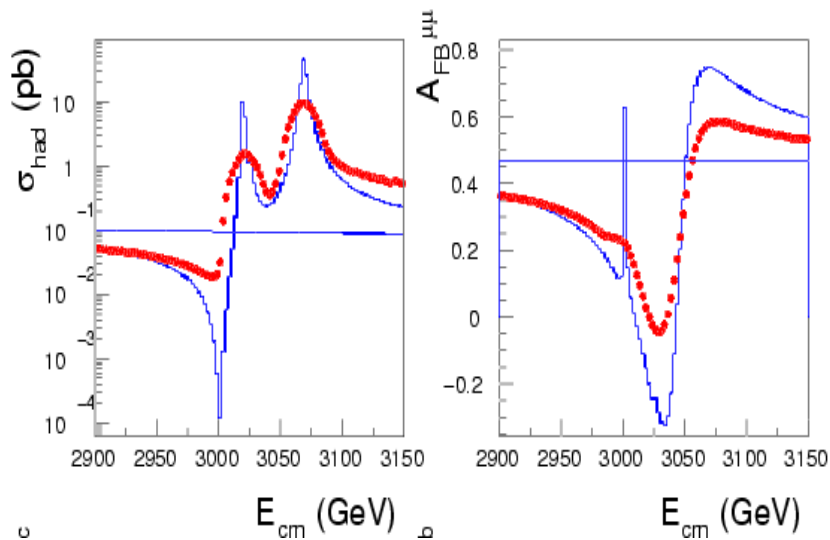
Figure 5: D-BESS model at CLIC. CLIC energy resolution limits its ability to disentangle nearby states expected in models with new strong dynamics.

2.1.3.6 *Contact Interactions*

New physics can enter through contact interactions, which are higher dimension operators in the effective Lagrangian as:

$$\mathcal{L} = \frac{g^2 \bar{\psi}\Gamma\psi\bar{\psi}\Gamma\psi}{\Lambda^2} \tag{4}$$

The MC is sensitive to $\Lambda \sim 200$ TeV, roughly equivalent to CLIC. Preliminary studies suggest that the forward angle block-out is not an issue here [11]. If polarization is not available at a MC, it may be at a disadvantage compared with CLIC in being able to disentangle the chiral structures of the new operators.

2.1.3.7 *Extra Dimensions*

These theories have extra dimensions that have a radius of curvature close to the Terascale. For gravity and any other interactions that occur in the bulk (in extra dimensions) one expects an excitation spectrum of standard model particles arising from excited modes in the extra dimensions.

From the perspective of energy frontier colliders, however, only the physics at the first (perhaps second) Kaluza-Klein (KK) mode will be relevant. All kinematically allowed KK-mode resonances are accessible to a multi-TeV Muon Collider. These include the Z' and γ' of the electroweak sector. The precise measurement of the Z' and γ' mass scales will determine the various electroweak symmetry breaking structures, and how these states couple to different fermion generations will determine bulk fermion localization.

In theories such as the Randall-Sundrum warped extra dimensions models [12], the graviton spectrum contains additional resonances (KK modes) that can be probed by a Muon Collider as shown in Fig. 6.
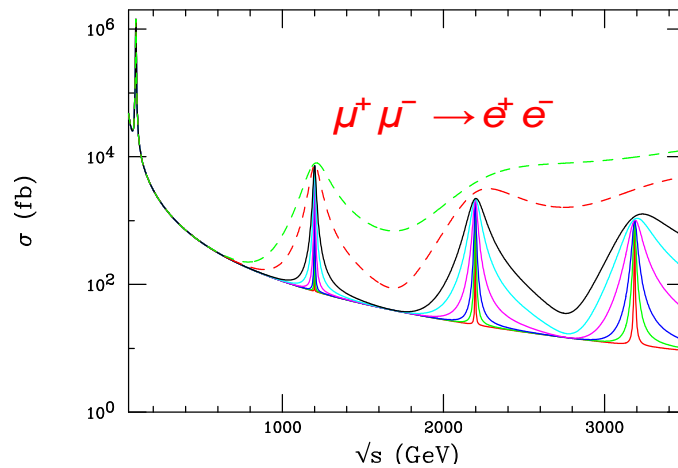
Figure 6: Graviton KK modes in a Randall-Sundrum model.

2.1.4 Summary

A multi TeV Muon Collider is required for the full coverage of Terascale physics. The physics potential for a Muon Collider at ~3 TeV and integrated luminosity of 1 ab^{-1} is outstanding. Particularly strong cases can be made if the new physics is SUSY or new strong dynamics. Furthermore, a staged Muon Collider can provide a Neutrino Factory to fully disentangle neutrino physics. If a narrow s-channel resonance state exists in the multi-TeV region, the physics program at a Muon Collider could begin with less than 10^{31} cm^{-2} s^{-1} luminosity.

Detailed studies of the physics case for a 1.5–4 TeV Muon Collider are just beginning. The goals of such studies are to: (1) identify benchmark physics processes; (2) study the physics dependence on beam parameters; (3) estimate detector backgrounds; and (4) compare the physics potential of a Muon Collider with those of the ILC, CLIC and upgrades to the LHC.

2.1.5 Acknowledgments

2.1.6 References

1. G. 't Hooft, (ed.), C. Itzykson, (ed.), A. Jaffe, (ed.), H. Lehmann, (ed.), P. K. Mitter, (ed.), I.M. Singer, (ed.), R. Stora, (ed.),"Recent Developments in Gauge Theories. Proceedings, NATO Advanced Study Institute, Cargese, France, August 26 - September 8, 1979", NATO Adv. Study Inst. Ser. B Phys. **59**, 1-438 (1980).
2. J. Bernabeu *et al.*, "EURONU WP6 2009 yearly report: Update of the physics potential of Nufact, superbeams and betabeams", arXiv:1005.3146 [hep-ph]; and the references therein.
3. E. Accomando *et al.* [CLIC Physics Working Group], "Physics at the CLIC multi-TeV linear collider", arXiv:hep-ph/0412251.
4. V. D. Barger, M. S. Berger, J. F. Gunion and T. Han, "Higgs boson physics in the s-channel at mu+ mu- colliders", Phys. Rept. **286**, 1 (1997) [arXiv:hep-ph/9602415].
5. S. Dittmaier and A. Kaiser, "Photonic and QCD radiative corrections to Higgs boson production in mu+mu- $\rightarrow$ f anti-f ", Phys. Rev. D **65**, 113003 (2002) [arXiv:hep-ph/0203120].
6. O. Buchmueller, R. Cavanaugh, D. Colling, A. De Roeck, M. J. Dolan, J. R. Ellis, H. Flacher, S. Heinemeyer *et al.*, "Supersymmetry and Dark Matter in Light of LHC 2010 and Xenon100 Data", arXiv:1106.2529 [hep-ph].
7. S. Chatrchyan *et al.* [CMS Collaboration], "Inclusive search for squarks and gluinos in pp collisions at sqrt(s) = 7 TeV," arXiv:1107.1279 [hep-ex].
8. J. B. G. da Costa *et al.* [Atlas Collaboration], "Search for squarks and gluinos using final states with jets and missing transverse momentum with the ATLAS detector in sqrt(s) = 7 TeV proton-proton collisions", Phys. Lett. B **701**, 186 (2011), [arXiv:1102.5290 [hep-ex]].
9. C. T. Hill and E. H. Simmons, "Strong dynamics and electroweak symmetry breaking", Phys. Rept. **381**, 235 (2003) [Erratum-ibid. **390**, 553 (2004)], [arXiv:hep-ph/0203079].
10. E. Eichten, K. D. Lane and J. Womersley, "Narrow technihadron production at the first muon collider", Phys. Rev. Lett. **80**, 5489 (1998), [arXiv:hep-ph/9802368].
11. E. J. Eichten and S. Keller, "Compositeness test at the FMC with Bhabha scattering", arXiv:hep-ph/9801258.

12. L. Randall and R. Sundrum, "A Large mass hierarchy from a small extra dimension", Phys. Rev. Lett. **83**, 3370 (1999), [arXiv:hep-th/9905221]; "An alternative to compactification", Phys. Rev. Lett. **83**, 4690 (1999), [arXiv:hep-th/9906064].

2.2 An Overview of Muon Colliders

Robert B. Palmer, Richard Fernow
Brookhaven National Lab, Upton, NY, 11973
Mail to: palmer@bnl.gov

2.2.1 Introduction

The idea of Muon Colliders was introduced around 1969 by Budker [1] and later developed by Skrinsky *et al.* [2]. Early U.S. design work on a Muon Collider was reported [3] at the Snowmass Workshop in 1996. Neutrino factories [4] use many of the same components, and will be discussed briefly in Section 2.2.2.

Some advantages of muons for a collider, as opposed to electrons, are:

1. Synchrotron radiation is proportional to E^4/m^4, and is thus strongly suppressed for muons, allowing muon acceleration and the collider to be circular and thus much smaller than a comparable energy e^+e^- collider (see Fig. 1).

2. Because the Muon Collider is circular, muon bunches collide many times, allowing larger emittances and fewer leptons for a given luminosity. The number of such collisions is limited by the muon lifetime to approximately 150 $<B>$, where $<B>$ is the average ring bending field in tesla. For an average field of 7 T, the lifetime corresponds to ~1000 turns, and thus this number of bunch crossings in each detector. In contrast, in an electron-positron linear collider the beams interact only once.

3. In a circular collider ring, there can be more than one detector (two in our design), which effectively doubles the luminosity.

4. Synchrotron radiation occurring during the bunch crossings (beamstrahlung) is strongly suppressed (proportional to E^4/m^4), resulting in a much smaller collision energy spread at a Muon Collider than at an e^+e^- collider.

5. s-channel Higgs production is enhanced by a factor of $(m_\mu/m_e)^2$, i.e., by ~40,000. This makes the observation of such production practicable, whereas with electrons it is not.
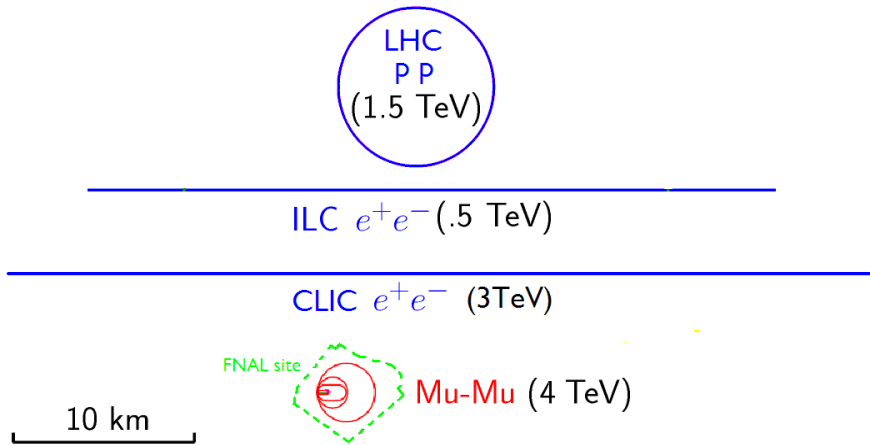
Figure 1: A comparison of collider sizes with their approximate effective center-of-mass energies.

But there are also challenges: selecting polarized muons is very inefficient; ring magnets and detectors must be shielded from decay electrons; acceleration and cooling must be very rapid to avoid decay losses; and, at higher energies, neutrino-induced radiation is a significant constraint.

Parameters of two colliders under study are given in Table 1.

Table 1: Latest machine parameters [5].

Parameter	Unit	Value	
Center of mass energy	TeV	1.5	3
Luminosity	10^{34} cm^{-2} s^{-1}	1.25	4.4
Beam-beam tune shift		0.087	0.087
Muons per bunch	10^{12}	2	2
Muon power (both beams)	MW	7.2	11.5
Normalized rms emittance $\varepsilon_{x,y}$	mm mrad	25	25
Normalized rms emittance ε_z	mm mrad	72,000	72,000
Repetition rate	Hz	15	12
Proton driver power	MW	4	3.2

The main collider components, numbered as in Fig. 2, include [6]:
1) A high intensity 8 GeV proton source, and a buncher that forms intense ($\sim 2 \times 10^{14}$ protons), short (~ 2 ns), bunches of protons at 15 Hz, with a total power of 4 MW

2) A liquid-metal target, able to withstand the 4 MW beam, in a ~ 20 T hybrid solenoid (water-cooled copper coils inside superconducting coils) to capture the pions; and a string of tapered solenoids to transport them to a lower field decay region.

3) A system of RF cavities to bunch the muons and phase rotate them into a train with both muon signs.

4) A system to separate the beam containing both signs into two beams, one of each sign.[1]

5) An ionization cooling system for all six dimensions (6D), to reduce the emittances sufficiently to allow the multiple bunches to be merged.

6) A system to merge the multiple bunches into single bunches, one of each sign.

7) 6D re-cooling, of the now larger combined bunches, to the lowest technically feasible emittances. At this point, the transverse emittances are approximately 10 times larger than is required, but the longitudinal emittance is approximately 100 times smaller.
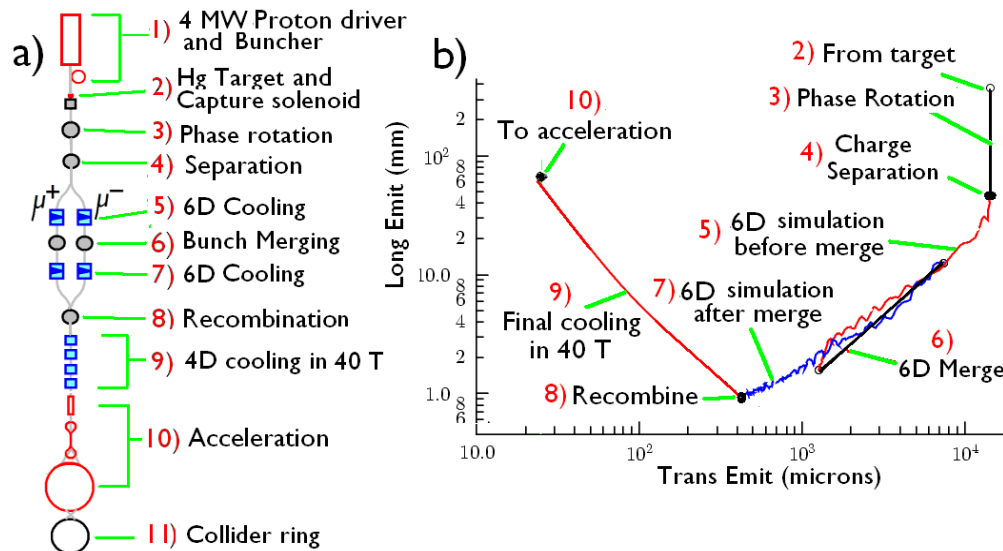
Figure 2: a) Schematic of a Muon Collider with numbered sub-systems (see text); b) longitudinal *vs*. transverse emittances from production to the start of acceleration. All components of this scheme have been simulated at some level, but with many caveats and without matching sections.

8) A system to recombine the muons of the two signs, with suitable spacing.

9) A final transverse cooling system using liquid hydrogen in high field (30–40 T) solenoids, at low energies, to achieve the required final transverse emittance. At the required low energies, the longitudinal emittance rises rapidly due to the adverse dependence of energy loss on energy, but this is acceptable.

[1] For one of the 6D cooling schemes (HFOFO Snake), this would be done later in the sequence.

10) Acceleration, initially in linacs, with frequencies first very low (using induction linacs), but rising (in normal conducting RF) as the bunches become shorter. When the RF frequency has risen to 201 MHz, superconducting cavities are employed. These linacs are followed by Recirculating Linear Accelerators (RLAs), and then one or more pulsed Rapid Cycling Synchrotrons (RCSs), or possibly further RLAs.

11) The collider ring has two low-beta insertions for two detectors. It must be nearly isochronous to maintain the very short (1 cm) bunches with reasonable RF. Tungsten shielding, and/or open midplane bending magnets are needed to keep the decay electrons from heating and quenching the superconducting coils. The detectors also have special shielding from these decay electrons. The ring is deep underground to control neutrino-induced radiation.

We will now briefly describe the Neutrino Factory, since it shares many of the above sub-systems, and will then discuss in more detail the individual systems in Sections 2.2.3–2.2.15.

2.2.2   Neutrino Factory

The main components of a Neutrino Factory are the same as for a collider, but instead of a collider ring, a storage ring with long straight sections is used to provide intense neutrino beams. The bunch requirements are less severe: more smaller-intensity muon bunches can be used, and far less cooling is needed. The beam energies under discussion are in the range 4–50 GeV compared with 0.75–1.5 TeV for the collider. The Neutrino Factory is described in greater detail in Section 3.1.

2.2.3   Proton Driver

The assumed proton driver (Fig. 3) is an upgraded version of Project X [7]. The current concept is based on a 3 GeV, 1 mA CW linac feeding 3 MW to multiple target stations. For the Muon Collider, the CW linac would be upgraded to 5 mA, and would also feed a 3–8 GeV pulsed linac giving 4 MW of proton power. This would be accumulated in one ring [8], and then bunched in a second ring, giving short trains of bunches at the required repetition rate of 15 Hz.
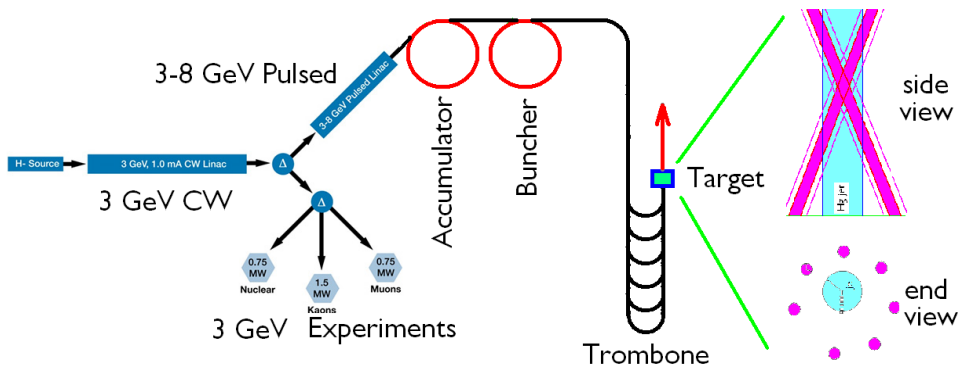
Figure 3: Schematic of Project X proton accelerator upgraded for use as a Muon Collider proton driver.

Merging these short trains into single bunches in a ring appears impractical from space-charge considerations, so it is proposed to extract the bunches of the train into separate (trombone) transport lines of differing lengths so that they arrive on the target at the same time. They interact with the mercury target by passing through it at small angles, with each bunch of the train intersecting the jet from a different azimuthal angle.

2.2.4   Target

The target must withstand extremely high pulsed-beam heating. The use of solid targets seems very difficult, while the use of a liquid-metal jet appears more straightforward. The liquid, when hit by the beam, is 'destroyed,' but the jet re-forms before the next proton bunch arrives. The demonstration of this concept in the MERIT experiment (see Sec. 2.2.16.1) at CERN [9] using a mercury jet and 24 GeV proton bunches with intensities of up to 30 Tp, gives us confidence in this solution.

The pions produced in the target are captured in the 15 cm bore of a 20 T axial magnetic field generated by an inner copper coil, and an outer superconducting solenoid. Additional superconducting solenoids are used to taper the field down to that used in the decay channel and subsequent phase rotation.

Figure 4 shows the cross section through a recent target system design [10] for a Neutrino Factory. The yellow sections are shields formed of tungsten carbide pellets cooled by flowing water. The blue elements are the mercury jet and a bath of liquid mercury that serves as a beam dump. The proton beam intersects the mercury jet at a small angle. For the Muon Collider, some modifications of this design will be required to allow multiple beams to intersect the jet.
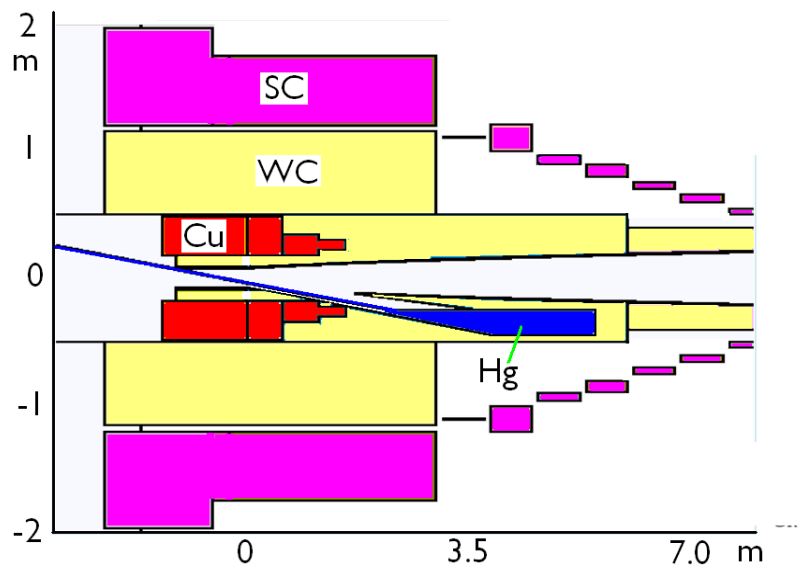
Figure 4: Cross section through the target station. Magenta represents superconducting coils, red represents copper coils, and yellow is used for the water-cooled tungsten carbide shielding.

2.2.5   Phase Rotation

The pions, and the muons into which they decay, have an extremely wide energy distribution (rms $\delta E/E \sim 100\%$), but they are produced in a relatively short interval of time as determined by the bunch length of the protons (~2 ns), plus a spread of the order of 1 ns from the decay kinematics. Such a huge bunch is hard to capture efficiently in an RF system, and difficult to transport or focus. It is convenient therefore to perform a phase rotation of that single bunch, with huge energy spread, but short duration, into a longer distribution with smaller energy spread, and to have this longer distribution in the form of a train of bunches at a convenient frequency of 201 MHz.

Figure 5 shows schematically how the concept works [11]. The beam is initially allowed to drift for 56 m, where it develops an energy-time correlation. Then, a 32 m channel containing RF cavities bunches this distribution using frequencies that fall as a function of distance. This is followed by 36 m of further RF with phases and frequencies chosen to decelerate the faster bunches, while accelerating the slower ones.
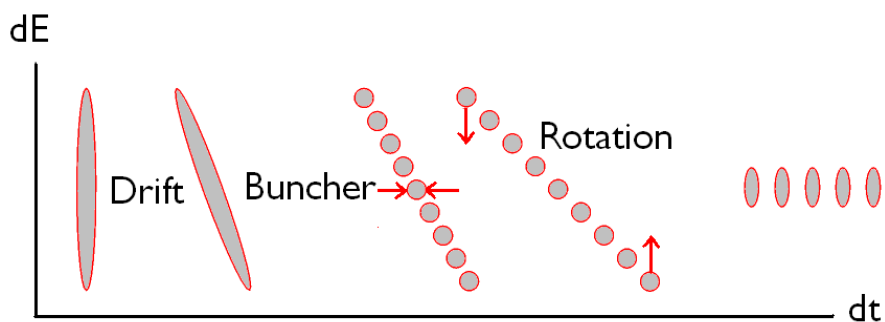
Figure 5: Concept of Neuffer phase rotation.

Figure 6 shows phase space plots both before (6a) and after (6b) the rotation. The red box encloses the 12 most intense sub-bunches that can be merged after initial 6D cooling. It is seen that after phase rotation these bunches have a much smaller energy spread but are spread over a longer time interval.
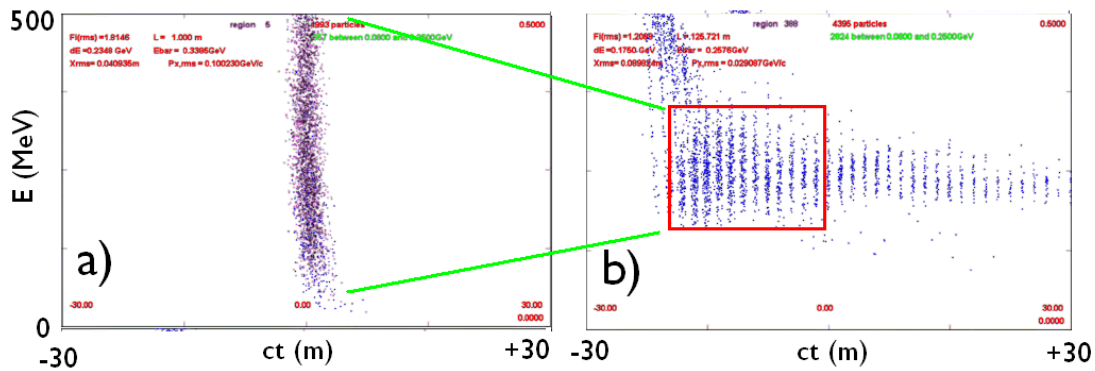
Figure 6: Phase plots of muons: a) shortly after their production; and b) after rotation. The red box at right covers 12 bunches that can be combined later in the system.

2.2.6   Charge Separation

Two of the 6D ionization cooling methods described later in Section 2.2.8 (RFOFO Guggenheim, or Helical Cooling Channel) require separate channels for the two signs of muons. Whichever method is used, it is necessary to first separate the charges.

Figure 7a shows a schematic of a system using bent solenoids for the separation [12]. An initial bend in the *x-z* plane generates dispersion in the *y* direction, displacing the positive and negative beams above and below the *x-z* plane. A septum then divides the beams of the two charges into two separate bent solenoids, one above the other. One of these immediately bends the beam back to its original direction in the *x-z* plane, correcting its dispersion. The second solenoid containing the other charge is extended straight for a distance, and then it too bends the beam back to the original direction, but now displaced in *x* from the beam of the other sign.
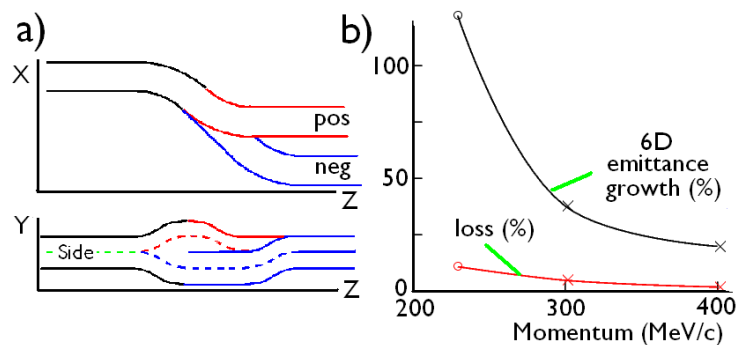
Figure 7: Charge separation: a) schematic of bent solenoids; b) emittance growth and losses *vs.* momentum of beams.

The main difficulty in this method is that no RF can be inserted during the operation, since RF would disturb the momenta and thus the subsequent dispersion

correction. Without RF, the bunch length grows, and muons can fall out of the following RF bucket and be lost. Use of higher solenoid fields and tighter bends reduces the path length and thus the resulting bunch length growth. Unfortunately, higher fields and stronger bends can cause non-linearities that increase the transverse emittances. Both these effects can be reduced if the momentum is increased, as shown in Fig. 7b.

Alternatively, 6D cooling could be started using the method that accepts both signs (the Helical FOFO Snake), and the charge separation done later when the emittances are smaller. This option is under study.

2.2.7   Introduction to Transverse Ionization Cooling

Electrons can be cooled using synchrotron radiation. Protons are cooled by stochastic methods or by interactions with a co-moving cold electron beam, but these methods are all too slow to cool muons with their limited lifetime. Only ionization cooling [13] appears feasible. Muons passing through an absorber lose momentum in 3 directions (see Fig. 8), while only the longitudinal momentum is restored by RF. This cooling is competing with growth from Coulomb scattering. In the linear case, the equilibrium emittance in this process is given by

$$\varepsilon_{x,y}(\mathbf{eq}) = \frac{\beta_{x,y}}{\beta_v} C(mat, E)$$

(1)

where

$$C(mat, E) = \frac{1}{2}\left(\frac{14.1\ MeV}{m_\mu}\right)^2 \frac{1}{L_R \frac{d\gamma}{ds}} .$$

(2)

$C(mat,E)$ depends on the absorber material and the muon energy and is smallest for hydrogen, followed by helium, lithium hydride and then lithium. It actually has a maximum value (see Fig. 9a) near the 200 MeV/c momentum commonly used in cooling channels. The choice of such a momentum is driven by a) using the least amount of re-acceleration, and b) avoiding the increase of longitudinal emittance from the negative slope of energy loss with energy at lower momenta (see Fig. 9b).
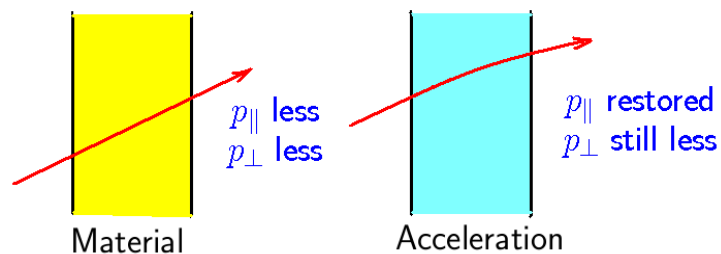
Figure 8: Transverse ionization principle.
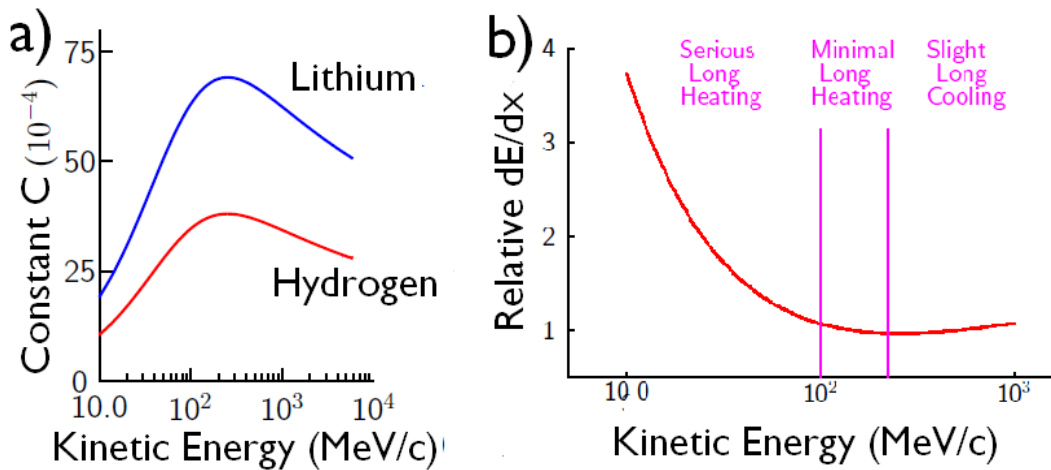
Figure 9: a) The constant C(*mat, E*) for hydrogen and lithium vs. muon kinetic energy; b) relative energy loss vs. muon kinetic energy.

From Eq. 1, one might assume that the strongest focusing, and thus lowest value of $\beta_{x,y}$ would always be preferred, but as β falls, the angular spread of the beam grows, making it very hard to avoid focusing non-linearities. It is thus desirable to lower β only as the emittance falls, keeping the ratio β/ε approximately constant. This requires a 'tapering' of the cooling channel to yield the highest cooling efficiency.

2.2.8   Six-dimensional Cooling Before Merge

2.2.8.1   *Introduction*

In some earlier designs, it was proposed to have some linear transverse cooling after the phase rotation and before any 6D cooling. However, this is not efficient. Straggling in such a channel causes the longitudinal emittance to rise, resulting in particles falling out of the RF bucket. It is significantly more efficient to go from the phase rotation straight into a 6D cooling lattice with appropriately large acceptance.

From the shape of *dE/dx vs.* energy (see Fig. 9b), ionization loss gives very weak cooling of *δE/E* at high energies, and thus very weak longitudinal cooling. At low energies it gives strong *δE/E* heating, which is why initial cooling is done at intermediate energies, around 130 MeV. In order to get significant reduction of *δE/E*, and thus significant longitudinal cooling, we employ geometries with dispersion that pass higher energy tracks through more ionizing material than low energy tracks. Figure 10 shows schematically the three ways that this can be done.
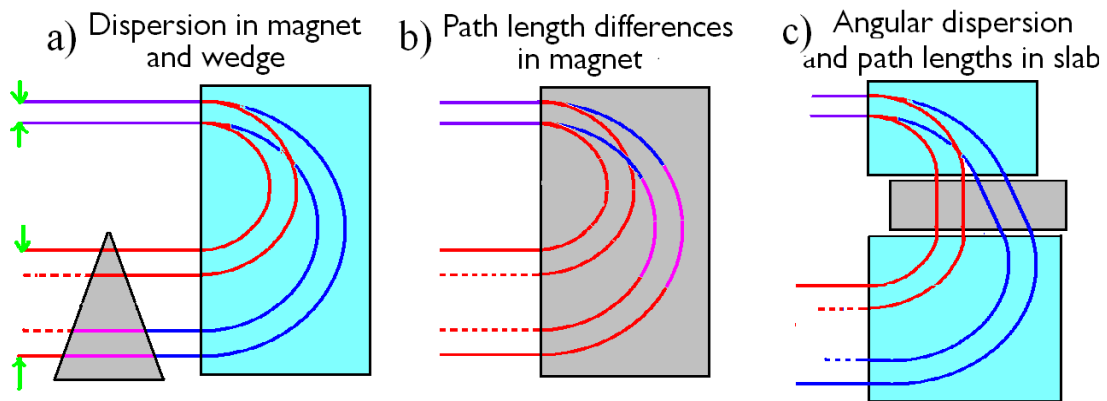
Figure 10: Emittance exchange methods: a) using dispersion and a material wedge; b) using path length differences in a material-filled magnet; c) using angular dispersion and a material slab.

2.2.8.2 *RFOFO Guggenheim*

The first method (Fig. 10a) is used in the RFOFO cooling channel [14] shown in Fig. 11a. Transverse focusing is provided by pairs of opposite polarity solenoids that surround the RF cavities. Dispersion is generated by tilting these solenoids such as to cause the orbits to form a gentle upward, or downward, helix. This helix arrangement is referred to as a "Guggenheim" geometry. Wedge-shaped hydrogen absorbers are placed at minima of the beta functions. Dispersion at these absorbers gives the required emittance exchange and allows, together with the still present transverse cooling, cooling in all six (6D) dimensions. Simulations [15] of this method are shown in Fig. 2b. These simulations used fields from a helical arrangement of technically plausible, superconducting coils.
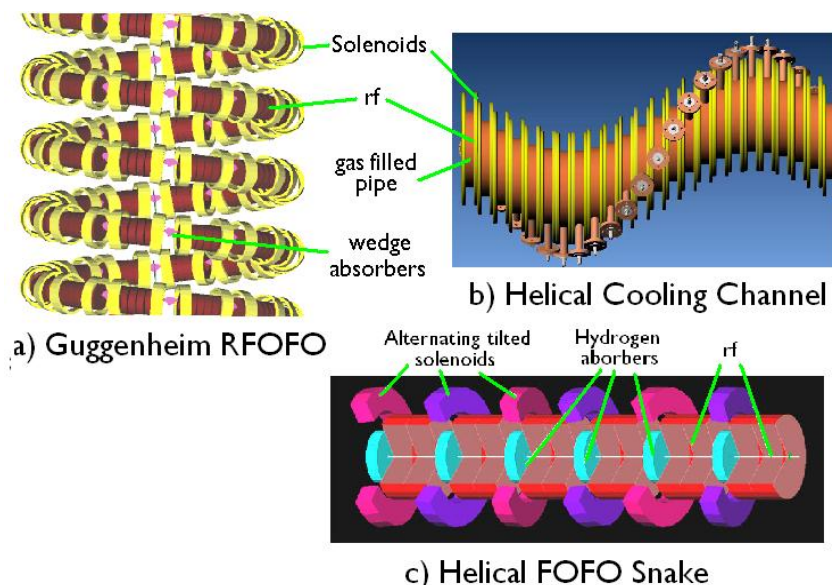
Figure 11: 6D cooling lattices: a) Guggenheim RFOFO; b) Helical Cooling Channel (HCC); c) Helical FOFO Snake.

In principle, an RFOFO lattice can be used in a ring instead of in a Guggenheim helix geometry, with kickers to inject and extract from the ring. However, to provide

adequate tapering, many rings would be needed. The kickers would be difficult and heating of the absorbers could become a problem. But the cost might be less, and ring cooling with an RFOFO or another lattice could be practical, especially after the emittance has fallen, and the bunches have already been merged.

This cooling method uses vacuum RF cavities in solenoidal fields up to ~5 T. A solution to the breakdown problem in such cavities (see Sec. 2.2.16.3) is essential.

2.2.8.3   *Helical Cooling Channel (HCC)*

The second method for emittance exchange (Fig. 10b) is the 'Helical Cooling Channel' (see Fig. 11b). The helical fields are generated by solenoid coils surrounding the helical beam trajectories [16]. An outer linear solenoid, not shown, is also sometimes needed to get the desired fields. The resulting orbits have longer paths for higher momenta than lower. When the beam pipe is filled with high-pressure hydrogen gas, the higher energy muons lose more energy than the lower, giving the required emittance exchange and thus the required 6D cooling.

The simulated performance [17] of the HCC is somewhat better than that of the RFOFO Guggenheim: it has larger acceptances, lower losses and uses less orbit length. The better performance probably arises from the continuous nature of the focusing, and benefits from gradient as well as solenoid focusing. In addition, the HCC has been more successful at getting adequate emittance exchange. Simulations have been performed with the helical field derived from analytic models and, in addition, by summing the fields of solenoids in the helical solenoid configuration shown in Fig. 11b. A technically plausible engineering design for integration of the superconducting coils and RF cavities, with suitable thermal separation and high pressure gas enclosure remains to be established.

This cooling method uses high pressure hydrogen gas in the RF, which is in solenoidal fields up to 15 T or more. Experiments have shown that the magnetic field is not a problem, but it remains to be shown that running intense ionizing radiation through the gas in high RF fields does not cause a problem (see Sec. 2.2.16.3). Experiments to study this have recently begun.

2.2.8.4   *Helical FOFO Snake*

Both of the above methods work for only one sign of muons, thus requiring the charge separation discussed in Section 2.2.6. The third method, the Helical FOFO Snake (see Fig. 11c), works simultaneously for both signs [18] by using smaller amplitudes of the helices, and parallel-faced hydrogen absorbers. The use of parallel-faced absorbers still generates emittance exchange by strong resonant angular dispersion that gives longer paths in the material for higher momentum tracks (see Fig. 10c).

2.2.8.5   *Choice of 6D Cooling Method*

Simulations of both the Guggenheim and the Helical Cooling Channels have achieved similar, very small emittances. The Helical FOFO Snake has currently been simulated only for larger initial emittances, but its use there would delay the need for charge separation, save hardware, and avoid the need for higher energies at the charge separation.

The choice between RFOFO Guggenheim and Helical Cooling Channel will depend on both experimental and simulation results. The vacuum RF used in the RFOFO

Guggenheim must operate in magnetic fields that have shown breakdown problems (Section 2.2.16.3). The beams in the Helical Cooling Channel pass through gas in the RF cavities, whose effect is not yet known, although currently under study. In addition, the relative costs and technical difficulties in the two methods have yet to be determined.

Although the three methods discussed above have been the most thoroughly studied, some simulation work has also been done on other methods for 6D cooling, including dipole-solenoid cooling rings [19] and anti-cyclotrons [20].

2.2.9   Merge

2.2.9.1   *Introduction*

The phase rotation system, discussed in Section 2.2.5, generated 12 bunches that were then cooled in six dimensions. The collider luminosity depends on the square of the number of muons per bunch, so it is desirable to merge these bunches into single bunches, one of each sign. After the merge, the emittances of the merged bunches will inevitably be greater, but they can now be re-cooled through 6D cooling channels similar or identical to those used before the merge.

2.2.9.2   *Simple Longitudinal Merge*

A simple way of merging [21] uses helical channels similar to those used in the HCC. An energy chirp is introduced in the bunches by 40 m of low gradient (1 MV/m) 270 MHz RF. The bunches are then allowed to drift without RF for a further 60 m. At this point the bunches are stacked in energy, all at the same time, and can be captured by 201 MHz RF, similar to that used at the restart of 6D cooling. The final longitudinal emittance is similar to that at the start, so re-cooling could be done in the same, or a similar 6D cooling channel. Figure 12 shows simulation of phase spaces in this longitudinal merge.
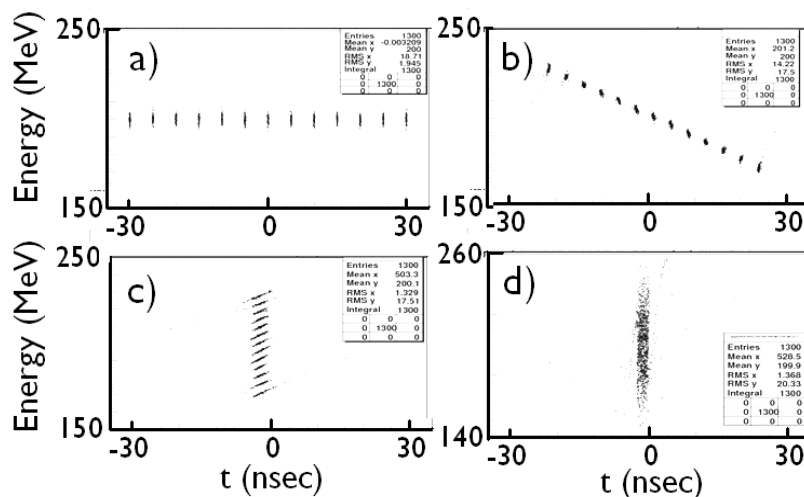
Figure 12: Simulation of phase spaces in a longitudinal merge: a) at end of first 6D cooling; b) after 40 m with 1 MV/m RF; c) after 60 m further drift; d) after capture with 201 MHz, 10 MV/m RF.

34

2.2.9.3   6D Merge

A problem inherent in the above simple longitudinal merging is that, after the merge, the relative longitudinal and transverse emittances do not naturally match into the following re-cooling. The longitudinal emittance is too large, while the transverse emittance, if not diluted, remains very small.

This problem can be removed by performing the merge in all 6 dimensions [22]. The merged bunches then have emittances very close to those in the first channel at a point well along that channel. A schematic of a method for this is shown in Fig. 13a. Lower frequency RF is used to combine groups of three bunches (Fig. 13b), reducing the total number of bunches from 12 to 4. A kicker is then used to send the four bunches into separate transports bringing them, all to the same time, but in four different transverse positions (Fig. 13c). When captured into a single channel, their transverse and longitudinal emittances are larger by similar factors, with none being increased as much as in the simple longitudinal merge. Figure 2b showed a simulation using a 6D merge, although that example used a merge of 21, rather than 12 bunches, resulting in greater increases in emittances than would a 12-bunch 6D merge.
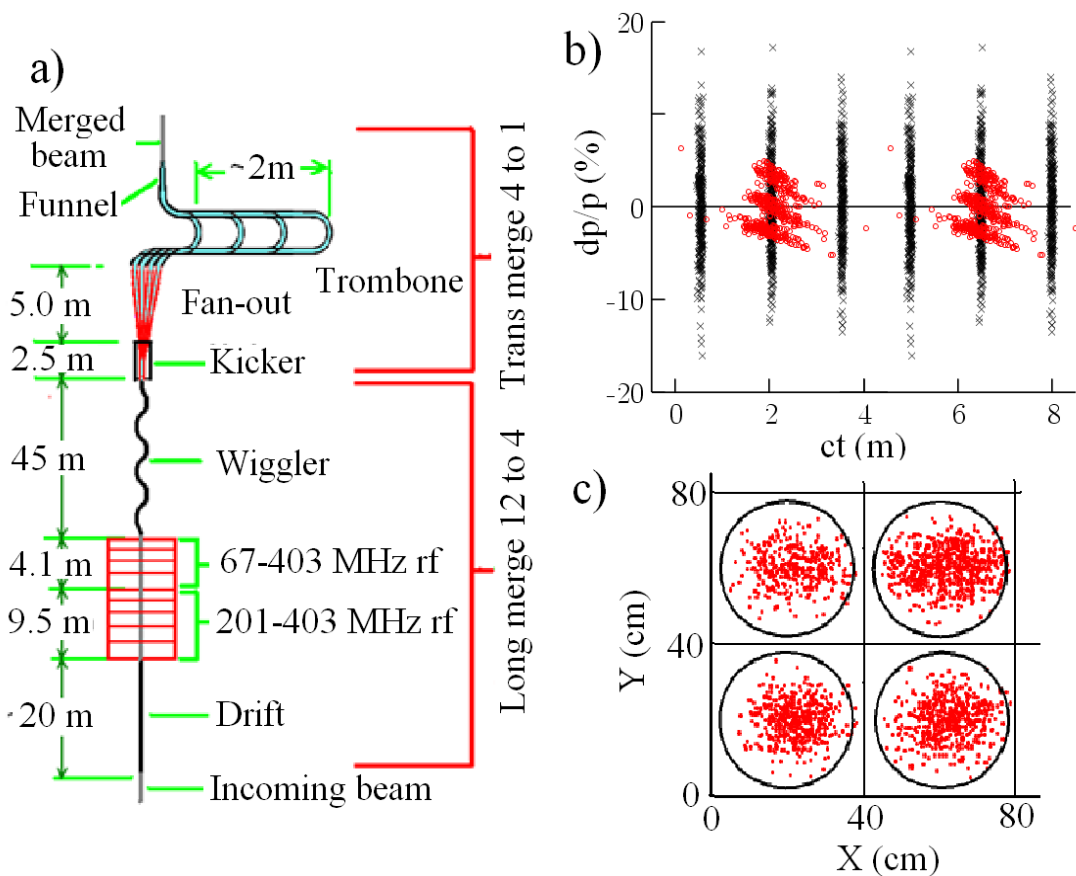
Figure 13: 6D merge: a) Schematic: the initial longitudinal merge combines groups of three, of the initial 12, into 4 combined bunches; followed by a transverse merge that combines the four into one; b) Longitudinal phase space before (black) and after merge (red); c) Four beams transverse locations before recapture into one.

2.2.10 Six-Dimensional Cooling After Merge

In the simulation shown in Fig. 2b, the six-dimensional cooling after the merge is taken down to lower emittances than in the cooling before the merge [15]. These simulations did not include any space charge effects. But analytic space charge estimates for the lower final emittances, combined with the greater number of muons in the single bunch, show significant space charge defocusing. In the transverse directions, this is not serious because of the very strong transverse magnetic focusing. But in the longitudinal direction, the analytic calculations show longitudinal defocusing several times larger than the RF focusing. Clearly, the simulation needs to be redone including space charge, and further parameter changes will undoubtedly be required. Increasing the frequency and gradient of the RF will help, but the final bunch lengths, and longitudinal emittances, will probably not be as small as plotted in Fig. 2b.

2.2.11 Final Transverse Cooling

2.2.11.1 *Introduction*

At the end of the 6D cooling, the transverse emittance is still about 10 times larger than that required for the design luminosity, but the longitudinal emittance is almost 100 times lower than is needed. This allows an approach to the final cooling that permits the longitudinal emittance to rise.

Such a situation is reached if cooling takes place at very low energies, where the equilibrium emittances are lower for two reasons: a) at lower momenta, the focusing from a given field is stronger, and b) the ionization energy loss *dE/dx* is greater, lowering the constant C(*mat, E*) in Eq. 2. Figure 14a shows the equilibrium emittances in hydrogen for three assumed solenoid fields, as a function of the muon energy. It is seen that the needed equilibrium emittance (about half of the final emittance required) is reached for any of the magnetic field values considered, but at ever lower energies as the field is reduced. Of course, the lower the energy, the greater the slope of *dE/dx vs. E*, and the greater the increase of longitudinal emittance.
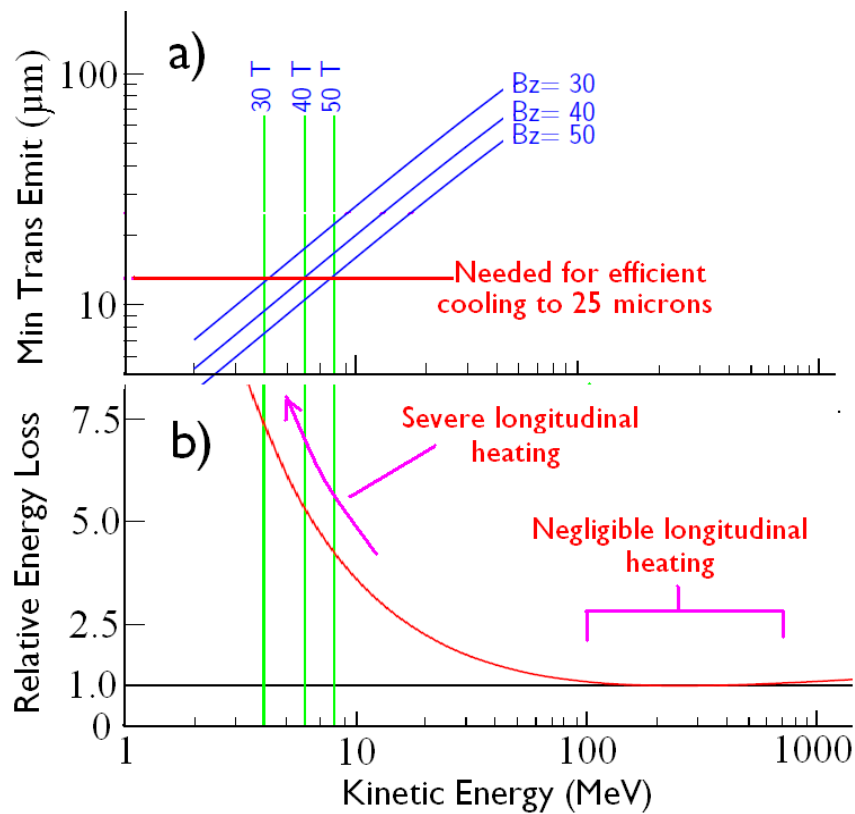
Figure 14: a) Equilibrium transverse emittance *vs.* energy for cooling in hydrogen in 30–50 T solenoid fields; b) relative energy loss.

2.2.11.2 *System of Cooling in 30–50 T Solenoids*

The proposed final cooling system [23] comprises a dozen or so stages. Each stage (see Fig. 15) consists of a high-field, small-bore solenoid, inside which the muons pass through a liquid-hydrogen absorber. Between each solenoid there is RF to reaccelerate and phase-rotate the muons, giving the required energy and energy spread for the following stage. The required RF frequencies are dictated by the ever increasing bunch lengths. The gradients assumed and RF types are shown on Fig. 16. There is also a field reversal to avoid an accumulation of canonical angular momentum.

For each stage, the initial energy, energy spread, and absorber length, are adjusted to minimize the ICOOL simulated negative slope of the ratio of longitudinal to transverse emittance. The resulting longitudinal and transverse emittances for optimized sequences using three fields are shown in Fig. 17.

We note that the 50 T case more than achieves our requirements, whereas 40 T just meets them and 30 T just misses. We expect that 30 T could likely be made acceptable with some adjustment of parameters. We adopt 40 T for the current design, with the option of accepting fields somewhat less if the R&D (discussed in Section 2.2.16.4) indicates that we must do so.

Figure 18 shows the relative lengths of components for the sequence using 40 T.
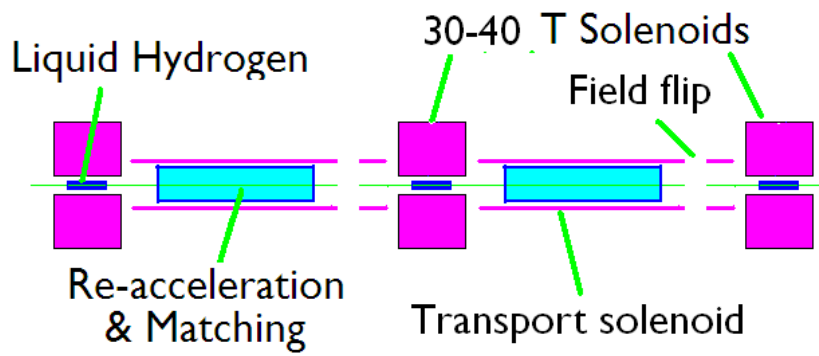
Figure 15: Schematic of two stages of Final Cooling.
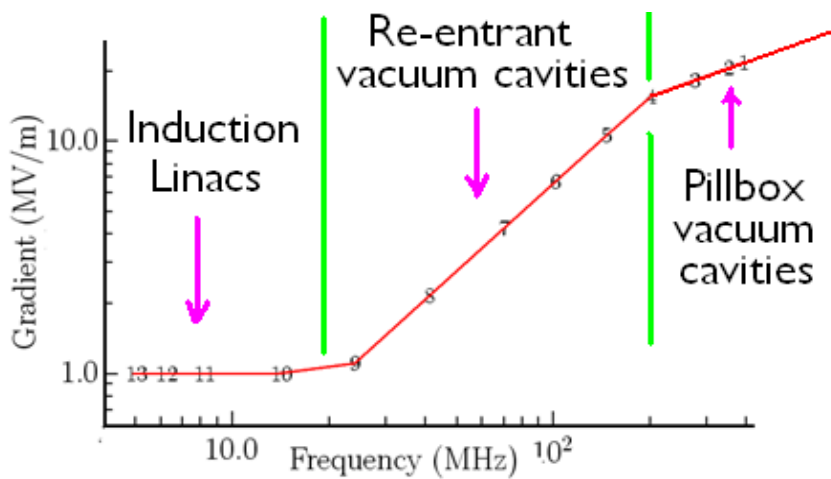
Figure 16: Frequencies and gradients of assumed RF systems used for re-acceleration.
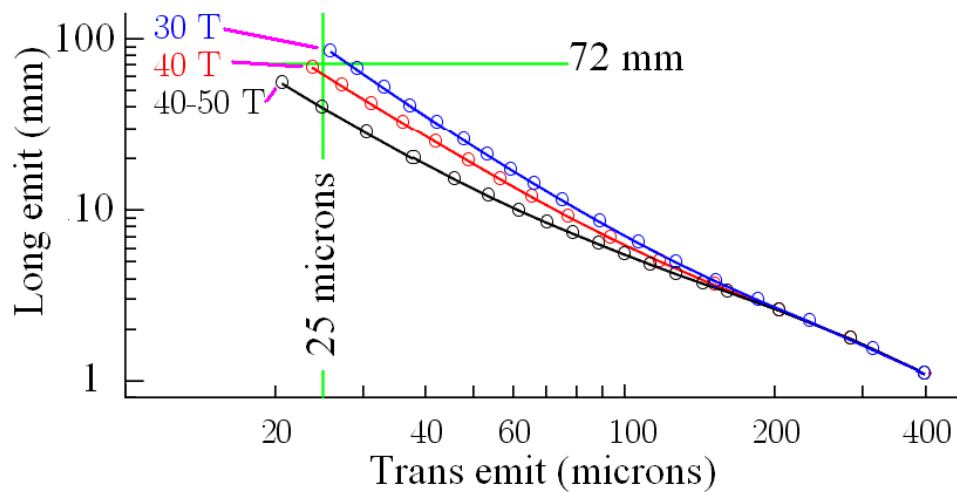
Figure 17: Longitudinal *vs*. transverse emittances for sequences of stages using three solenoid fields.
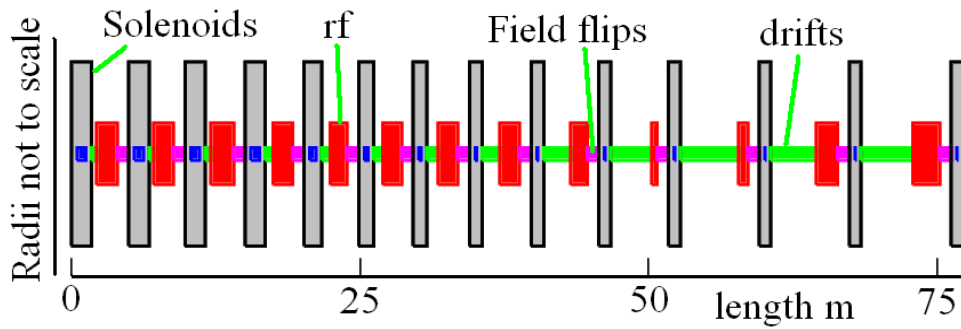
Figure 18: Schematic showing the lengths of the components of the optimized sequence of final cooling stages using 40 T solenoids.

The above simulations did not include the needed matching and re-accelerations, assuming that they could be performed without significant emittance dilution. Analytic estimates were made of re-acceleration frequencies, likely acceleration gradients, and decay losses in this re-acceleration, transverse matching, drifts, and field flips.

Progressing down the sequences, the longitudinal emittances grow, and the energies fall, resulting in ever longer bunches and ever lower RF gradients. At the end, the rms bunch length is of order 3 m, and the re-accelerations must be done with induction linacs.

A complete simulation of matching and re-acceleration has been done for only one case—that between the last two solenoids in a 50 T sequence. Figure 19a shows the dimensions of the 50 T magnets, the re-acceleration (in this case an induction linac), the field flip, and the transport coils that also achieved the required adiabatic transverse matching. Figure 19b gives the simulated longitudinal and transverse emittances and shows, as required, negligible emittance dilutions.

Analytic estimates of space-charge effects in the final cooling design find them to be less of a problem than at the end of the 6D cooling. In all stages, reasonable increases in RF and transport focusing appear to keep the space-charge defocusing smaller than the focusing provided by the RF and transport solenoids. At present, these calculations are only approximate, and full simulations are needed.
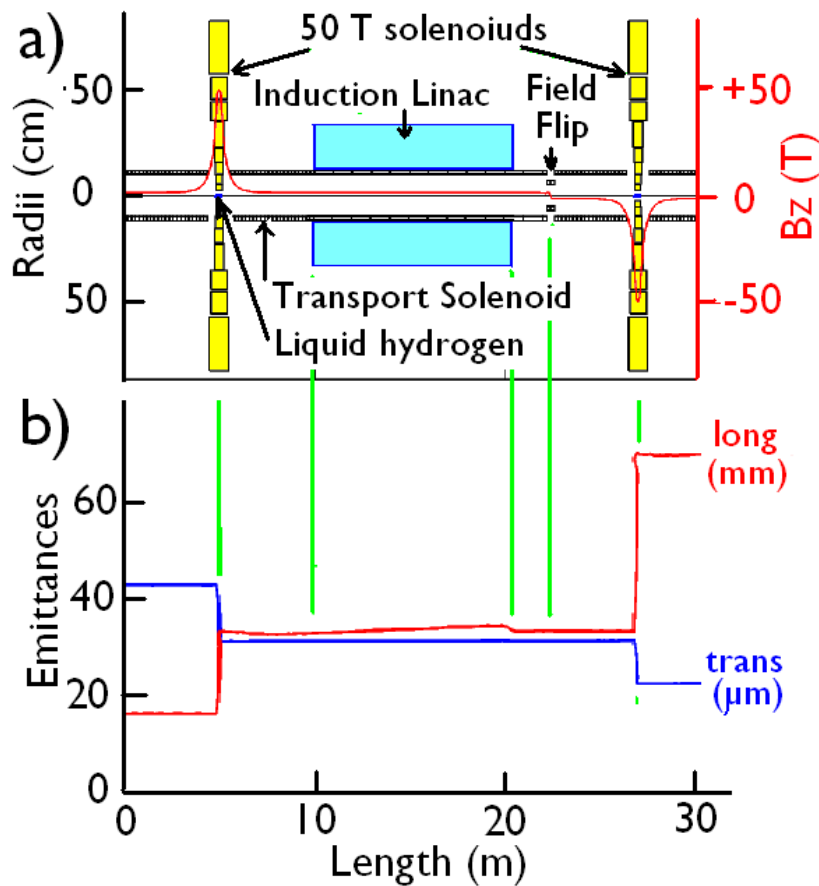
Figure 19: The matching, re-acceleration and field flip between the last two stages of the 50 T sequence of final cooling: a) component dimensions; b) evolution of longitudinal and transverse emittances along the channel.

2.2.11.3 *Other Schemes for Final Cooling*

There are also studies ongoing of at least two alternatives to the above Final Cooling system. Lithium lenses can provide the cooling material and, with an axial current, the required focusing [24], but no plausible simulation has yet reached the required transverse emittance of 25 μm.

The other concept is to use Parametric Ionization Cooling (PIC) [25] and/or Reverse Emittance Exchange (REMEX) using dispersion and wedges. Again, no simulation has yet shown cooling to the required emittances.

2.2.12 Acceleration

The bunches emerging from Final Cooling have very low energy (~6 MeV), large longitudinal emittance, and thus long bunch length. They can only be accelerated by very low frequency room-temperature RF. The gradients used, and cavity types, as a function of frequency, are shown in Fig. 16. As the beams gain energy, higher frequencies can be used until, at an energy around 400 MeV, 201 MHz superconducting RF can be employed.

Preliminary parameters and layouts for the superconducting acceleration for the 1.5 TeV collider are shown in Fig. 20. Acceleration starts with a simple linac that accelerates from 400 MeV to 1.5 GeV, followed by two Recirculating Linear Accelerators (RLAs) [26]. These RLAs have dog-bone geometries in order to simplify the design of the fan-outs.

	E (GeV)		turns	leng (m)	<grad>
	1) .4-1.5	Linac		linac =140	4.0 MV/m
	2) 1.5-12.5	RLA	n=4.5	linac = 306	4.0 MV/m
	3) 12.5-100	RLA	n=6.5	linac = 1250	5.6 MV/m
	4)100-400 RCS	n=23		Both in TeVatron tunnel	2.1 MV/m
	5)400-750 RCS	n=27		circ(ring)= 6283	2.1 MV/m
	both RCS pulsed at 15 Hz				
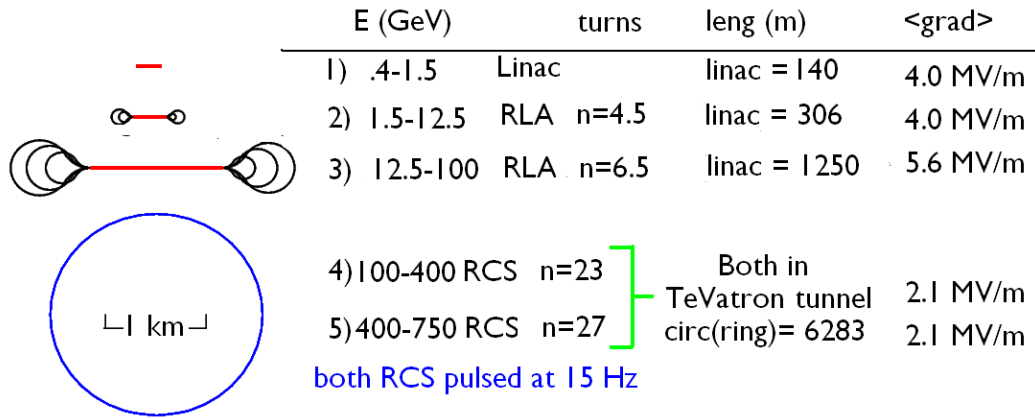
Figure 20: Superconducting acceleration systems with energies, turns, lengths, and average RF gradients.

Following the two RLAs, which take the energy to 100 GeV, there are two options. The more economical one is to use two pulsed Rapid Cycling Synchrotrons (RCSs) [27]. In the second of these synchrotrons, the circumference would be very large if only 1.8 T pulsed dipoles were used. The circumference is much reduced if such pulsed dipoles are interleaved with fixed 8 T superconducting dipoles (see Fig. 21). At injection, the pulsed dipoles oppose the fixed ones. At ejection, they work together. Using this solution, both RCSs can possibly be housed in the existing Fermilab Tevatron tunnel, giving a very cost-effective solution. However, the average accelerating gradients in these rings would be only 2.1 MV/m, leading to relatively high decay losses. The estimated transmission through all acceleration is only 63%.

The alternative option would be to use one or more additional RLAs with average accelerating gradients of around 6 MV/m, resulting in a 10% reduction of decay losses, and raising the total transmission through acceleration to 70%. Transmission is very important because it determines the needed proton driver power, space charge in the proton bunch compressor, and loading and space charge in the cooling channel. The choice between further RLAs or RCSs will depend on tradeoffs between cost and performance.
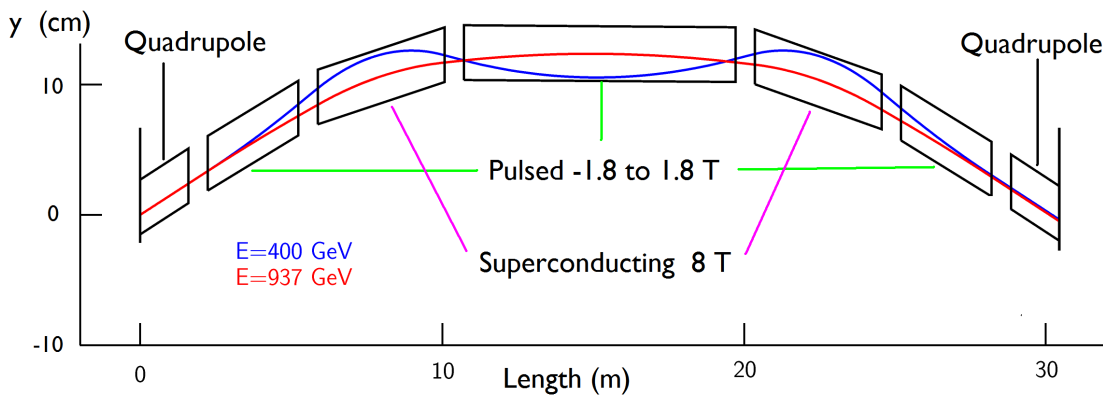
Figure 21: Alternating fixed and pulsed dipoles in the second RCS.

For the 3 TeV collider, either an additional (and larger) RCS, or another RLA would be added.

2.2.13 Collider Ring Lattices

Lattice parameters near the IPs for collider rings [5,28] at the two energies are shown in Fig. 22. In the lower energy ring the β at the IP is 1 cm, and it is 0.5 cm at the higher energy. This reduction at the higher energy was achieved by using a triplet final focus instead of the doublet at the lower energy. The maximum betas are 48 and 94 km, respectively. The momentum acceptances $\delta p/p$ of both rings are similar. The longitudinal emittances are also the same because the smaller bunch length is compensated by the greater momentum spread δp. However, considerably more RF (250 MV at 800 MHz) is needed at 3 TeV, compared with that at 1.5 TeV (20 MV at 800 MHz), to keep the bunch short.
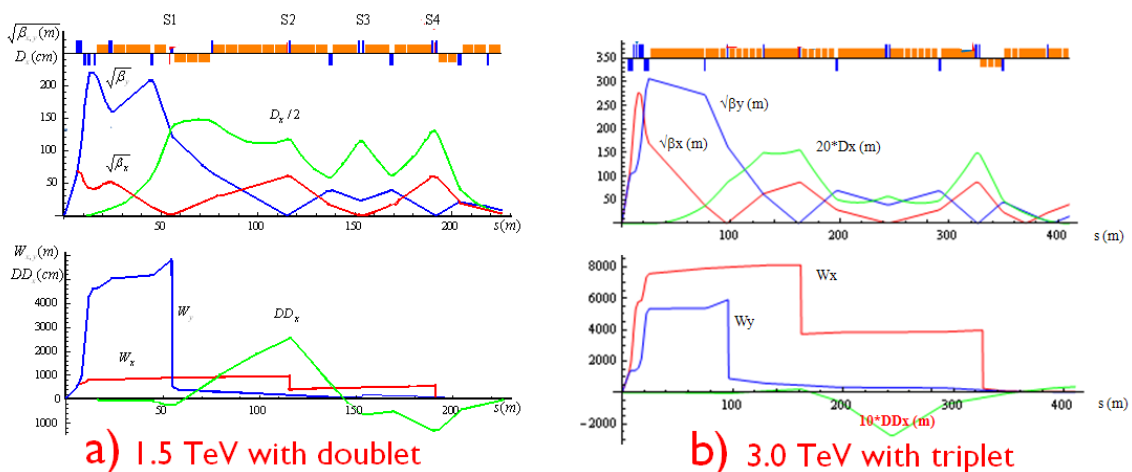
Figure 22: Lattice parameters near IP for a) 1.5 TeV , and b) 3.0 TeV.

2.2.14 Radiation

2.2.14.1 *Introduction*

There are three radiation challenges associated with the collider ring: a) electrons from muon decays showering in components and arriving in the detector as background. This will be discussed below in section 2.2.15, under MDI; b) radiation from these decays heating the superconducting magnet components and requiring excessive wall power to cool them; and c) neutrino-induced radiation giving low, but finite doses of radiation outside the site boundaries. In each of these cases, it is desirable to have the minimum number of circulating muons for the luminosity achieved.

2.2.14.2 *Beam Collimation*

Since the luminosity is proportional to the square of the density of muons, the tails of Gaussian distributions contribute relatively less to the luminosity than the core. Thus, collimating the tails of the transverse distributions would result in an improvement of luminosity for a given current, and an improvement in signal to decay backgrounds. A similar situation is present in luminosity contributions as a function of the number of lifetimes of the beam in the ring. Extracting the beam before all the muons have decayed again results in an improvement of luminosity for given radiation levels.

Where the collimation will be made will depend on operating criteria, but clearly one should include collimation capabilities. The collimation should probably be initiated at very low energies, where metal jaws would be effective. At high energies, electrostatic deflectors may be needed for such scraping [3]. Extraction systems and dumps to allow for early dumping of the beams should also be included.

2.2.14.3 *Neutrino-induced Radiation*

The neutrino-induced radiation is a particularly difficult issue [3,29]. It is present in a relatively narrow band exiting the earth in a wide circle around the site (see Fig. 23). Assuming divergences of the beams to be small compared with $1/\gamma$, the radiation intensity in Sieverts for a uniform bend field B is given in Equation 3, and for straight sections of length L in Equation 4. The divergence assumption is violated close to an IP, making these criteria too conservative there, but good everywhere else.

$$R_B = 4.4 \; 10^{-24} \frac{N_\mu \, f \, E^3 \, t \, <B>}{D \, B} \tag{3}$$

$$R_L = 6.7 \; 10^{-24} \frac{N_\mu \, f \, E^3 \, t \, <B> \, L}{D} \; . \tag{4}$$

In the above equations, R_B and R_L represent, respectively, the radiation dose in Sv integrated over a time interval t, from a uniform bend region or straight section of length L, N_μ is the number of muons in one ring, f is the repetition rate, E is the energy in TeV in one ring, t is the exposure time per year (taken here to be 10^7 seconds), $<B>$ is the average bending field around the ring, B is the local bend field in the magnet producing the radiation, and D is the depth in meters (taken here to be 135 m). Given a maximum

acceptable[2] off-site radiation level, we can calculate the maximum straight section length, and the minimum bending field that will give an acceptable radiation level.
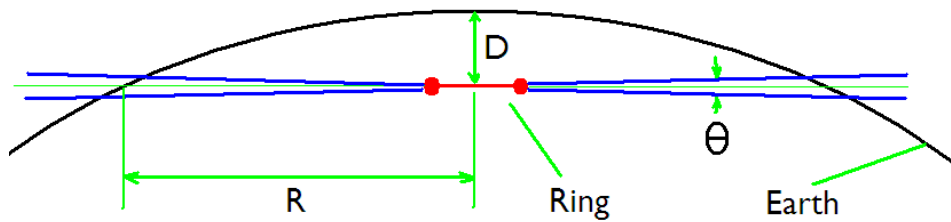
Figure 23: Schematic of neutrino radiation distribution from a ring at a depth *D* below the surface of a spherical earth.

For our parameters and an off-site limit of 0.1 mSv (10 mrem), then for the 1.5 TeV collider, the maximum straight section length is 2.4 m and the minimum bending field is 0.25 T. For 3.0 TeV, the maximum straight length is only 0.28 m and the minimum field is 1.5 T. These are severe constraints that the current designs do not meet. Possible mitigation actions include:

1) Allowing a higher off-site radiation level.
2) Using greater depths.
3) Making all quadrupoles into combined field magnets with the required minimum dipole component.
4) Placing weak dipoles over other components, such as RF and drifts.
5) Using collimation and beam dumping to decrease the radiation for a given luminosity.
6) Buying land in areas of maximum neutrino radiation and limiting access there.

2.2.15 Machine Detector Interface

Detailed studies have started to simulate background radiation near a detector, with shielding designed to reduce it [30]. Simulated radiation levels in the tunnels near the IP and in the detector are shown in Fig. 24. Shielding cones with an opening angle of 10° at the IP appear to be required. With these, it is found that the background rate in silicon trackers is about 10% of that in the LHC at 10^{34} cm^{-2} s^{-1}, so similar detectors should be able to operate well.

---

[2] Fermilab management guidance is to assume an off-site limit of 0.1 mSv, which is 10% of the federally mandated limit.
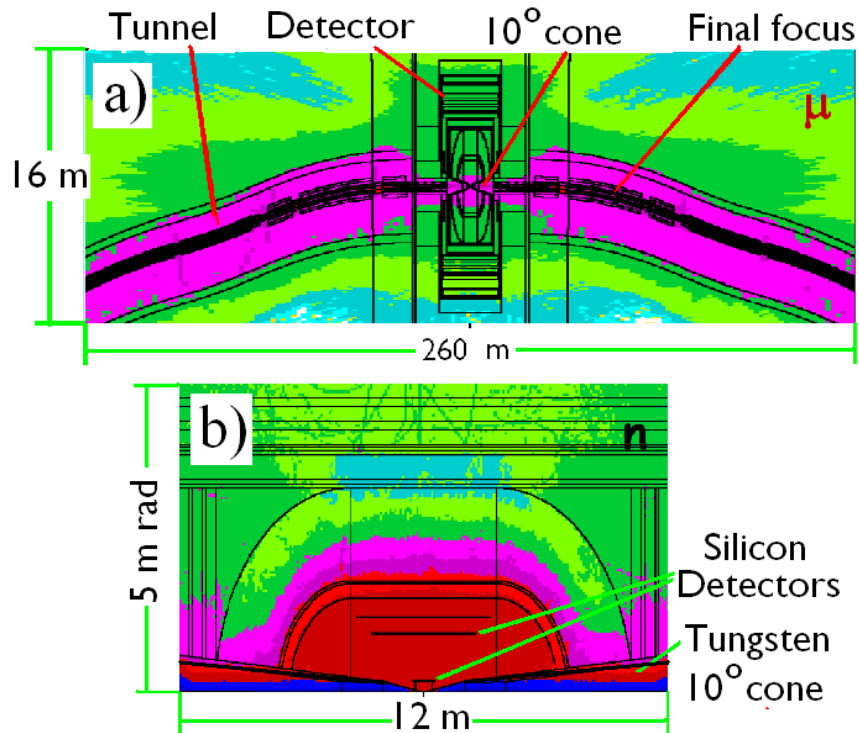
Figure 24: Radiation at the IP; a) radiation level in the tunnels approaching the IP, and in the detector; b) detail of the detector with silicon tracking planes.
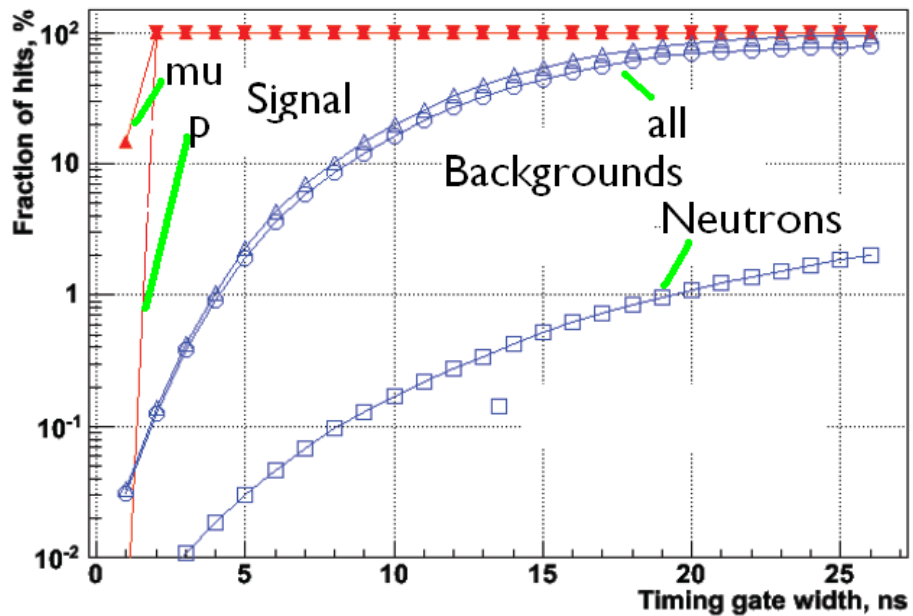
Figure 25: Simulated signal and background tracks vs. timing cuts.

Output from these simulations has been formatted to allow simulation of physics event reconstruction in the presence of the background. A very important result has

already emerged [31]: if local detector timing can be set to the order of 2 ns about the calculated time of arrival of relativistic tracks from the IP, then almost all background tracks are eliminated (see Fig. 25). Thus, it appears that the events can have adequate cleanliness.

2.2.16 Experimental Program and Technical Challenges

2.2.16.1 *Liquid Mercury Target R&D*

Figure 26 shows the liquid-mercury target experiment (MERIT). The target was tested [9] in a proton beam at CERN and demonstrated multi-megawatt capability for the Neutrino Factory parameter regime. However, the individual proton bunches used in that experiment (30 Tp at 24 GeV) deposited less energy than the collider specification of 200 Tp at 8 GeV. The challenge, through simulation, is to extrapolate the MERIT data to the collider requirements.
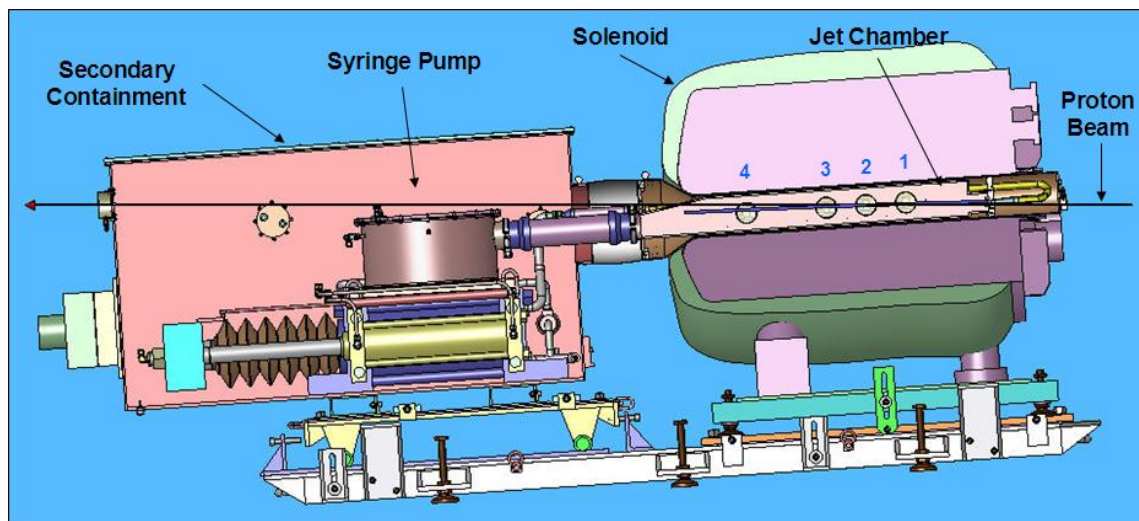
Figure 26: Schematic of the MERIT mercury-jet target experiment.

2.2.16.2 *The Ionization Cooling Experiment (MICE)*

An experiment to demonstrate ionization cooling, MICE (see section 3.4) is under construction at Rutherford Appleton Lab (RAL) in the UK [32]. At an early stage, experiments with LiH wedges should demonstrate emittance exchange without re-acceleration. In later stages, transverse cooling with re-acceleration will be achieved (see Fig. 27).
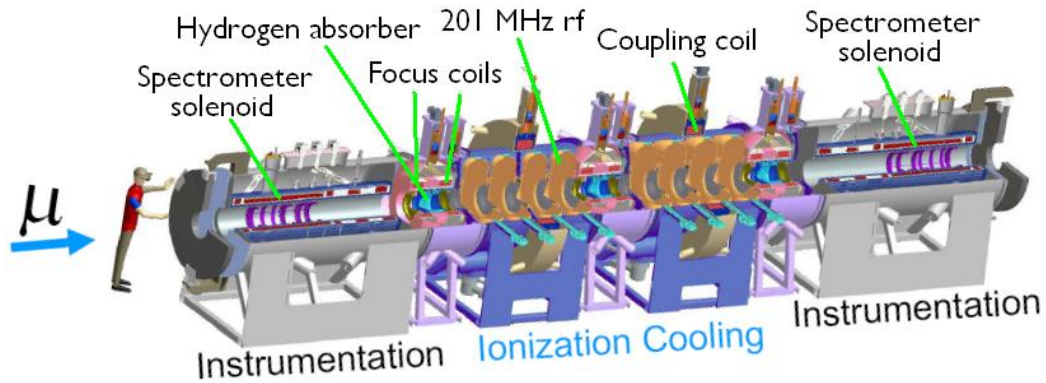
Figure 27: Layout of the Muon Ionization Cooling Experiment (MICE).

2.2.16.3 *RF Breakdown in Magnetic Fields*

Experiments by the MuCool program [33,34] at Fermilab (see section 3.7) in both Lab G and the MuCool Test Area (MTA) have shown damage and/or reduced RF gradients for both 805- and 201-MHz cavities operated in an axial magnetic field. Figure 28a shows some data on breakdown gradients at both frequencies. Maximum observed gradients are plotted as a function of the axial magnetic field on the nearest cavity surface.

Figures 28b and 28c show trajectories of field-emitted electrons with magnetic fields of zero and 1 T. It has been proposed that such electrons, when focused by the magnetic field, cause damage on the impacted surfaces. The damage mechanism is thought to be fatigue from cyclical strains caused by the pulsed heating in successive RF cycles [35].
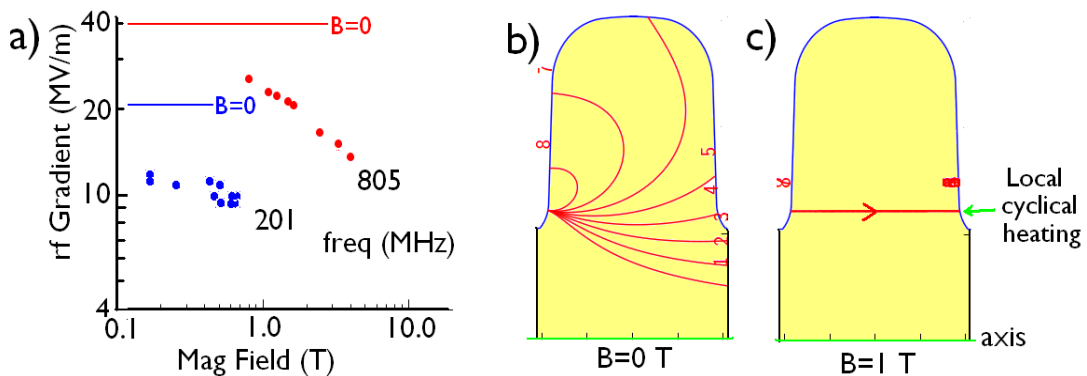
Figure 28: RF breakdown in magnetic fields; a) breakdown gradients in 805 and 201 MHz pillbox cavities as a function of axial magnetic fields; b) simulated electron trajectories with no field; c) simulated electron trajectories with 1 T magnetic field.

These observed gradients are well below the gradients specified for the collider design, and assumed above in the simulations of phase rotation, 6D cooling, and re-acceleration in Final Cooling. Several approaches to improve the situation are under study:

1) It has been shown [34] that RF in high-pressure hydrogen gas does not show any dependence on an external magnetic field, but it is not yet known whether there will be other effects when an ionizing beam passes through the gas in the

presence of RF. An experiment to test this is currently under way at the MTA. If no problem is found, then this technique would provide solutions for phase rotation, the Helical Cooling Channel, or hybrid forms of the RFOFO Guggenheim channel. But it does not solve the problem for the Final Cooling re-acceleration, where fields of up to 3 T are required for transverse space-charge control, and scattering from the gas would be unacceptable.

2) A cavity with the magnetic field perpendicular to the electric field along the high gradient surfaces (magnetic insulation) has been tested [36]. The surface gradients achieved were more than twice as large as those with the same field perpendicular to the surface but, because of a more damaging breakdown mechanism, not as good as without a magnetic field. When the lower acceleration for a given surface field in magnetically insulated open-iris cavities is included, the accelerating gradient appears not to be sufficient.

3) Tests in magnetic fields [37] showing severe damage of copper surfaces, have shown no damage on the beryllium windows exposed to the same fields. If the model described above is correct, then the low density of beryllium allows the focused electrons to penetrate more deeply into the cavity wall, thus giving less local heating and fatigue. In addition, beryllium is harder than copper and thus less subject to fatigue. An experiment using beryllium buttons is imminent. Designs for a beryllium walled cavity, and an 'all beryllium' cavity are also under way.

4) Improvements in surface treatments, including Atomic Layer Deposition (ALD) should suppress the initial electron field emission [38], and there are plans to test this.

2.2.16.4 *High Field HTS 30-40 T Solenoids for Final Cooling*

Another challenge is to build the small bore 30–40 T, all superconducting, solenoids for the final cooling. HTS materials have sufficient current density even at 50 T, but there are many hurdles. The highest HTS superconducting field achieved in an insert is 33.8 T [39]. A 32 T all-superconducting magnet is under construction at the NHMFL. An SBIR-funded study by a BNL/PBL [40] collaboration is building HTS coils that, when tested in the 19 T resistive magnet at NHMFL, could reach a field approaching 40 T.

R&D is also going on at Fermilab [41] where small HTS coils have been wound and tested in a 14 T commercial superconducting solenoid, giving a maximum field of 18.3 T.

2.2.16.5 *Radiation Shielding for Collider Ring Magnets*

For the 1.5 TeV collider, the total muon beam power is 7.2 MW, of which approximately 2.4 MW ends up as decay electron energy, while the balance goes to neutrinos. If the efficiency of the cryogenic refrigerator at 4 K is 20% of the Carnot efficiency, and not more than 10 MW is devoted to cooling the 4 K, 10 T dipoles, then shielding is required to reduce the 2.4 MW to less than 27 kW, i.e., the shielding must have a leakage of less than about 1%.

Two solutions are under study:

1) Constructing a thick tungsten beam pipe that is cooled by room temperature water inside a cosine theta, possibly elliptical, dipole. An earlier study [3] of a

4 TeV collider (see Fig. 29a) using a 5 cm thick tungsten pipe had a better-than-needed 0.27 % leakage. The thickness required for 1% leakage in the 1.5 TeV case is under study.

2) Building dipoles with open mid-planes with room temperature tungsten absorbers on either side to absorb the electrons on the inside, and synchrotron radiation on the outside. A design (see Fig. 29b) concept for this approach has achieved a 5% leakage, but not yet the required 1%.

R&D is also needed on the quadrupoles and dipoles in the interaction region. Here the apertures and fields are greater than in the arcs, but the thermal leakage does not have to be kept so low because there are relatively fewer such magnets.
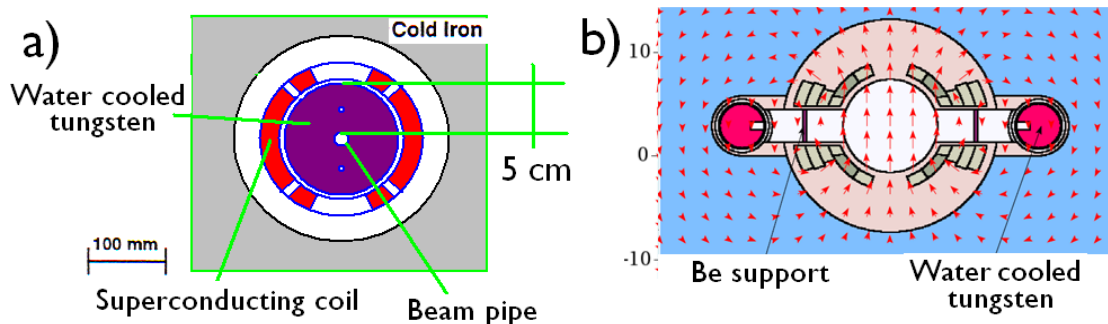
Figure 29: Shielding for ring dipoles: a) tungsten beam pipe in a 1998 study; b) open mid-plane dipole [42].

2.2.16.6 *R&D on Hydrogen Absorbers*

A liquid hydrogen absorber has been built [43] for MICE by collaborators at KEK, and tested at the Fermilab MTA. R&D may be needed for the wedge-shaped absorbers used in an RFOFO Guggenheim cooling channel. A displaced cylindrical absorber would be practical, but its performance needs simulation. For a Muon Collider or Neutrino Factory, forced-flow absorbers would be needed. Designs for similar systems serving as hydrogen targets have been successfully operated at several laboratories.

2.2.17 Summary Tables

2.2.17.1 *Muon Transmission*

Table 2 gives a preliminary summation of simulated muon losses from phase rotation to collider ring. These results are based on simulations of just one of the 6D cooling systems (RFOFO Guggenheim), using a phase rotation scheme designed for a Neutrino Factory, and using a bunch merging channel that worked with 21, rather than 12, bunches. It is seen that the muon beam transmission is only 5.4 %.

Using this estimate, for 2×10^{12} muons of each sign in the ring, we would need 1.67×10^{14} protons on target with a proton beam power of $15 \times 1.67 \times 10^{14} \times 8 \times 10^9 \times 1.6 \times 10^{-19} = 3.2$ MW. This gives us a margin of 20% from the specified 4 MW.

There is reason to believe that (with the new phase rotation, simpler merge, and better matching) the efficiency will be better than this estimate, in which case less than

4 MW of proton power would be needed. On the other hand, the effects of space charge may go in the other direction.

Table 2: Muon transmission

Parameter	Transmission	Cumulative	Muons per proton
After rotation with p=226±100 MeV/c		1.0	0.22
21 best bunches	0.7	0.7	0.153
Charge separation	0.95	0.66	0.145
6D cool before merge	0.47	0.31	0.068
6D merge	0.88	0.27	0.057
6D cool after merge	0.48	0.13	0.029
Final 40 T cooling	0.7	0.092	0.020
Room-temperature acceleration	0.84	0.077	0.017
Superconducting acceleration	0.7	0.054	0.012

2.2.17.2 *Wall Power Requirements*

The power estimates in Table 3 were derived assuming: a) cryogenic losses of 2.4 W per m of cold lengths, b) calculated energy losses in hydrogen absorbers; c) cryogenic efficiencies of 20% of Carnot; d) 60% RF generation efficiency; e) 15 MW to power the copper pion capture coil; f) estimates from simulation of beam energy deposited in front-end focusing solenoids assuming a 50% reduction from added shielding; g) hysteresis and ohmic heating estimates for the RCSs; h) 10 MW to cool the tungsten shields in the ring dipoles; and other, hopefully reasonable, assumptions.

The 3 TeV case assumes that the machine runs at 12 Hz rather than at the 15 Hz used for 1.5 TeV. This reduces the proton power and lowers both RF and cryogenic loads in all components except the final acceleration and collider ring, where they are increased. The lower losses in the earlier components appear to just balance the increases at the end, resulting in the same total wall power estimate for both machines.

Table 3: Wall power estimates in MW.

Subsystem	1.5 TeV	3.0 TeV
Proton driver	20	16
Target and taper	15.4	12.3
Decay and phase rotation	5.4	4.3
6D cool before merge	20.7	16.6
Merge	1.6	1.3
6D cool after merge	6.2	5.0
Final 40 T cooling	1.7	1.4
Normal conducting acceleration	4.2	3.4
Superconducting Linac	3.5	2.8
Superconducting RLAs	28.6	24.7
Superconducting RCSs	23.1	40.6
Collider ring	15.3	17.4
TOTALS	**146**	**146**

These summations did not assume either beam collimation, or early beam ejection to improve the luminosity to background ratios. If this were done, one would probably want to increase the repetition rate of the 3.0 TeV machine to restore the luminosity. This would somewhat increase the total wall power at the higher energy. The estimate has no doubt left out many, hopefully smaller, power needs; so these estimates are surely somewhat optimistic, but they should give the right scale for the power needs.

2.2.17.3 *Comparison with CLIC*

Table 4 gives a comparison of parameters between the 3 TeV Muon Collider and the 3 TeV CLIC electron-positron machine.

Table 4: Comparison of parameters with 3.0 TeV CLIC

Parameter	Unit	Muon Collider	Muon Collider	CLIC Electron
Center of mass energy	TeV	1.5	3	3
Luminosity	10^{34} cm^{-2} s^{-1}	1.25 (x2)[a]	4.4 (x2)[a]	2 (5.9)[b]
Accelerator length/circumference [c]	km	6	12	42
Leptons per bunch	10^{12}	2	2	0.0037
Normalized rms emittance, $\varepsilon_{x,y}$ [d]	mm mrad	25	25	0.66/0.02
IP beam, $\sigma_{x,y}$ [d]	μm	6	3	0.04/0.001
Repetition rate	Hz	15	12	50
Lepton power total	MW	7.2	11.5	28
Proton beam power	MW	4.0	3.2	-
Wall power [e]	MW	146	146	560

[a]The luminosity numbers for the Muon Collider should be multiplied by 2 if the luminosities of the two detectors are added.

[b]The CLIC luminosity is for those interactions within 1% of the beam energy. Its luminosity for all energies is 5.9 10^{34}.

[c]The largest structures in both machines, the accelerations, are more than 3 times smaller for the Muon Colliders.

[d]The beam sizes and emittances are dramatically larger in the muon case, meaning that tolerances and vibration are of much less concern for the muons.

[e]The wall power estimates for the Muon Collider clearly have large uncertainties, but relative to CLIC they reflect the lower lepton beam powers and the expected higher efficiencies of the multi-pass ring superconducting accelerator used for the muons.

2.2.18 Conclusions

Either a 1.5 TeV Muon Collider or a 3 TeV Muon Collider can easily fit on the FNAL site (see Fig. 30).

There has been a lot of recent design and simulation progress: a new capture magnet design; a shorter phase-rotation channel; a more efficient charge separation; two new merge designs; more complete 6D cooling simulations; analytic space-charge and RF-loading calculations; an acceleration sequence with better transmission; new detector background studies, and more.
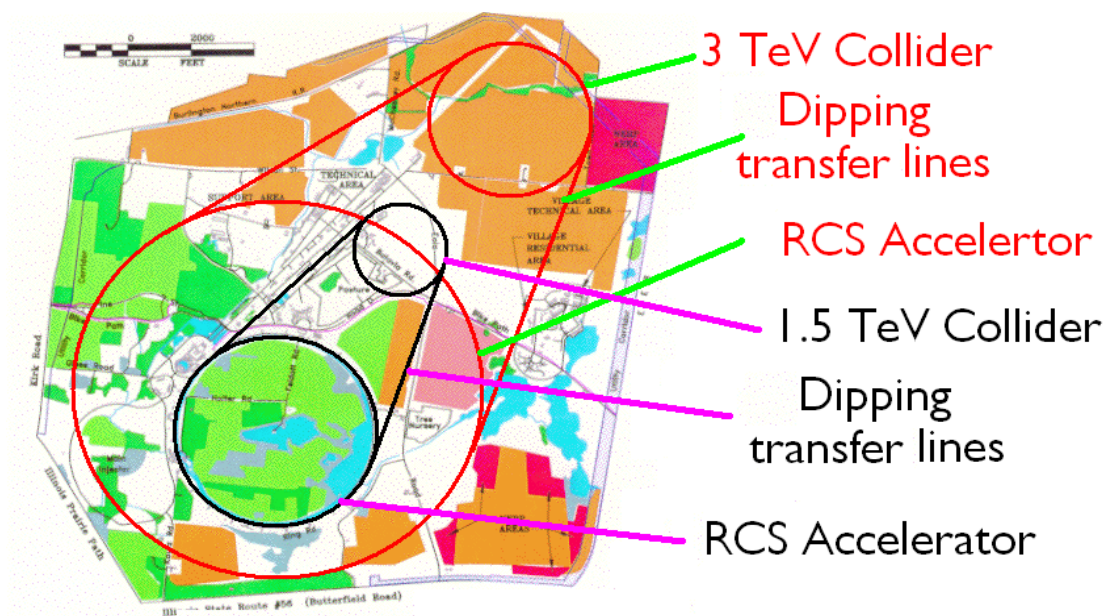
Figure 30: Sizes of 1.5 and 3.0 TeV Muon Colliders relative to FNAL site. Ring sizes are approximately correct, but locations on the site are arbitrary.

There has also been steady progress in component development and experiments:

a) The MERIT mercury target experiment has established that a liquid metal target is a plausible solution for the Muon Collider requirements.

b) The MuCool Test Area now has a proton beam, and tests of RF cavities with high pressure hydrogen in that beam are under way.

c) Magnetic insulation to fix the problem of obtaining the needed RF gradient in a magnetic field has been tested and shown to exhibit an unexpected breakdown mechanism that rules it out as a solution.

d) Tests of beryllium buttons and/or a beryllium-walled cavity, are imminent.

e) The muon beam at MICE has been commissioned.

The estimated performance of a Muon Collider, when compared with the CLIC electron-positron collider, shows:

a) luminosities equal or greater than CLIC's

b) estimated wall power approximately 1/3 of CLIC

c) easier tolerances

d) a much smaller footprint

The greatest challenges presently envisioned are:

a) space charge and other coherent effects in late 6D cooling, and final cooling, where simulations have only now just begun. Coherent effects in acceleration and in the collider ring have not yet been studied and could also be significant.

b) RF breakdown in magnetic fields, where several solutions are being tested;

c) collider ring designs, particularly at 3 TeV, meeting an agreed neutrino-induced radiation criterion, and adequate radiation shielding.

Thus, establishing the feasibility of a Muon Collider is getting closer.

2.2.19 References

1. G. I. Budker, "Accelerators and colliding beams," 7th International Conference on High-Energy Accelerators, Yerevan, USSR, 27 Aug - 2 Sep 1969, p. 33, extracts in AIP Conf. Proc. 352 (1996) 4; G. I. Budker, "Research work on the colliding beams of the Novosibirsk Institute of Nuclear Physics (present state of experiments and perspectives)," 15th International Conference on High Energy Physics, 26 Aug - 4 Sep 1970, Kiev, USSR, p. 1017, extracts in AIP Conf. Proc. 352 (1996) 5.
2. A. N. Skrinsky, "Intersecting storage rings at Novosibirsk," International Seminar on Prospects of High-Energy Physics, Morges, Switzerland, Mar 1971, extracts in AIP Conf. Proc. 352 (1996) 6.
3. Muon Muon Collider: Feasibility Study, Snowmass 1996, BNL-52503, Fermilab Conf.-96/092, LBNL-38946; C. Ankenbrandt *et al.*, "Status of Muon Collider Research and Development and Future Plans", Phys. Rev. ST-AB 2 (1999) 081001.
4. M. Apollonio *et al.*, "Accelerator design concept for future neutrino facilities", J. Inst. 4:P07001, 2009.
5. Y. Alexahin, "Muon collider lattice design status", Muon Collider Workshop, Telluride, CO, June 2011; https://indico.fnal.gov/conferenceOtherViews.py?view=standard&confId=4146
6. R. Palmer *et al.*, "A complete scheme for a muon collider", Proc. COOL 2007, Bad Kreuznach, Germany, p. 77.
7. S. Nagaitsev, "Project X: a new multi-MW proton source at Fermilab", Proc. PAC 2011, New York.
8. G. Flanagan *et al.*, "Using Project X as a proton driver for muon colliders and neutrino factories", Proc. IPAC 2010, Kyoto, Japan, p. 4452.
9. K. McDonald *et al.*, "The MERIT high-power target experiment at the CERN PS", Proc. IPAC 2010, Kyoto, Japan, p. 3527.
10. H. Kirk *et al.*, "A solenoid capture system for a muon collider", Proc. PAC 2011, New York.
11. D. Neuffer *et al.*, "Muon capture in the front end of the IDS neutrino factory", Proc. IPAC 2010, Kyoto, Japan, p. 3500.
12. R. Palmer & R. Fernow, "Charge separation for muon collider cooling", Proc. PAC 2011, New York.
13. A.N. Skrinsky, V.V. Parkhomchuk, "Methods of cooling beams of charged particles", Sov. J. of Nucl. Phys. 12 (1981) 3; D. Neuffer, "Principles and applications of muon cooling", Part. Accel. 14:75, 1983.
14. R. Palmer *et al.*, "Ionization cooling ring for muons", Phys. Rev. ST-AB 8, 061003 (2005).
15. R. Palmer & R. Fernow, "Tapered six-dimensional cooling channel for a muon collider", Proc. PAC 2011, New York.
16. Y. Derbenev & R. P. Johnson, "Six-dimensional muon beam cooling using a homogeneous absorber: concepts, beam dynamics, cooling decrements, and equilibrium emittances in a helical dipole channel", Phys. Rev. ST-AB 8, 041002 (2005).
17. K. Yonehara *et al.*, "A helical cooling channel system for muon colliders", Proc. IPAC 2010, Kyoto, Japan, p. 870.
18. Y. Alexahin, "Circularly inclined solenoid channel for 6D ionization cooling of muons", Proc. PAC 2009, Vancouver, CA, p. 727.
19. A. Garren *et al.*, "6D $\mu\pm$ cooling using a solenoid-dipole ring cooler for a muon collider", Nuc. Instr. Meth. Part. Res. A, to be published.

20. K. Paul *et al.*, "End to end simulation of an inverse cyclotron for muon cooling", Proc. PAC 2011, New York.
21. C. Yoshikawa *et al.*, "Use of a helical channel with large slip factor for bunch recombination", NFMCC technical note 564, May 2011; C. Yoshikawa *et al.*, "Bunch coalescing in a helical channel", NFMCC technical note 566, July 2011; http://nfmcc-docdb.fnal.gov/
22. R. Palmer & R. Fernow, "Six-dimensional bunch merging for muon collider cooling", Proc. PAC 2011, New York.
23. R. Palmer *et al.*, "Muon collider final cooling in 30-50 T solenoids", Proc. PAC 2011, New York.
24. V. Balbekov, "Muon cooling with lithium lenses and high field solenoids", presented at MAP Winter Meeting, 1 March 2011; http://www.jlab.org/conferences/muon2011/program.html
25. J. Maloney *et al.*, "EPIC muon cooling simulations using COSY Infinity", Proc. PAC 2011, New York.
26. S.A. Bogacz *et al.*, "Recirculating linear accelerators for future muon facilities", Proc. IPAC 2010, Kyoto, Japan, p. 3602.
27. D. Summers *et al.*, "Muon acceleration to 750 GeV in the Tevatron tunnel for a 1.5 TeV μ+μ- collider", Proc. PAC 2007, Albuquerque, NM, p. 3178.
28. Y. Alexahin *et al.*, "Conceptual design of the muon collider ring lattice", Proc. IPAC 2010, Kyoto, Japan, p. 1563.
29. B. King, "Potential hazards from neutrino radiation at muon colliders", Proc. PAC 1999, New York, p. 318.
30. Y. Alexahin *et al.*, "Muon collider interaction region design", Phys. Rev. ST-AB 14, 061001 (2011).
31. N. Terentiev, "Vertex and tracker silicon detector hits for MARS/ILCroot simulated beam background in 1.5 TeV muon collider", Muon Collider workshop, Telluride, CO, June 2011; R. Raja, "Towards a compensatable muon collider calorimeter with manageable backgrounds", Muon Collider workshop, Telluride, CO, June 2011; https://indico.fnal.gov/conferenceOtherViews.py?view=standard&confId=4146
32. L. Coney, "Status of the MICE muon ionization cooling experiment", Proc. PAC 2009, Vancouver, CA, p. 1680.
33. J. Norem *et al.*, "Dark current, breakdown, and magnetic field effects in a multicell, 805 MHz cavity", Phys. Rev. ST-AB 6, 072001 (2003); A. Moretti *et al.*, "Effects of high solenoidal magnetic fields on RF accelerating cavities", Phys. Rev. ST-AB 8, 072001 (2005); Y. Torun *et al.*, "The MuCool Test Area and RF program", Proc. IPAC 2010, Kyoto, Japan, p. 3780.
34. P. Hanlet *et al.*, "High pressure RF cavities in magnetic fields", Proc. EPAC 2006, Edinburgh, Scotland, p. 1364.
35. D. Stratakis *et al.*, "Effects of external magnetic fields on the operation of high-gradient accelerating structures", Nuc. Instr. Meth. Phys. Res. A 620 (2010) 147.
36. A. Moretti & Z. Qian, "Box cavity results and plans", MAP Friday Meeting, 30 July 2010; https://indico.fnal.gov/categoryDisplay.py?categId=133
37. A. Hassanein *et al.*, "Effects of surface damage on RF cavity operation", Phys. Rev.ST-AB 9, 062001 (2006); R. Palmer *et al.*, "RF breakdown with external magnetic fields in 201 and 805 MHz cavities", Phys. Rev. ST-AB 12, 031002 (2009).
38. J. Norem, "ALD update", MAP Friday Meeting, 25 March 2011; https://indico.fnal.gov/categoryDisplay.py?categId=133
39. D. Larbalestier, "Prospects for very high field superconducting magnets made from high temperature superconductors", MAP Friday Meeting, 29 January 2010; https://indico.fnal.gov/categoryDisplay.py?categId=133
40. SBIR grant to Particle Beam Lasers, Inc.
41. E. Barzi *et al.*, "YBCO conductors and insert coil technology for high magnetic fields",

MAP Friday Meeting, 13 May 2011;
https://indico.fnal.gov/categoryDisplay.py?categId=133

42. Nikolai Mokhov, **"**MARS simulation of ring energy deposition", Muon Collider Workshop, Telluride, CO, June 2011,

43. https://indico.fnal.gov/conferenceOtherViews.py?view=standard&confId=4146

44. S. Ishimoto *et al.*, "Liquid hydrogen absorber for MICE", Proc. IPAC 2010, Kyoto, Japan, p. 421.

3 Accelerator R&D towards a Neutrino Factory and Muon Collider

3.1 The International Design Study for the Neutrino Factory

J. Scott Berg

Brookhaven National Laboratory; P.O. Box 5000; UPTON NY 11973-5000, USA

A. Blondel

University de Geneve, 24, Quai Ernest-Ansermet, 1211 Geneva 4, Suisse

A. Bross, J. Morfin

Fermi National Laboratory, P.O. Box 500, Batavia, IL 60510-5011, USA

K. Long, Jürgen Pozimski

Imperial College London; South Kensington Campus; London SW7 2AZ; UK

P. Soler

School of Physics and Astronomy, Kelvin Building, University of Glasgow, Glasgow G12 8QQ, Scotland, UK

R. Tsenov

Department of Atomic Physics, St. Kliment Ohridski, University of Sofia, 5 James Bourchier Boulevard, BG-1164 Sofia, Bulgaria

M. Zisman

Lawrence Berkeley National Laboratory, 1 Cyclotron Road, Berkeley, CA 94720, USA

On behalf of the IDS-NF collaboration

Mail to: jsberg@bnl.gov

3.1.1 Introduction

The phenomenon of neutrino oscillations, arguably the most significant advance in particle physics over the past decade, has been established through measurements on neutrinos and anti-neutrinos produced in the sun, by cosmic-ray interactions, in nuclear reactors, and using beams produced by high-energy particle accelerators [1]. In consequence, we know that the Standard Model is incomplete and must be extended to include neutrino mass, mixing among the three neutrino flavors, and therefore lepton-flavor non-conservation. These observations have profound implications for the ultimate

theory of particle interactions and for the description of the structure and evolution of the Universe. In particular:

- Mixing among the three massive neutrinos admits the possibility that the matter-antimatter (CP) symmetry is violated via the neutrino-mixing matrix;
- If a neutrino is to be distinguished from its antineutrino counterpart it is necessary to assign a conserved "lepton number" to the neutrino. At present there is no theoretical justification for such a conserved quantum number. If lepton number is not conserved, then a neutrino is indistinguishable from an antineutrino, i.e. the neutrino is a Majorana particle; a completely new state of matter; and
- The neutrino abundance in the Universe is second only to that of the photon and so, even with a tiny mass, the neutrino may make a significant contribution to the dark matter which is known to exist. Therefore, the neutrino may play an important role in determining the structure of the Universe.

These exciting possibilities justify an energetic and far-reaching program.

3.1.1.1 *The Neutrino Factory*

In the Neutrino Factory, beams of electron and (anti-) muon-neutrinos are produced from the decay of muons circulating in a storage ring. As the muon charge-to-mass ratio is large, the neutrinos carry away a substantial fraction of the energy of the parent muon, hence, high neutrino energies can readily be achieved. Time dilation is beneficial, allowing sufficient time to produce a pure, collimated beam. Charged-current interactions induced by "golden channel," $\nu_e \rightarrow \nu_\mu$, oscillations produce muons of charge opposite to those produced by the anti-muon neutrinos in the beam and thus a magnetized detector is required. The additional capability to investigate the "silver" ($\nu_e \rightarrow \nu_\tau$) and "platinum" ($\nu_\mu \rightarrow \nu_e$) channels makes the Neutrino Factory the ideal place to look for oscillation phenomena that are outside the standard, three-neutrino-mixing paradigm. It is thus the ideal facility to serve the precision era of neutrino oscillation measurements.

The baseline specification for the Neutrino Factory, developed within the International Design Study for the Neutrino Factory (the IDS-NF), has been optimized for the discovery of CP-invariance violation, the determination of the mass hierarchy, and the determination of θ_{13} [2]. The optimum requires two distant detectors, one at the "magic baseline," 7000–8000 km, the second at a source-detector distance in the range 2500–5000 km. The sensitivity to non-standard interactions improves as the stored-muon energy is increased, reaching a plateau at around 25 GeV [3]. A baseline stored muon energy of 25 GeV has therefore been adopted. The baseline accelerator facility provides a total of 10^{21} muon decays per year split between the two distant neutrino detectors.

The performance of the IDS-NF baseline in terms of the 3σ discovery reach for CP violation, the mass hierarchy, and θ_{13} is shown in Fig. 1. The discovery reach is presented in terms of the fraction of all possible values of δ (the "CP fraction") and plotted as a function of $\sin^2 2\theta_{13}$. The discovery reach of the Neutrino Factory is significantly better than realistic alternative facilities, particularly for small values of θ_{13}. Recent results hint that θ_{13} may be large, i.e., close to the present upper bound [4]. In this case, a re-optimization of the baseline Neutrino Factory will still yield superior

56

performance. As an example, Fig. 1 shows the performance that may be obtained with 10 GeV stored muons illuminating a detector at a distance of 2000 km from the source.
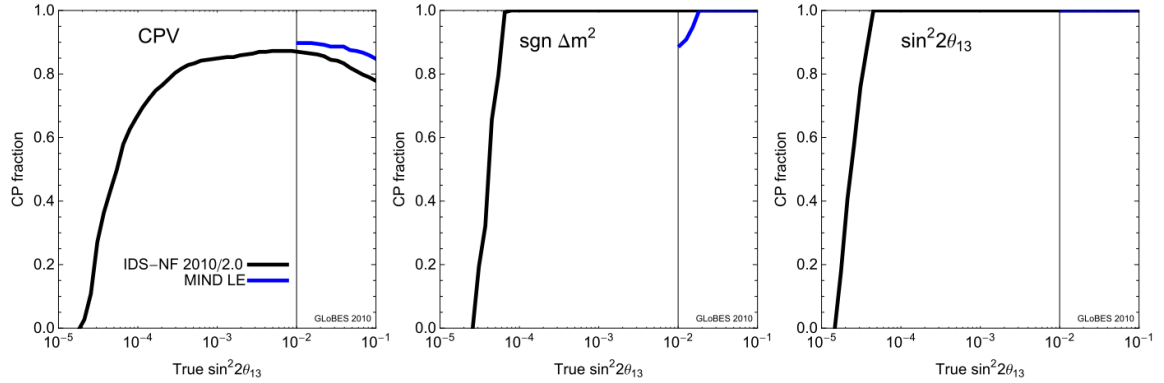
Figure 1: The discovery potential at 3σ for CP violation (left panel), the mass hierarchy (central panel), and $\sin^2 2\theta_{13}$ (right panel). The discovery reach is plotted in terms of the CP fraction as a function of $\sin^2 2\theta_{13}$. The performance of the IDS-NF baseline is shown as the black solid line. The Neutrino Factory re-optimized for large $\sin^2 2\theta_{13}$ is shown as the blue solid line.

3.1.2 Layout and Components of the Neutrino Factory Accelerator Complex

A schematic diagram of the Neutrino Factory accelerator facility is shown in Fig. 2. Muons are produced by bombarding a target with protons, resulting in the production of pions, which decay to muons. Pions and muons of both signs are captured and focused in a high-field solenoid channel designed to maximize the number of muons transported to the muon storage ring.

The captured muons have a large energy spread and a large transverse emittance, both of which need to be reduced so that the beam can be accelerated efficiently. This is accomplished by turning a single, large-emittance bunch into a train of bunches each with a small emittance. The bunches initially have different energies spanning the range that the muons had before bunching. Phase rotation is therefore employed to give all the bunches the same mean energy and a reasonable energy spread. The transverse emittance of the bunch train is then reduced using ionization cooling.

Table 1: Parameters characterizing the muon beam produced by the accelerator facility. Muon decays are a total for all signs and detector baselines.

Parameter	Value
Muon total energy [GeV]	25
Production straight muon decays in 10^7 s	10^{21}
Maximum RMS angular divergence of muons in production straight	$0.1/\gamma$
Distance to intermediate baseline detector [km]	3000–5000
Distance to long baseline detector [km]	7000–8000
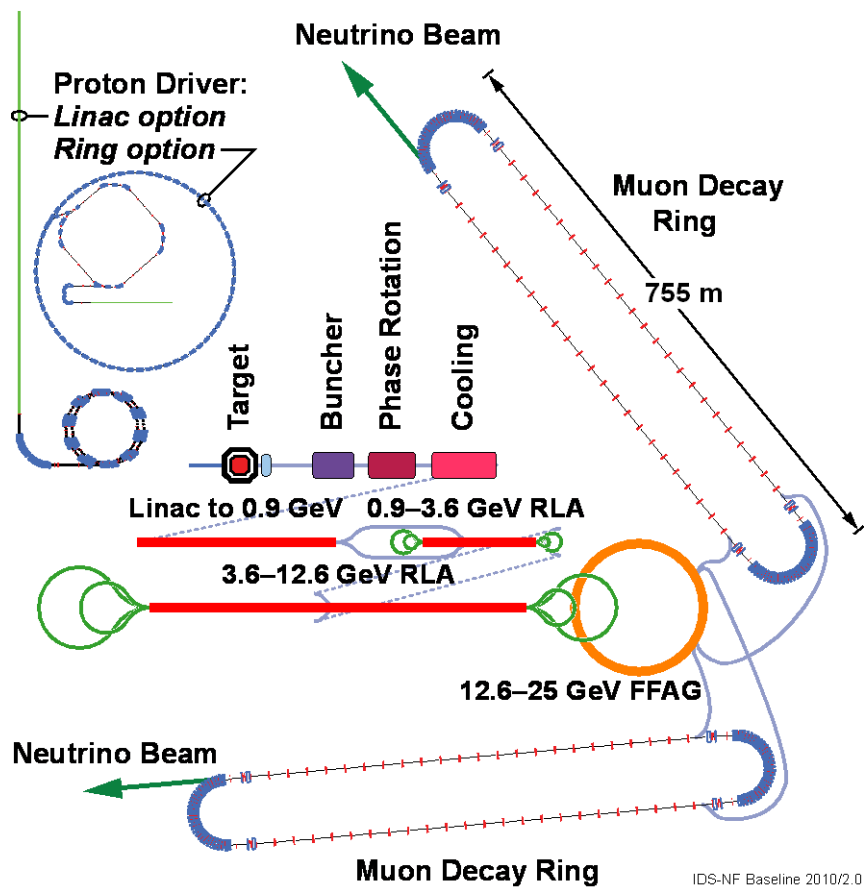
Figure 2: Layout of the IDS-NF Accelerator Systems.

After the beam has a more reasonable emittance, it is accelerated to the final energy. To keep the efficiency of acceleration high, different acceleration schemes are used in different energy ranges. The first stage of acceleration is performed using a linac because the large transverse emittance and the variation of velocity with energy make it impractical to recirculate the low-energy beam through the cavities. The linac is followed by two recirculating linear accelerators, in each of which the beam makes multiple passes through the accelerating structures. The final stage of acceleration is performed using a linear non-scaling fixed-field alternating-gradient accelerator, which allows many more passes through the cavities.

Finally the beam is injected into two racetrack-shaped decay rings, the straight sections of which are pointed at the two distant detectors. The rings have very long straight sections to ensure that a large fraction of the muons are moving toward the detector when they decay.

3.1.2.1 *Proton Driver*

At the start of the accelerator chain, a proton driver capable of delivering an average power of 4 MW is required. Several boundary conditions define the proton beam parameters necessary to produce the desired number of muons in the storage rings of the Neutrino Factory (see Table 2). The proton-beam energy must be in the multi-GeV range in order to maximize the pion production. In addition, the Neutrino Factory requires a particular time structure consisting of 3 very short bunches separated by

120 μs. The short bunch length of 1–3 ns rms is dictated by the efficiency of the muon-beam capture and the bunch separation is constrained by beam loading in the downstream muon accelerator and the recovery time of the mercury-jet target.

Table 2: Parameters characterizing the proton beam parameters.

Parameter	*Value*
Proton beam energy [GeV]	5–15
Average beam power on target [MW]	4
Repetition rate [Hz]	50
Pulse duration [ns]	1–3
Bunches per 50 Hz cycle	3
Bunch separation [μs]	120

In order to achieve such short bunches, a dedicated bunch compression scenario needs to be designed carefully in order to deal with very strong space-charge forces. Several proton driver schemes fulfilling these requirements have been proposed (see Fig. 2).

In the CERN Neutrino Factory scenario [5], which would be based on the proposed 5 GeV high-power version of the Superconducting Proton Linac (SPL) [6] and be able to deliver 10^{14} protons at a repetition rate of 50 Hz. The chopped beam from the SPL would be injected into an isochronous accumulator ring in which 120 ns long bunches are formed without the need for an RF system. The beam parameters after accumulation are obtained as a compromise between the competing requirements of minimizing the heating of the injection foil, maximizing the aperture, and adequate compensation of the space-charge forces. The beam parameters are set to allow for RF phase-rotation in the downstream compressor ring. The size of the two rings is determined by the requirement that successive bunches must arrive at the correct location in the compressor ring. The compressor ring has a large phase-slip factor, which is needed for fast phase rotation. The most recent design of the SPL and more details of the CERN proton driver scenario can be found in [7, 8].

A proton driver for a Neutrino Factory situated at Fermilab [9] would be based on an upgrade of the proposed Project X linac. Fermilab is currently designing a high intensity proton source that will deliver beam at 3 GeV and at 8 GeV and is designed such that it can be upgraded to deliver the full beam power (4 MW at 8 GeV) required for the Neutrino Factory. Just as in the CERN scheme, additional accumulator and compressor rings will be needed to provide the correct time structure. At injection into the accumulation ring there will be a stripping system, foil or laser based, to convert the H^- ions to protons. The front end of Project X will have a programmable chopper so that beam will be injected into three RF buckets in the accumulation ring. After injection is complete, the RF bucket voltage will be increased to shorten the bunches. The accumulated protons will then be transferred to a separate bunch-shortening (compressor) ring. Bunch rotation will be used to achieve the final bunch length (2 ns). The three bunches will be extracted with the proper spacing (120 μs). The accumulation, bunch shortening, and targeting will be done at 50 Hz, as required for the Neutrino Factory. Project X will be located within the Tevatron ring at Fermilab.

A Neutrino Factory sited at the Rutherford Appleton Laboratory (RAL) [10] would be served by a proton driver based on an upgrade to the ISIS pulsed-proton source. A

common proton driver for the spallation neutron source and the Neutrino Factory is proposed in the framework of the ongoing ISIS megawatt-upgrade program. In such a scenario, the proton drivers for both facilities would share the same source, chopper, linac, accumulator, and acceleration up to 3.2 GeV. After extraction, a number of bunches would be sent directly to the neutron-spallation target while three others would be injected into a second RCS where, after acceleration to somewhere between 6.4 GeV and 10.3 GeV followed by bunch compression, the beam would be extracted towards the Neutrino Factory pion-production target. For the ISIS megawatt upgrade to be compatible with the Neutrino Factory, an 800 MeV H^- linac has been designed, candidate lattices for the 3.2 GeV booster RCS have been identified, and preliminary parameters for the final RCS ring have been proposed.

3.1.2.2   *Target*

The proton beam will be brought into collision with a target, producing pions that decay into muons. Since a solid target is likely to be damaged by a proton beam of the intensities that are required, a liquid-mercury-jet target has been chosen as the baseline. For the high proton-beam energies under consideration, a target material with high atomic number is preferred.

The target must operate in a high magnetic field to maximize the capture of the pions, which are emitted with a large transverse momentum. Extensive studies of the target have been performed to find the optimal proton-beam energy and target-station geometry [2]. These parameters have determined the specification of the proton beam energy and emittance. The mercury jet must have sufficient velocity for the mercury target to be reformed between proton beam pulses. The resulting parameters for the jet are given in Table 3, and a diagram of the target region is shown in Fig. 3.

Table 3: Parameters of the mercury jet target.

Parameter	*Value*
Jet diameter [mm]	8
Jet velocity [m/s]	20
Jet/solenoid axis angle [mrad]	96
Proton beam/solenoid axis angle [mrad]	96
Proton beam/jet angle [mrad]	27
Solenoid field at target/jet crossing [T]	20
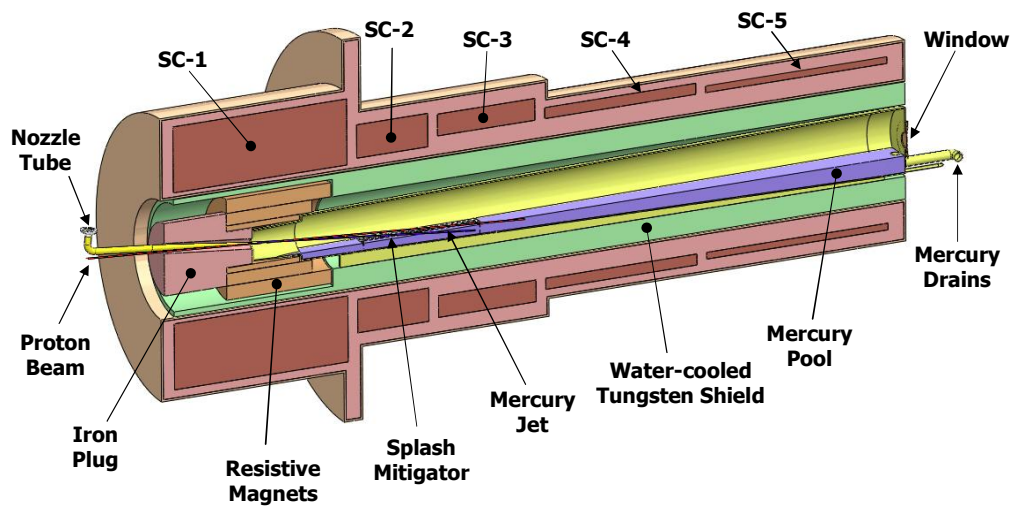
Figure 3: Cross-section of target region as envisioned in the IDR, showing the outer superconducting coils (SC-*n*), inner resistive solenoids, shielding, and portions of the mercury handling system.
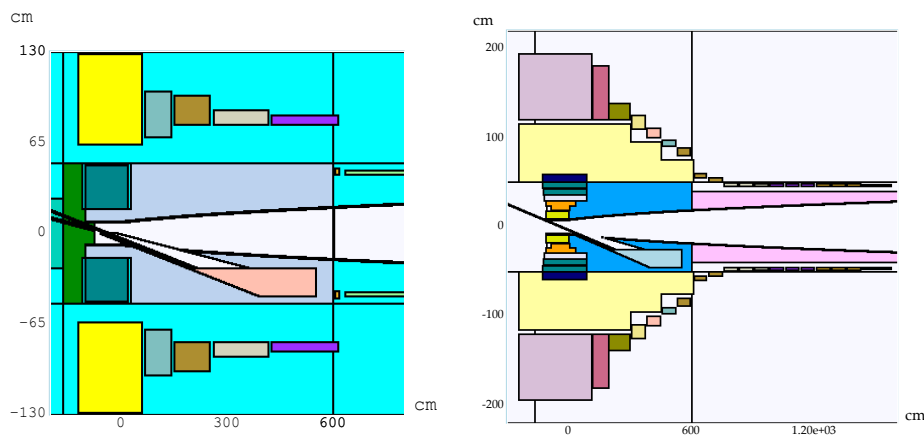
Figure 4: Target geometry from the IDS-NF (left), and a recent version of the improved target geometry (right). Note the differing scales (magnets corresponding to the downstream magnets in the right-hand figure are not shown in the left-hand figure). The inner radius of the solenoids has increased from 65 cm to 120 cm, and additional shielding has been added in the region between the inner warm and outer superconducting coils.

The biggest challenge in the design of the target is to achieve the high magnetic fields required in a region in which the radiation-dose is very high. The large magnetic field is reached using a 14 T superconducting coil outside a 6 T copper insert. A series of superconducting magnets downstream from the target/beam crossing serves to reduce the field, thereby reducing the beam divergence and transporting the beam to the muon front end. There must be sufficient shielding in front of the superconducting magnets to keep the cryogenic loads manageable and to prevent the coils from quenching from the instantaneous energy deposition. A revision to the IDS-NF baseline target station geometry is being prepared in which additional shielding is introduced at the expense of larger solenoids. The result of a recent study of the revised shielding is compared to the baseline in Fig. 4.

3.1.2.3 *Muon Front End*

The Neutrino Factory muon front end consists of a pion decay channel and longitudinal drift, followed by an adiabatic buncher, phase-rotation system, and ionization-cooling channel. It is designed to optimize the number of muons that can be transmitted through the downstream accelerator complex. The present design is based on the lattice presented in the Neutrino Factory Study 2A report [11] and subsequently developed in the ISS [12] with several modifications: the taper from the target solenoid has been adjusted; the solenoid-field strength in the drift, buncher, and phase rotation sections has been reduced from 1.75 T to 1.5 T; the whole system has been shortened; and the thickness of the lithium-hydride absorbers in the cooling section has been increased. These changes result in the same muon-capture performance in a shorter bunch train, reducing requirements on some systems downstream of the muon front end.

Downstream of the target solenoid, the magnetic field is adiabatically reduced from 20 T to 1.5 T over a distance of 15 m to capture a secondary-pion beam with a large energy spread. As the initial proton bunch and subsequently the pion bunch is relatively short in time, the pions and their daughter muons develop a position-energy correlation in the decay channel as required for the following sections of the muon front end. The drift channel is followed by a buncher section that uses RF cavities to form the muon beam into a train of bunches and a phase-energy rotating section that decelerates the leading high-energy bunches and accelerates the late, low-energy bunches, so that each bunch has the same mean energy.

Buncher

The IDS-NF baseline design delivers a bunch train that is less than 80 m long, a significant improvement over the ISS-design which delivered a 120 m long bunch train containing the same number of muons. A shorter bunch train will help to ease the challenging kicker requirements for the muon FFAG and decay rings, and may allow the decay rings to be made shorter. For the present design, to capture particles around a reference momentum of $p_0 = 233$ MeV/c, with the intent of capturing muons from an initial kinetic energy range of 50 MeV to 400 MeV, the buncher length is 31.5 m. With these parameters, the RF cavities decrease in frequency from 320 MHz to 230 MHz over the length of the buncher. The initial geometry for the placement of the RF cavities uses $0.4 - 0.5$ m long cavities placed within 0.75 m long cells. The 1.5 T solenoid focusing of the decay region is continued through the buncher and the rotator section that follows. The linear ramp of cavity frequency that is required theoretically is approximated by a sequence of RF cavities that decrease in frequency along the 33 m beam transport allotted to the buncher. The number of different RF frequencies is limited to a manageable 13 and the linear ramp in gradient is approximated by the placement and gradient of the cavities in the buncher. Table 4 shows a summary of the RF cavities that are needed in the buncher, rotator, and cooling sections.

Table 4: Summary of front-end RF requirements.

	Length [m]	Number of cavities	Frequencies [MHz]	Number of frequencies	E_{peak} [MV/m]	P_{peak}
Buncher	33	37	319.6–233.6	13	4 to 7.5	1-3.5 MW/freq.
Rotator	42	56	230.2–202.3	15	12	2.5 MW / cav.
Cooler	75	100	201.25	1	15	4 MW / cav.
Total	**150**	**193**	**319.6–201.25**	**29**		**562 MW**

Rotator

In the rotator section, the RF bunch-spacing between the reference particles in each bunch is shifted away from the integer and phased such that the high-energy reference particle is stationary and the low-energy one is uniformly accelerated to arrive at the same energy as the first reference particle at the end of the rotator. This is accomplished using an RF gradient of 12 MV/m in 0.5 m long RF cavities within 0.75 m long cells (Fig. 5). The RF frequency decreases from 230.2 MHz to 202.3 MHz in steps by grouping adjacent sets of cavities into the same RF frequency. The 42 m long RF rotator then contains 56 RF cavities grouped into 15 frequencies. At the end of the rotator, the RF frequency reaches that of the ionization cooling channel (201.25 MHz). The average momentum at the rotator is 230 MeV/c.
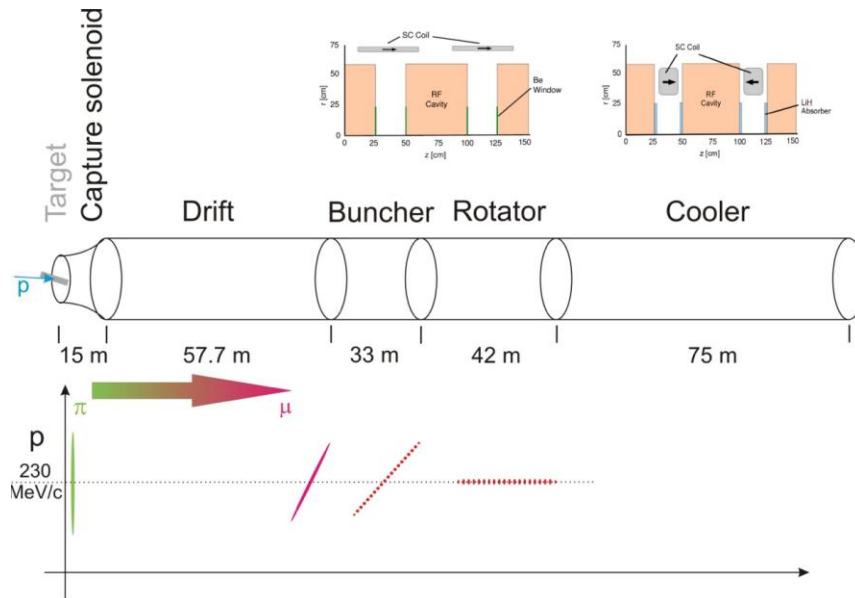
Figure 5: Schematic overview of the muon front end. The lattice design of the Buncher, Rotator and Cooler are shown in the top row, while the bottom row shows the development of the particle burst into a bunch train within the front end.

Cooler

The baseline cooling-channel design consists of a sequence of identical 1.5 m long cells (Fig. 6). Each cell contains two, 0.5-m-long RF cavities, with 1.1 cm thick lithium hydride (LiH) discs at the ends of each cavity (4 per cell), and a 0.25 m spacing between cavities. The LiH discs provide the energy-loss material for ionization cooling. The

cells contain two solenoid coils with opposite polarity, which produce an approximately sinusoidal variation of the magnetic field in the channel with a peak value on-axis of 2.8 T, providing transverse focusing with $\beta_\perp = 0.8$ m.
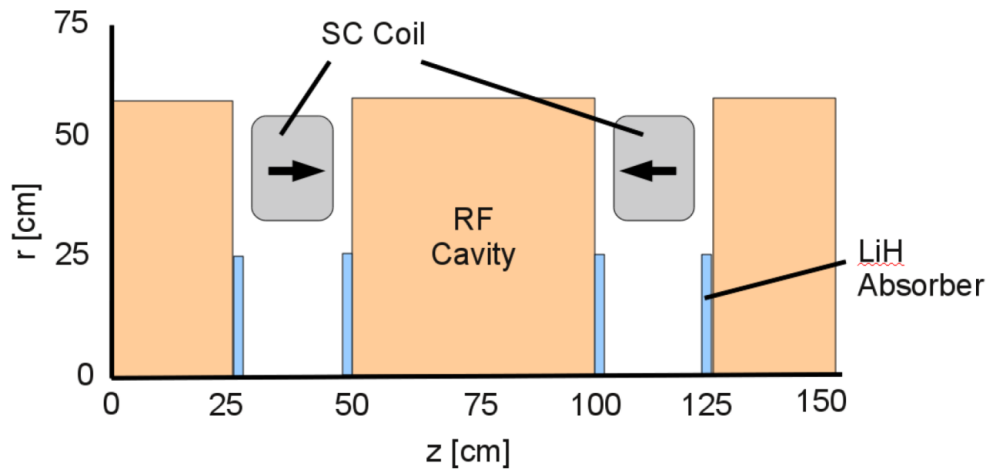
Figure 6: Schematic diagram of one cell of the ionization cooling lattice.

Two independently-developed codes have been used for tracking simulations of the muon front end by the Monte Carlo method: ICOOL version 3.20; and G4beamline version 2.06. Both codes use semi-analytic procedures to compute electromagnetic fields. Good agreement is shown in the muon yield from the two codes (see Fig. 7). The input beam for both simulations has been generated using MARS 15.07. The effect of the cooling can be measured by counting the number of simulated particles that fall within a reference acceptance that approximates the expected acceptance of the downstream accelerator. Using the output from our reoptimized buncher and rotator, we have tracked particles through the cooling channel, and obtain, within the reference acceptances, 0.19 muon per 8 GeV incident proton.
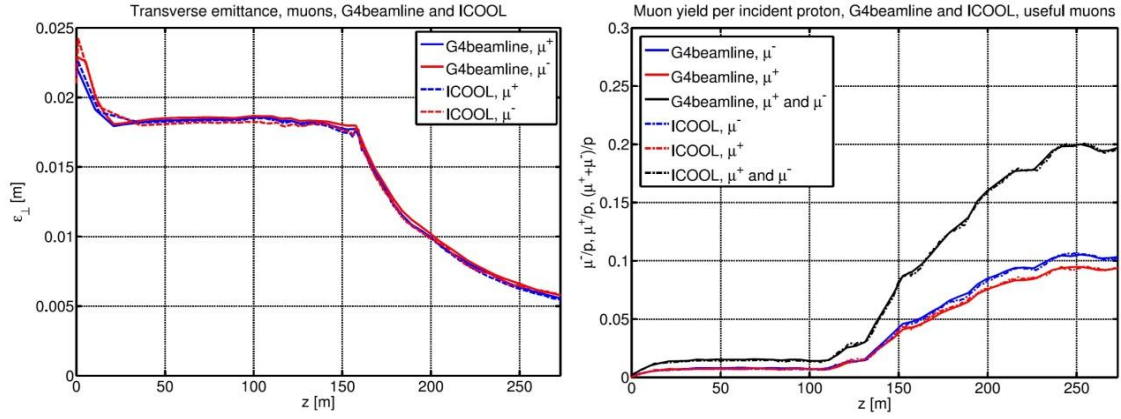
Figure 7: Performance of the bunching and cooling channel as a function of distance along the channel simulated using the ICOOL and the G4beamline codes. Left: The evolution of transverse emittance (computed over all bunches). Right: The evolution of the number of muons within a reference acceptance. The cooling section starts at $s = 155$ m, where the rms transverse emittance is 0.018 m and 0.08 μ per proton are in the reference acceptance.

The performance of the bunching and phase rotation channel, along with the subsequent cooling channel, is displayed in Fig. 7, which shows, as a function of the distance down the channel, the number of muons within a reference acceptance. The phase rotation increases the number of "accepted" muons by a factor of four. A critical feature of the muon production, collection, bunching, and phase rotation systems is that together they produce bunches of both signs (μ^+ and μ^-) at roughly equal intensities. This occurs because the focusing systems are solenoids, which focus both signs, and the RF systems have stable acceleration for both signs, separated by a phase difference of π. The Neutrino Factory muon front end captures a substantial proportion of the muons produced by the Neutrino Factory target. Longitudinal capture is achieved using a buncher and energy-time phase-rotation system, while transverse capture is achieved using a high-field solenoid adiabatically tapered to 1.5 T and is enhanced by ionization cooling. Overall, the muon front end increases the capture rate of muons in the nominal accelerator acceptance by a factor 10.

Front-end RF

The requirements for the normal-conducting RF cavities in the muon front end are summarized in Table 4. The cavities are 50 cm long with peak field gradients in the range 4 MV/m to 15 MV/m, with the highest voltage required for the 201 MHz cavities. Empirical evidence suggests that magnetic fields overlapping RF cavities, as present in the muon front end, may induce breakdown in the cavities [13, 14]. Simulations of the performance of the muon front end using a reduced field have shown that only if the achievable RF gradient falls dramatically below the nominal value, is there a significant effect on muon transmission. In order to mitigate this technical risk, several alternative lattices have been developed (see reference [2]).

Front-end Magnets

The 1.5 T solenoids for buncher and rotator must accommodate the beam pipe, with a 30 cm radius and must also accommodate RF cavities with radii of 60 cm. This can be achieved using coils with an inner radius of 68 cm and a conductor radial thickness

of 4 cm, so that the cavities fit entirely within the coils. A coil length of 50 cm spaced at 75 cm intervals leaves a gap of 25 cm between the coils, matching the periodicity of the cooling channel and enabling access for room temperature services such as vacuum and RF power feeds. The required current for these coils is 47.5 A/mm^2 to give a total current of 0.95 MA-turns. The coils are therefore large enough to accommodate the beam pipe, RF and diagnostics, and shielding. A smaller radius could be used in the first 60 m, where there is no RF. The 135 m transport requires 180 such magnets. The cooling system requires strong alternating-sign coils that are placed between RF cavities. These coils (see Table 5) produce an on-axis solenoid field that varies from +2.8 T to −2.8 T over a 1.5 m period, following an approximately sinusoidal dependence. Maximum fields in the cooling cell volume are 5 T near the coil surfaces; 100 such coils are needed in an 80 m cooling system.

Table 5: Summary of front-end magnet requirements.

	Length [m]	Inner radius [m]	Radial thickness [m]	Current density [A/ mm^2]	Number
Initial transport	0.5	0.68	0.04	47.5	180
Cooling channel	0.15	0.35	0.15	±107	100

There are significant particle losses along the beam line and these will result in a large energy deposition in the superconducting magnets and other equipment. Two main risks have been identified: energy deposition by all particles may cause superconducting equipment to quench; and energy deposition by hadrons and other particles may activate equipment, preventing hands-on maintenance. In currently operating accelerators, uncontrolled hadronic losses must be less than ≈1 W/m to allow "hands-on" maintenance without additional time, distance, or shielding constraints. Magnets are expected to quench with beam losses above a few tens of W/cm^3. Several schemes are envisaged to control the beam losses and reduce them below these values. Particles with a high momentum, outside of the acceptance of the front end, can be removed using a pair of chicanes, where dispersion is induced in the beam by means of tilted solenoids and high-momentum particles are passed onto a beam dump. The chicane would be followed by a proton absorber removing low momentum protons taking advantage of the different stopping distance of protons compared with other particles in material. Additionally, particles with transverse amplitude outside of the acceptance of the front end may be removed using transverse collimators.

3.1.2.4 *Acceleration*

The muon beam must be accelerated from a total energy of 244 MeV to 25 GeV. This is made more challenging by the large transverse and longitudinal emittances of the beam. Acceleration will be performed in four stages with three different types of accelerators, each chosen to give the best efficiency for its energy range. Throughout the system, 201.25 MHz superconducting RF cavities will be used to accelerate the beam. Tables 6 and 7 give the parameters for the acceleration system, while Fig. 8 shows a conceptual layout of the acceleration systems.

Table 6: Overall parameters for the acceleration system.

Parameter	Value
Initial total energy [MeV]	244
Final total energy [GeV]	25
Normalized transverse acceptance [mm]	30
Normalized longitudinal acceptance [mm]	150
RF frequency [MHz]	201.25
Maximum RF gradient [MV/m]	17

Table 7: Parameters for acceleration stages

Type	Linac	RLA	RLA	FFAG
Min. total energy [GeV]	0.244	0.9	3.6	12.6
Max. total energy [GeV]	0.9	3.6	12.6	25
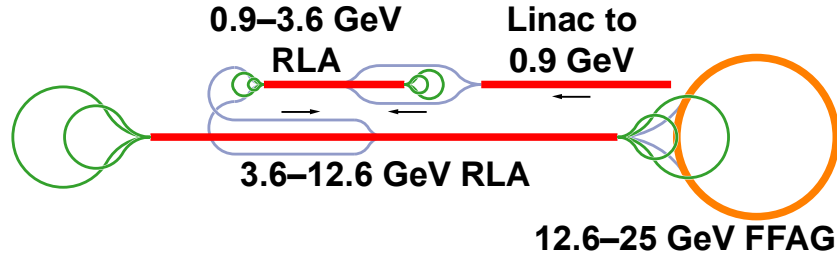
Figure 8: Structure of the acceleration systems.

Linac

A rough measure of the efficiency of acceleration is the number of passes that the beam makes through an RF cavity. However, due to the beam's large emittance and energy spread, as well as its significant velocity variation with energy, recirculating the beam through the RF cavities at the lowest energies would be impractical, resulting in excessive beam loss and emittance growth. Thus, acceleration begins with a linac. The linac consists of three types of cells (shown in Fig. 9), which increase in length and add more RF voltage per cell as the beam accelerates and the transverse geometric emittance decreases. Acceleration starts far off-crest to capture the large longitudinal emittance, then the RF phase moves approximately linearly with length to the crest by the end of the linac.

To improve the transverse acceptance of the linac, we are in the process of re-designing the linac to use only the first two types of cells, with larger aperture cavities for the later cells having a gradient of 15 MV/m.

RLAs

Once the muon beam has reached a sufficiently high energy (0.9 GeV), two recirculating linear accelerators (RLAs) are used. The first RLA raises the beam energy to 3.6 GeV, the second takes the beam energy to 12.6 GeV. Both RLAs include a

number of arcs, each designed to return muons of a particular energy to the linac at the appropriate phase, allowing the beam to make 4.5 passes through the accelerating structures. A dog-bone geometry has been chosen for the RLAs since it gives better beam separation at the switchyard for a given energy gain in the linac, allowing a larger number of passes through the linac. The beam is injected into the center of the linac to reduce the RF phase mismatch resulting from the velocity variation of the beam as it is accelerated.

The switchyard and arc crossings in the RLAs are particularly challenging due to the large beam emittances. To simplify these sections, provide additional space between beam lines, and simplify the matching between the linac and the arcs, the designs presented in the IDR will be updated. Chicanes injecting into the RLA linacs will be re-designed to add more space. The arcs will be re-designed to match into the linacs better: the ordering of magnets will change (defocusing quadrupoles at the ends), and the cell lengths will be made comparable to the linac cell lengths. The arc crossings will be re-designed to avoid changing the vertical height unnecessarily. The linac quadrupole strengths will also be adjusted to use a beta-beat to improve the matching into the arcs.

FFAG

The final acceleration stage will use a non-scaling fixed-field alternating-gradient (FFAG) accelerator. This machine has a single arc with a very wide energy acceptance, allowing the beam to accelerate over its full range in the same arc. This avoids the switchyard in the RLAs which limits the number of passes through the cavities. The lattice consists of nearly identical triplet cells, with RF cavities in most of the long drifts. Table 8 summarizes the important parameters of the ring.
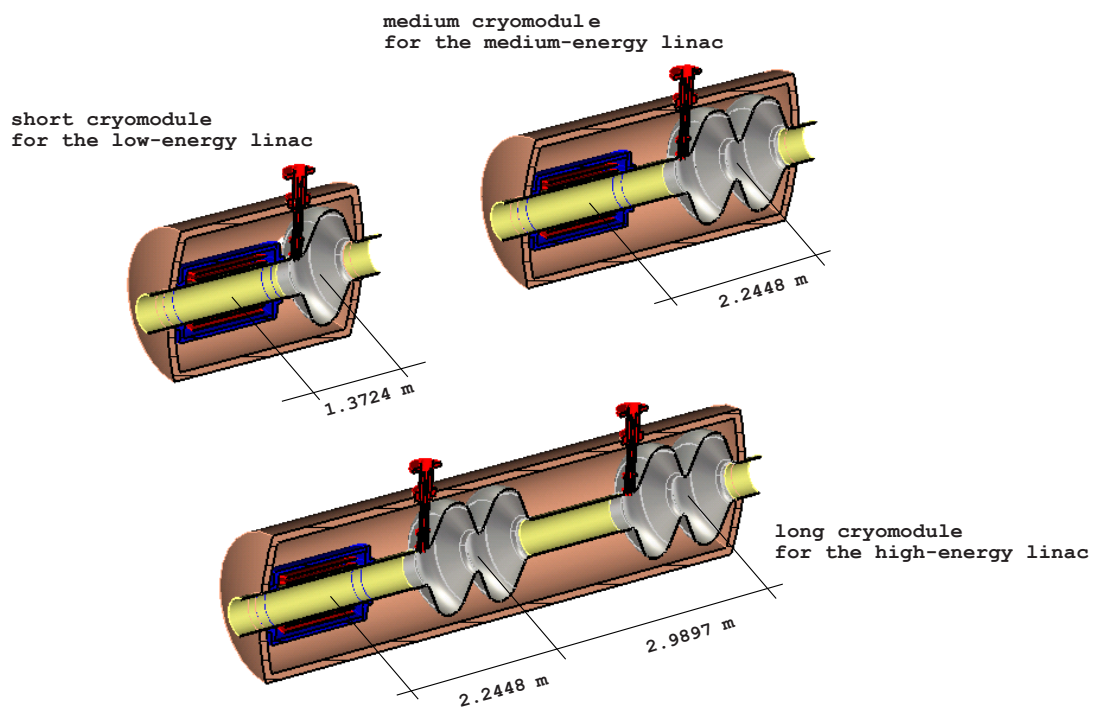
Figure 9: Different modules in the linac.

Table 8: Parameters of the FFAG ring.

Parameter	Value	
Cells	64	
Circumference [m]	667	
RF cavities	48	
On-crest energy gain per cavity [MeV]	25.5	
Quadrupoles	D	F
Length [m]	2.3	1.1
Aperture radius [mm]	137	163
Maximum field [T]	6.1	4.3

The most challenging parts of the FFAG lattice are the insertions for injection and extraction. The required magnet aperture is large, the kicker rise/fall time must be short and the beam energy is relatively high. In addition, since three beam pulses arrive in rapid succession, there must be three separate pulse-forming networks for each kicker. The parameters of the kicker magnets are given in Table 9.

Table 9: Parameters for kicker magnets in the FFAG. "Pattern" gives the arrangement of kickers in successive cells: − means an inward kick, + means an outward kick, and ○ means an empty drift. There are septa in the cells adjacent to the two end kickers. Each system injects or extracts both muon beam signs simultaneously.

Parameter	Injection	Extraction
Kickers	2	4
Pattern	−○−	++○○++
Kicker field [T]	0.089	0.067
Septum field [T]	0.92	1.76
Kicker/septum length [m]	4.4	4.4

3.1.2.5   *Muon Storage Rings*

Intense bursts of neutrinos and anti-neutrinos are generated by the decays of the muon bunches in long straight sections in dedicated storage rings. The neutrinos are directed through the Earth to detectors at distances of between 2500 km and 5000 km and between 7000 km and 8000 km at angles to the surface of ~18° and ~36°, respectively.

Different geometries of storage rings [2] have been studied, of which the most flexible are based on race-track lattices (Fig. 10), which are built to point towards the two neutrino detectors. The return straight can be used for collimation, RF and tune control. An alternative is a triangular lattice with two production straights that can be pointed in different directions and so send neutrinos to combinations of detectors.

Based on the proton driver described above, a decay ring of 1.6 km in circumference can accommodate the equally-spaced, 250 ns long bunch trains and can allow time intervals of at least 100 ns between the neutrino bursts. The production straights for the race-track design are 600.2 m long, giving an efficiency of 37.5% and the tunnel depth for the far detector ring of this size is 444 m. To keep the neutrino beams reasonably well focused, the muon beam's rms divergence angle should not add more than about

10% to the natural $1/\gamma$ angle of the decay cone, implying large β–functions (~150 m) in the long production straights. Matching these β–functions to values of ~14 m in the arcs (chosen to reduce the size of the beam and maximize transmission) is accomplished by dedicated matching sections at the end of each straight, which also eliminate the high dispersion in the arcs. A detailed description of the decay ring lattice can be found in [2]. Simulations of the race-track decay ring using the code Zgoubi [15] prove that the neutrino angular distribution will meet the Neutrino Factory requirements. Additional simulations showed that, assuming the predicted energy spread of the muons is achieved, the bunches in the bunch train will not merge sooner than twice the lifetime of the muons, so no RF need be installed in the decay ring.

Studies of the beam instrumentation in the decay ring—essential for the correct prediction of the expected neutrino flux at the far detector—have been performed [2]. To measure the muon divergence, systems utilizing Cherenkov radiation and optical transition radiation have been considered. The muon beam energy can be monitored by spin-polarization measurements. An efficient collimation system must be developed to cope with the high muon-beam power along with a beam injection system able to cope with large beams with the short time-gaps between the bunch trains.
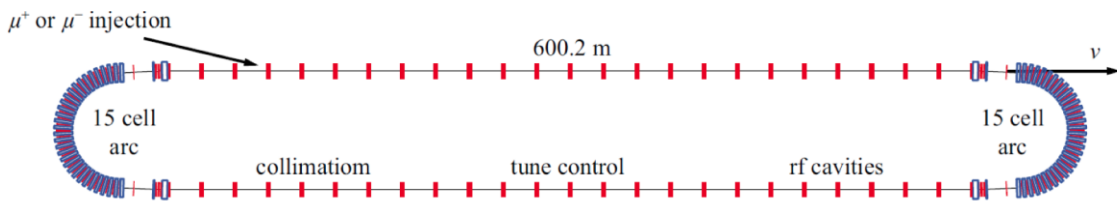
Figure 10: Race-track design for the Neutrino factory storage rings.

3.1.3 The Neutrino Detectors

The IDS-NF baseline for the Neutrino Factory includes having two Magnetized Iron Neutrino Detectors (MINDs), one with a fiducial mass of 100 kton at ~4000 km and another with a fiducial mass 50 kton at ~7500 km (the "magic baseline") [2]. The detector is optimized to carry out the detection of the "golden channel" through the wrong-sign muon signature. This strategy is more efficient for resolving degeneracies in the neutrino-oscillation formulae and provides better sensitivity than, for example, measuring the golden and the "silver" channel simultaneously.

The baseline MIND detector presented in the IDR has a cuboidal geometry with a cross-sectional area of 15×15 m^2 and length of either 63 m or 125 m, depending on the mass of the detector. The thickness of each plane of iron is 3 cm, followed by two planes of scintillator, each with a thickness of 1 cm. The three planes form a module of thickness 5 cm. The lateral resolution requirement is 1 cm, which is provided by having co-extruded scintillator bars 15 m long and 3.5 cm wide, read out using optical fibers and silicon photo-multipliers (SiPMT). A 1 T dipole field was assumed.

The simplified geometry and magnetic field were adopted to allow comparison with previous simulations. However, a more realistic octagonal geometry (14 m octagonal iron plates as shown in Fig. 11) with a toroidal field of between 1 T and 2.2 T over the whole fiducial area is now being studied. These parameters can be achieved with a

100 kA/turn current traversing the center of the MIND plates, which have been shown to be feasible to manufacture.

The baseline for the Neutrino Factory includes one or more "near" detectors located close to the end of the production straights. It is necessary to have one near detector for each of the straight sections of the storage ring at each of the two polarities, so four near detectors designed to carry out measurements are essential for the sensitivity of the oscillation-physics program to be achieved. The near-detector measurements that are essential for the neutrino oscillation analysis include the determination of the neutrino flux through the measurement of neutrino-electron scattering and the measurement of the neutrino-beam properties that are required for the flux to be extrapolated with accuracy to the far detectors. In addition, it will be necessary to measure the charm production cross sections and the neutrino-nucleon deep inelastic, quasi-elastic, and resonant-scattering cross sections.

The intense neutrino beam delivered by the Neutrino Factory makes it possible to carry out a unique neutrino-physics program at the near detectors. This program includes fundamental electroweak and QCD physics, such as measurements of parton distribution functions as a function of Q^2 and Bjorken x, QCD sum rules, nuclear re-interaction effects, strange particle production, and a precise measurement of $\sin^2\theta_W$. The near detector must also be capable of searching for new physics, for example by detecting tau-leptons, which are particularly sensitive probes of non-standard interactions at source and at detection. Tau neutrino detection is also important in the search for sterile neutrinos.
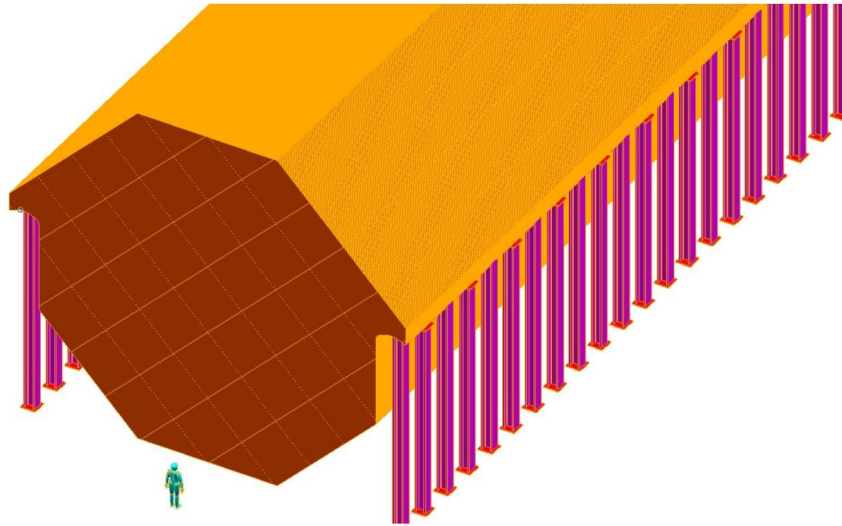
Figure 11: Schematic drawing of the Magnetized Iron Neutrino Detector (MIND).

3.1.4 The Neutrino Factory as Part of the Muon Physics Program

The properties of the muon make it a unique tool for particle physics. In addition to the decays that provide intense, high-energy, electron neutrino beams, the great precision with which properties such as $g - 2$ can be calculated using the Standard Model makes it an ideal tool in the search for new phenomena. Furthermore, the observation of charged-lepton flavor violation (cLFV) in muon decay, predicted in

many models, would revolutionize current theories, while the muon's comparatively large mass and point-like nature make it an appealing candidate to provide multi-TeV lepton-antilepton collisions at a Muon Collider.

Neutrino oscillations involve processes in which lepton flavor is not conserved. Therefore, processes such as $\mu \to e\gamma$, $\mu \to eee$, and muon-to-electron conversion in the field of the nucleus ($\mu N \to eN$) will occur. Rates for such cLFV processes can be calculated in the Standard Model extended to take into account neutrino oscillations but they are minuscule (of the order of 10^{-54}) and so the observation of such processes would be a clear signal of new physics. To achieve the requisite sensitivities, intense muon beams are required and the techniques proposed for the Neutrino Factory, such as high power, pulsed proton beams with short (~10 ns) bunches, pion capture in solenoidal fields, the manipulation of muon beams of large emittance, and FFAG acceleration are of great relevance.

A Muon Collider [16] offers crucial advantages over an e^+e^- collider of the same center-of-mass energy and luminosity because the muon mass is roughly 200 times that of the electron. The large muon mass leads to a relatively low rate of synchrotron radiation, making it possible to design a circular machine in which 100% of multi-TeV $\mu^+\mu^-$ collisions occur within ~0.1% of the nominal center-of-mass energy of the collider. In addition, should the Higgs boson be discovered and have the expected coupling proportional to mass, the Muon Collider could be used as a "Higgs Factory" at which detailed studies of its properties may be carried out.

A conceptual design for the Muon Collider has been proposed [17] in which the systems that make up the Neutrino Factory form the "front end" of the Muon Collider. Indeed, should the techniques required to realize the Neutrino Factory be demonstrated, the principal accelerator-system challenge that would remain for the Muon Collider would be the development of an ionization-cooling system that could reduce all six phase-space dimensions of the muon beams such that a luminosity in excess of 10^{34} cm^{-2} s^{-1} could be achieved. Therefore, the implementation of the Neutrino Factory is desirable to mitigate the technical risks presented by the Muon Collider.

The Neutrino Factory is the facility of choice for the study of neutrino oscillations: it has excellent discovery reach and offers the best precision on the mixing parameters, particularly in the difficult region of small θ_{13}. The ability to vary the stored-muon energy and perhaps the detector technology can provide the flexibility to respond to developments in our understanding and the discovery of new phenomena. The R&D program required to make the Neutrino Factory a reality will directly benefit the development of the Muon Collider and experiments that seek to discover cLFV. A comprehensive muon-physics program is compelling indeed.

3.1.5   References

1. C. Amsler et al, "Review of Particle Physics", in "Physics Letters B", 667, 1, (1008).
2. S. Choubey et al, the IDS-NF collaboration, "Interim Design Report", https://www.ids-nf.org/wiki/FrontPage/Documentation?action=AttachFile&do=get&target=IDS-NF-020-v1.0.pdf.
3. J. Kopp, M. Lindner, and T. Ota, "Discovery reach for non-standard interactions in a neutrino factory," Phys. Rev. D 76 (2007) 013001, arXiv:0702269 [hep-ph].
4. K. Abe et al, T2K Collaboration, "Indication of Electron Neutrino Appearance from an Accelerator-produced Off-axis Muon Neutrino Beam", Phys. Rev. Lett. **107**, 041801,

arXiv:1106.2822 [hep-ex] (2011);
P. Adamson et al, MINOS Collaboration, "Improved search for muon-neutrino to electron-neutrino oscillations in MINOS", Submitted to: Phys. Rev. Lett. arXiv:1108.0015 [hep-ex] (2011).

5. A. Blondel (Ed.) et al, "ECFA/CERN studies of a European neutrino factory complex", CERN-2004-002 (2004).

6. B. Autin *et al.*, "Conceptual design of the SPL, a high-power superconducting H⁻linac at CERN", CERN-2000-012 (2000).
F. Gerigk *et al.*, "Conceptual design of the SPL II: A high-power superconducting H⁻ linac at CERN", CERN-2006-006, (2006);
F. Gerigk *et al.*, "Layout and Machine Optimization for the SPL at CERN", CERN-ATS-2010-208, (2010).

7. M. Aiba, "Feasibility Study of Accumulator and Compressor for the 6-bunches SPL based Proton Driver", CERN-AB-2008-060, (2008).

8. R. Garoby, E. Benedetto, M. Aiba, and M. Meddahi, "Linac-based Proton Driver for a Neutrino Factory", CERN-NEUTRINO-FACTORY-NOTE-157 (2009).

9. S. D. Holmes, "Project X—Reference Design Report", Project-X-doc-776 (2010).

10. C.R. Prior, "Muon Storage Rings for the Neutrino Factory", Proceedings of the US Particle Accelerator Conference, PAC'09, Vancouver, Canada, May 2009. J. Pasternak, M. Aslaninejad, K. Long and J. Pozimski, "Feasibility of a common proton driver for a neutron spallation source and a neutrino factory", Proceedings of the 23rd Particle Accelerator Conference (2010).

11. C. Albright et al, "The neutrino factory and beta beam experiments and development", physics/0411123 (2004).

12. M. Apollonio *et al.*, "Accelerator Design Concept for Future Neutrino Factories", J. Inst. P07001 (4) (2009).

13. A. Moretti *et al.*, "Effects of high solenoidal magnetic fields on RF accelerating cavities," Phys. Rev. ST Accel. Beams 8 (2005) 072001.

14. R. B. Palmer *et al.*, "RF breakdown with external magnetic fields in 201 and 805 MHz cavities," Phys. Rev. ST Accel. Beams 12 (2009) 031002.

15. F. Méot, "6D Beam Dynamics Simulations in FFAGs using the ray-tracing code ZGOUBI", ICFA Beam Dynamics Newsletter 43, *op.cit.*

16. M. M. Alsharo'a *et al.*, "Recent progress in neutrino factory and muon collider research within the muon collaboration," Phys. Rev. ST Accel. Beams 6 (2003) 081001.

17. R. B. Palmer, "Muon collider progress," in Proceedings of the 23rd Particle Accelerator Conference [473], pp. 652–656.

3.2   The Muon Accelerator Program

Steve Geer, Fermilab, Batavia, IL 60510
Mail to: sgeer@fnal.gov

Mike Zisman, LBNL, Berkeley, CA 94720
Mail to: mszisman@lbl.gov

3.2.1   Introduction

Multi-TeV Muon Colliders and high intensity Neutrino Factories have captured the imagination of the particle physics community. These new types of facility both require an advanced muon source capable of producing $O(10^{21})$ muons per year. The muons must be captured within bunches, and their phase space manipulated so that they fit

within the acceptance of an accelerator. In a Neutrino Factory (NF), muons from this "front end" are accelerated to a few GeV or a few tens of GeV, and then injected into a storage ring with long straight sections. Muon decays in the straight sections produce an intense neutrino beam. In a Muon Collider (MC) the muons must be cooled by a factor $O(10^6)$ to produce beams that are sufficiently bright to give high luminosity in the collider. Bunches of positive and negative muons are then accelerated to high energy, and injected in opposite directions into a collider ring in which they collide at one or more interaction points.

Over the last decade our understanding of the concepts and technologies needed for Muon Colliders and Neutrino Factories has advanced, and it is now believed that, within a few years, with a well focused R&D effort (i) a Neutrino Factory could be proposed, and (ii) enough could be known about the technologies needed for a Muon Collider to assess the feasibility and cost of this new type of facility, and to make a detailed plan for the remaining R&D. Although these next NF and MC steps are achievable, they are also ambitious, and will require an efficient and dedicated organization to accomplish the desired goals with limited resources. The Muon Accelerator Program (MAP) has recently been created to propose and execute this R&D program.

3.2.2   The Birth of MAP

The Muon Collider Collaboration was formed in 1996, and consisted of about 100 particle physicists and accelerator scientists and engineers from U.S. laboratories and universities. The initial work on the overall Muon Collider concept resulted in the "Muon Collider Feasibility Study Report" in June 1996 [1]. The Neutrino Factory concept emerged in 1998 [2]. The collaboration was subsequently renamed the "Neutrino Factory and Muon Collider Collaboration" (NFMCC). From 1997 to 2010 the NFMCC pursued both NF and MC design and simulation studies [3–5], together with component development and proof-of-principle demonstration experiments. In late 2006, the Muon Collider R&D effort was complemented by the addition of the Muon Collider Task Force (MCTF) hosted by Fermilab. This approximately doubled the support in the U.S. for NF and MC R&D. By 2009 the NFMCC + MCTF community, together with their international partners (MICE [6], EMMA [7], MERIT [8], IDS-NF [9]) had made significant progress, completing a series of NF design feasibility studies [3], completing the proof-of-principle target experiment MERIT, launching the Muon Ionization Cooling Experiment (MICE), initiating a hardware component development program (MuCool), building the MuCool Test Area at Fermilab, and making steady progress with muon cooling channel studies.

Given these achievements, in October 2009 the DOE requested the Fermilab Director to put in place and host a new national Muon Accelerator R&D organization (Muon Accelerator Program, MAP [10]) to replace and streamline the NFMCC+MCTF activities, with an expectation of increased funding. MAP is now in place and functioning. The MAP R&D plan was reviewed in August 2010, and MAP became a formal and fully functional entity with the signing of its management plan in March 2011.

3.2.3   MAP Mission and Goals

The MAP mission is described in a mission statement:

"…to develop and demonstrate the concepts and critical technologies required to produce, capture, condition, accelerate, and store intense beams of muons for Muon Colliders and Neutrino Factories. The goal of MAP is to deliver results that will permit the high-energy physics community to make an informed choice of the optimal path to a high-energy lepton collider and/or a next-generation neutrino beam facility. Coordination with the parallel Muon Collider Physics and Detector Study and with the International Design Study of a Neutrino Factory will ensure MAP responsiveness to physics requirements."

To accomplish this mission, the main desired MAP R&D deliverables over the next few years are:

1. A Design Feasibility Study Report for a multi-TeV MC including an end-to-end simulation of the MC accelerator complex using demonstrated, or likely soon-to-be-demonstrated, technologies, an indicative cost range, and an identification of further technology R&D that should be pursued to improve the performance and/or the cost effectiveness of the design.

2. Technology development and system tests that are needed to inform the MC-design feasibility studies, and enable an initial down-selection of candidate technologies for the required ionization cooling and acceleration systems.

3. Contributions to the International Neutrino Factory Design Study (IDS-NF) to produce a Reference Design Report (RDR) for a NF.

3.2.4 Achievements in the First Year

The present fiscal year (FY11) has been a transition year for MAP. It is the first year that the new organization has been responsible for formulating the plan and steering the R&D. In addition to establishing the organization, some significant FY11 milestones have been accomplished:

1. **A new beam line.** The Mucool test Area (MTA) is a critical R&D facility at Fermilab built to enable tests of muon cooling channel components. In FY11, MAP has succeeded in completing and commissioning a beam line from the end of the Fermilab linac to the MTA. This is a major enhancement of the test facility. The first measurements with beam have also been made (see item 2).

2. **Cooling channel RF technologies; narrowing the options.** It has been found that the maximum operating gradient for normal conducting copper vacuum cavities is reduced when operated in an axial magnetic field of a few Tesla. If our present designs for muon cooling channels are to work, we must find a way to mitigate this effect. At the end of FY10 there were four different ideas on how to solve the problem. The MAP strategy is to build hardware to test these ideas in the MTA, and to do this as rapidly as is practical, until a solution emerges. In FY11 one of the ideas (so-called magnetic insulation) was tested in the MTA. These tests resulted in a deeper understanding of what happens with dark current electrons in the appropriate magnetic geometry, and have enabled the magnetic insulation option to be eliminated from the list of candidate solutions. A second candidate solution is to use a normal conducting cavity filled with hydrogen gas at high pressure. This technology had already been shown to work in a magnetic field, but had not been tested with an ionizing beam. In FY11, the first measurements of a test cavity of this type have been made using the new MTA beam. Further measurements, with both the magnetic field and beam, are

expected soon. Finally, preparations are being made for testing next year a third candidate solution, which uses beryllium within the cavity in regions of high surface field. Thus, we anticipate that within the first 18 months, MAP will have tested three out of the four proposed ways to mitigate the effects of magnetic field on RF operation.

3. **MICE magnets.** The MICE experiment at RAL will test a short section of a muon cooling channel in a muon beam, measuring the response of each incoming muon to the channel. This experiment not only provides an essential test of the simulation programs used to design and study muon cooling channels, but will also provide a demonstration of the cooling channel technologies. The large spectrometer solenoids used in the experiment have proven to be more challenging than originally anticipated, and need to be modified. In FY11 significant engineering studies were completed to evaluate the needed modifications, and a plan to complete the modifications established. Execution of the plan should be completed in FY12. This prepares the way for testing a cooling channel section in a muon beam in FY14–15.

4. **IDS-NF Interim Report.** The NF design studies are being pursued within the framework of the "International Design Study for a Neutrino Factory" which, as its name suggests, is a fully international endeavor, and includes many significant MAP contributions. The IDS-NF desires to produce a "Reference Design Report" in two years' time. The milestone this year was to produce an interim report. This report was successfully completed and reviewed by ECFA.

5. **Significant improvements in MC design.** Muon Collider design and simulation studies are essential to understand what hardware is needed to achieve a given performance, to guide R&D priorities, and to understand the implications of measured component performance. The MC design and simulation studies are naturally focused on the things that are unique to Muon Colliders. In FY11 these studies resulted in (i) an updated design for the proton target area to enable the target area solenoids to work in the hostile radiation environment created by the interaction of a 4 MW primary beam, (ii) a first design of a system to separate the positive from the negative muons before they are cooled, which is needed for most cooling channel designs, (iii) improved designs for merging within the cooling channel a string of muon bunches into a single bunch, needed to increase collider luminosity, (iv) improved collider lattice designs that include magnet studies to understand options that enable the dipoles and quadrupoles to operate in an environment in which the muons are decaying to produce high energy electrons, and (v) significant advances in machine-detector interface studies (see 7 below).

6. **Establishing a vision for upgrading Project X.** One of the motivations for a new high power proton source at Fermilab is to facilitate options for the laboratory's long-term future, in particular, a Neutrino Factory and/or Muon Collider. It is therefore important that there is a clear concept of how Project X might evolve into a 4 MW proton source with the bunch structure required by a NF and/or MC. To arrive at this concept requires a joint effort between the Project X and MAP teams. A MAP-Project X task force has now been formed, and has already developed an initial concept for the required Project X upgrade.

7. **Reaching out to the community: machine-detector interface studies and the Muon Collider 2011 meeting.** As the MC accelerator R&D proceeds it is

important that there is a good connection with the particle physics community. To facilitate this there is a machine-detector interface group within MAP that iterates on the final focus design and provides background files for detector studies. A new MC physics and detector group has been initiated outside of MAP to engage theorists and detector experts in assessing MC detector performance and final focus requirements, and a community-wide MC meeting was held in June 2011 (Muon Collider 2011) to bring together people interested in the accelerator R&D, the detectors, and the physics program, and to discuss status and R&D opportunities.

3.2.5 A Vision for the Future

MAP is focused on developing muon-based options for the future of particle physics. In the U.S., this is coupled to a vision for the future of the accelerator complex at Fermilab. That vision is illustrated in Figs. 1–3. It begins with Project X, a new proton source that can support a world class intensity frontier physics program (Fig. 1). The next possible step would be to upgrade Project X to provide a 4 MW beam, and add a NF (Fig. 2). Finally, the complex could be upgraded to add a site-filling MC with a center-of-mass energy of 3–4 TeV (Fig. 3).

3.2.6 Summary

MAP is a new R&D organization that has been established to pursue Muon Collider and Neutrino Factory R&D. The planned MAP R&D builds upon progress over the last decade. In its first year of existence MAP has integrated the ongoing R&D from the NFMCC and MCTF into one coherent effort, and has made some significant progress. The R&D program is ambitious, but is motivated by a strong muon-based vision for the future.
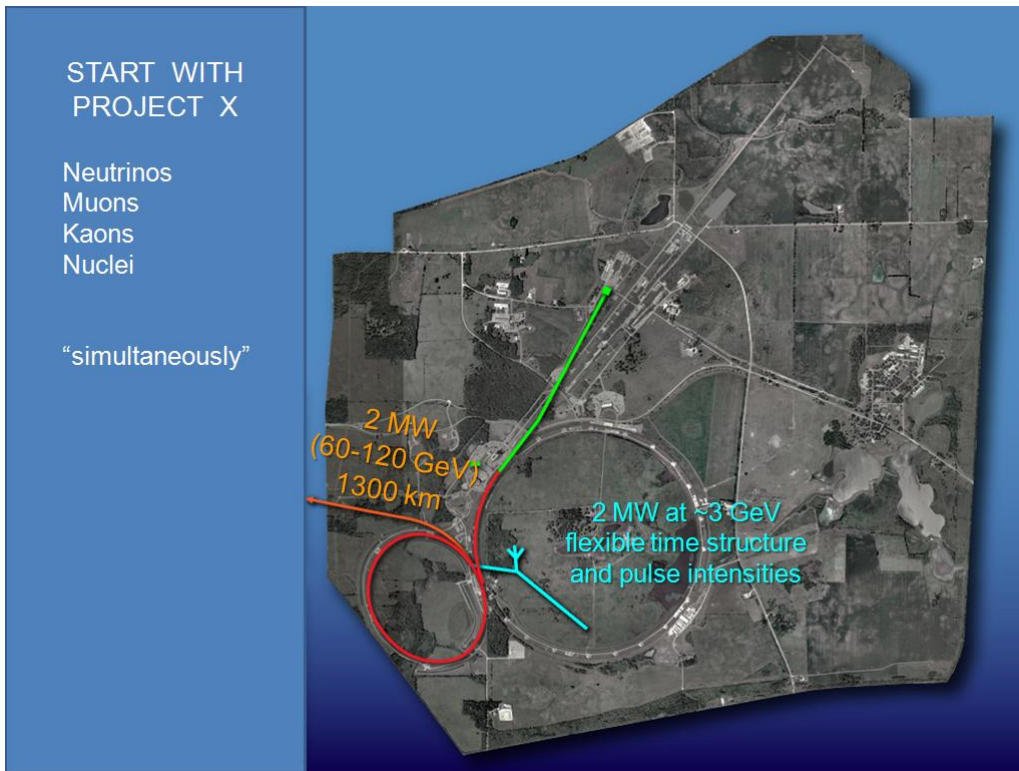
Figure 1: A vision for the future: Project X (Step 1).
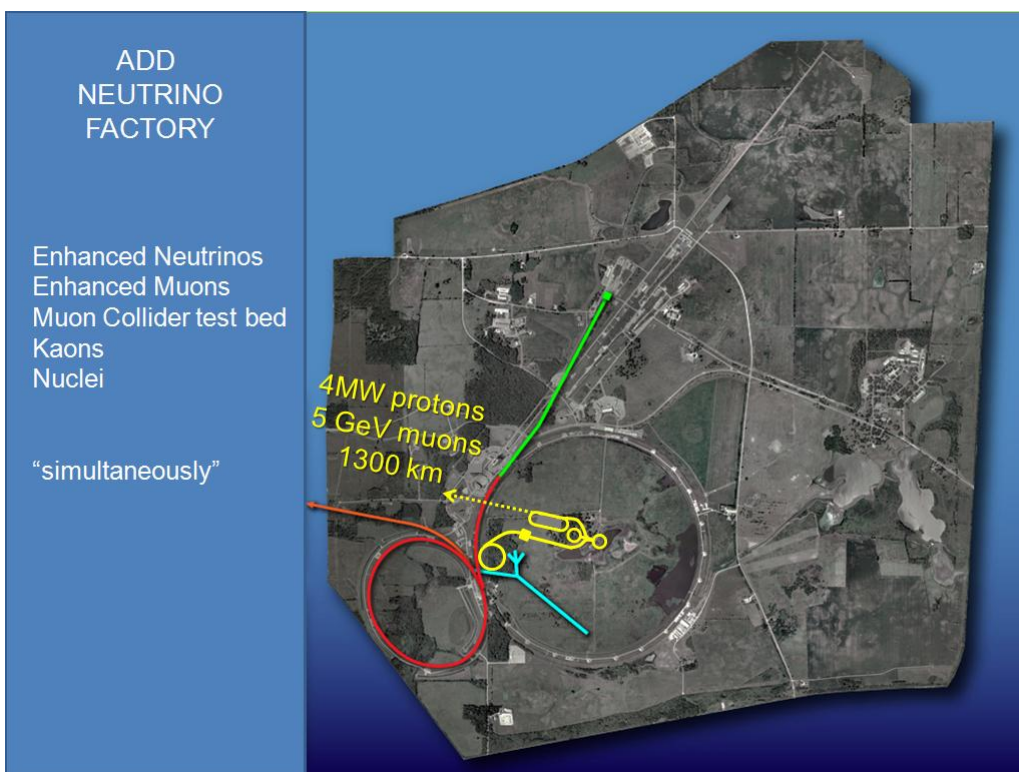
Figure 2: A vision for the future: A Neutrino Factory (Step 2).
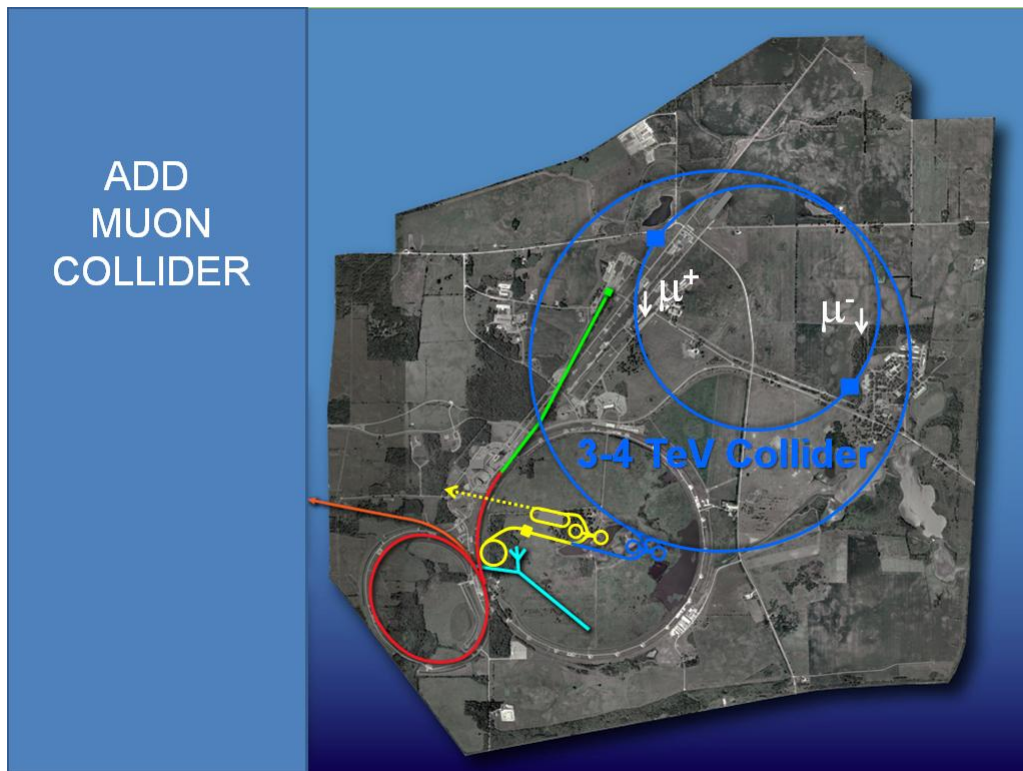
Figure 3: A vision for the future: A multi-TeV Muon Collider (Step 3).

3.2.7 References

1. R. Palmer, A. Tollestrup and A. Sessler (Eds.), "Muon Muon Collider: Feasibility Study," BNL-52503, FERMILAB-CONF-96/092, LBNL-38946; C. Ankenbrandt *et al.* (Muon Collider Collaboration), "Status of muon collider research and development and future plans," Phys. Rev. ST Accel. Beams 2 081001 (1999); M. Alsharo'a *et al.* (Muon Collider Collaboration), "Recent progress in neutrino factory and muon collider research within the Muon Collaboration," Phys. Rev. ST Accel. Beams, 6 081001 (2003).
2. S. Geer, "Neutrino beams from muon storage rings: Characteristics and physics potential," Phys. Rev. D 57, 6989 (1998).
3. S. Geer, H. Schellman (Eds.) hep-ex/0008064; N. Holtkamp, D. Finley (Eds.) Fermilab-Pub-00/108-E.; B. Autin, A. Blondel, J. Ellis, CERN-99-02; DeRujula A, Gavela M, Hernandez P. Nucl. Phys. B547 (1999) 21; Y. Mori, J. Phys. G: Nucl. Part. Phys. 29 (2003) 1527:1536; S. Osaki, R. Palmer, M. Zisman, J. Gallardo (Eds.) BNL-52623; S. Berg et al. (ISS Accelerator Working Group) arXiv:0802.4023v1, 2008.
4. S. F. King, K. Long, Y. Nagashima, B.L. Roberts, O. Yasuda (Eds.), "Physics at a Future Neutrino Factory and Super-beam Facility," Reports on Prog. in Physics 72, 10621, 2009.
5. D. Neuffer, AIP CP 721, p. 407 (2004).
6. See the MICE website: http://mice.iit.edu/
7. J.S. Berg (EMMA Collab.) AIP Conf. Proc. 981, 330 (2008).
8. H. Kirk et al. (MERIT Collab.) Proc. 2007 Part. Accel. Conf., pp. 646:648.
9. IDS website: https://www.ids-nf.org/wiki/FrontPage
10. See the MAP website: http://MAP.fnal.gov/

3.3 Machine-Detector Interface

Nikolai V. Mokhov, Fermilab, Batavia, IL, USA
Mail to: mokhov@fnal.gov

3.3.1 Introduction

In order to realize the high physics potential of a Muon Collider (MC) a high luminosity of $\mu^+\mu^-$-collisions at the Interaction Point (IP) in the TeV range must be achieved ($\sim 10^{34}$ cm^{-2}s^{-1}). To reach this goal, a number of demanding requirements on the collider optics and the IR hardware—arising from the short muon lifetime and from relatively large values of the transverse emittance and momentum spread in muon beams that can realistically be obtained with ionization cooling [1]—should be satisfied. These requirements are aggravated by limitations on the quadrupole gradients [2] as well as by the necessity to protect superconducting magnets and collider detectors from muon decay products [3, 4]. The overall detector performance in this domain is strongly dependent on the background particle rates in various sub-detectors. The deleterious effects of the background and radiation environment produced by the beam in the ring are very important issues in the Interaction Region (IR), detector and Machine-Detector Interface (MDI) designs. This report is based on studies presented very recently [5, 6].

3.3.2 Sources of Background and Radiation Load

There are three sources of beam-induced backgrounds and radiation loads in the MC:
- incoherent e^+e^- pair production at the interaction point
- beam halo loss on limiting apertures, and
- muon beam decays.

The first source, with its 10 mb cross section, gives rise to backgrounds in detector of 3×10^4 electron pairs per bunch crossing. It can be handled with the appropriate design of the MDI components assisted by the high solenoidal field of the detector. The second source is taken care of by the beam halo collimation (extraction) far upstream of IR.

Muon decays are thus the major challenge. At 0.75 TeV, with 2×10^{12} muons in a bunch, one has 4.28×10^5 decays per meter of the lattice in a single pass, and 1.28×10^{10} decays per meter per second for two beams. Electrons from muon decays have mean energy of approximately 1/3 of that of the muons. These ~250 GeV electrons, generated at the above rate, travel to the inside of the ring magnets, and radiate a lot of energetic synchrotron radiation photons tangent to the electron trajectory. Electromagnetic showers induced by these electrons and photons in the collider components generate intense fluxes of muons, hadrons and daughter electrons and photons, which create high background and radiation levels both in a detector and in the storage ring at the rate of 0.5–1 kW/m (to be compared to a few W/m in hadron colliders). Without corresponding mitigation measures, the quench stability and cryogenic issues in superconducting magnets and background loads to a detector have a potential of obviating the idea of a high-energy Muon Collider.

3.3.3 IR Lattice

The basic parameters of the muon beams and of the collider lattice necessary to achieve the desired luminosity are given in section 2.2. The major problem to solve was correction of the chromaticity of IR quadrupoles in such a way that the dynamic aperture remained sufficiently large and did not suffer much from a large beam-beam tune shift. To achieve these goals, a new approach to the IR chromaticity correction was developed [1] which we refer to as a three-sextupole scheme. The IR layout and beam sizes for $\beta^* = 1$ cm are shown in Fig. 1.
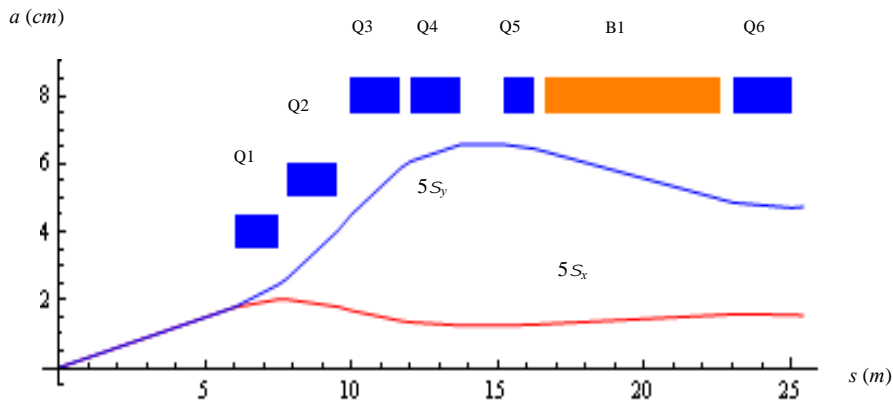
Figure 1: Beam sizes and aperture of the final focus.

3.3.4 IR Magnet Design

The IR doublets are made of relatively short quadrupoles (no more than 2 m long) to optimize their aperture according to the beam size variation and allow placing protecting tungsten masks in between them. The first two quadrupoles in Fig. 1 are focusing ones and the next three are defocusing ones. The space between the 4th and 5th quadrupoles is reserved for beam diagnostics and correctors. The cross sections of MC IR quadrupoles feature two-layer shell-type Nb_3Sn coils and cold iron yokes. The coil aperture ranges from 80 mm (Q1) to 160 mm (Q3 to Q5). The nominal field in the magnet coils is ~11–12 T, whereas the maximum field reaches ~13–15 T. As can be seen, all the magnets have ~12% margin at 4.5 K, which is sufficient for stable operation with an average heat deposition in magnet mid-planes up to 1.7 mW/g. Operation at 1.9 K would increase the magnet margin to ~22% and the quench margin by a factor of 4.

The specifics of the heat deposition distributions in the MC dipoles—with decay products inducing showers predominantly in the orbit plane—require either a very large aperture with massive high-Z absorbers to protect the coils or an open midplane design [1-3]. It has been shown [7] that the most promising approach is the open mid-plane design, which allows decay electrons to pass between the superconducting coils and be absorbed in high-Z rods cooled at liquid-nitrogen temperature, placed far from the coils. The coils are arranged in a cos-θ configuration [1, 7]. The coil aperture in the IR dipoles is 160 mm, the gap height is 55 mm with supporting Al-spacers, and the magnetic length is 6 m. The nominal field is 8 T.

3.3.5 Energy Deposition in IR Magnets

Energy deposition and detector backgrounds are simulated with the MARS15 code [8]. All the related details of geometry, material distributions and magnetic fields for lattice elements and tunnel in the ±200-m region from IP, detector components [9], experimental hall and machine-detector interface (Fig. 2) are implemented in the model. To protect the superconducting magnets and detector, 10 and 20-cm tungsten masks with $5\sigma_{x,y}$ elliptic openings are placed in the IR magnet interconnect regions and a sophisticated tungsten cone inside the detector [3, 4] was implemented into the model and carefully optimized. It is assumed that the 0.75 TeV muon beam is aborted after 1000 turns. The cut-off energy for all particles but neutrons is 200 keV, while neutrons are followed down to thermal energies (~0.001 eV).
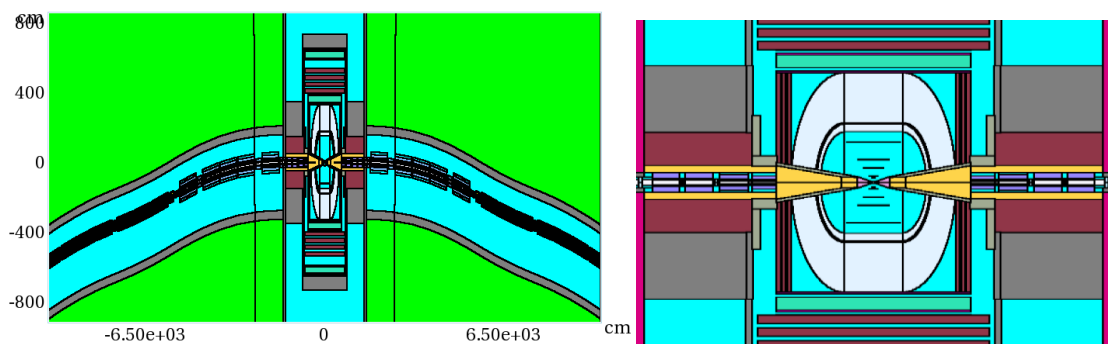
Figure 2: MARS15 model of IR (left) and MDI (right).

Calculated power density (absorbed dose) profiles are shown in Fig. 3 for the second and fifth final focus quadrupoles and in Fig. 4 for the first IR dipole. The right side in these plots is toward the ring center; the peak energy deposition is on this side for the IR dipoles and defocusing quadrupoles.

The open midplane design for the dipoles provides for their safe operation. The peak power density in the IR dipoles is about 2.5 mW/g, safely below the quench limit for the Nb_3Sn superconductor-based coils at their 1.9-K operation temperature. At this temperature, the first four quadrupoles are operationally stable, while the level in the next three IR quadrupoles is 5−10 times above the limit. This heat load could be reduced by use of a tungsten liner in the magnet aperture.

82
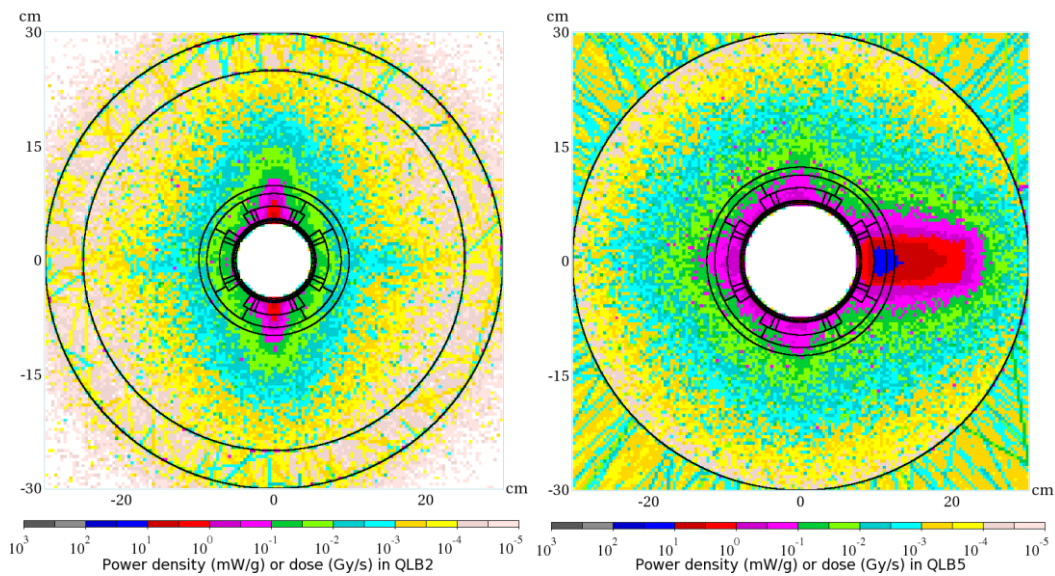
Figure 3: Power density (absorbed dose) profiles in the QLB2 focusing quadrupole (left) and QLB5 defocusing quadrupole (right).
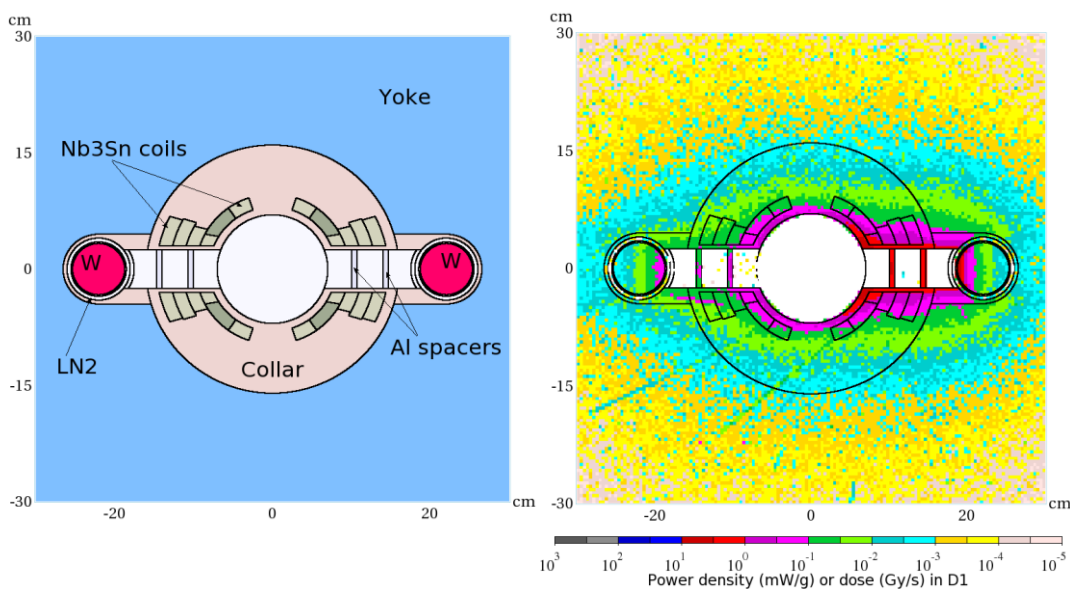
Figure 4: MARS15 model of the first IR dipole (left) and power density profiles in it (right).

3.3.6   MDI and Detector Backgrounds

In the IR design assumed, the dipoles close to the IP and tungsten masks in each interconnect region (needed to protect magnets) help reduce background particle fluxes in the detector by a substantial factor. The tungsten nozzles with 10–20° outer angle in the 6 to 600 cm region from the IP (as proposed in the very early days of MC [10] and optimized later [1,3]), assisted by the detector solenoid field, trap most of the decay electrons created close to the IP as well as most of incoherent e^+e^- pairs generated in the IP. With sophisticated tungsten, iron, concrete and borated polyethylene shielding in the MDI region (Fig. 2), total reduction of background loads by more than three orders of

magnitude is obtained. With such an IR design, the major source of backgrounds in the detector is muon decays in the region of about ±30 m from the IP.

Figure 5 (left) shows muon flux isocontours in the MC IR. Note that the cut-off energy in the tunnel concrete walls and soil outside is position-dependent and can be as high as a few GeV at 50–100 m from the IP compared with 0.2 MeV close to the IP. These muons—with energies of tens to hundreds of GeV—illuminate the entire detector. They are produced by energetic photons from electromagnetic showers generated by decay electrons in the lattice components. The neutron isofluences inside the detector are shown in Fig. 5 (right). The maximum neutron fluence and absorbed doses in the innermost layer of the silicon tracker for a one-year operation are at a 10% level of that in the LHC detectors at the nominal luminosity. More work is needed to further suppress the very high fluences of photons and electrons in the tracker and calorimeter which exceed those at proton colliders.
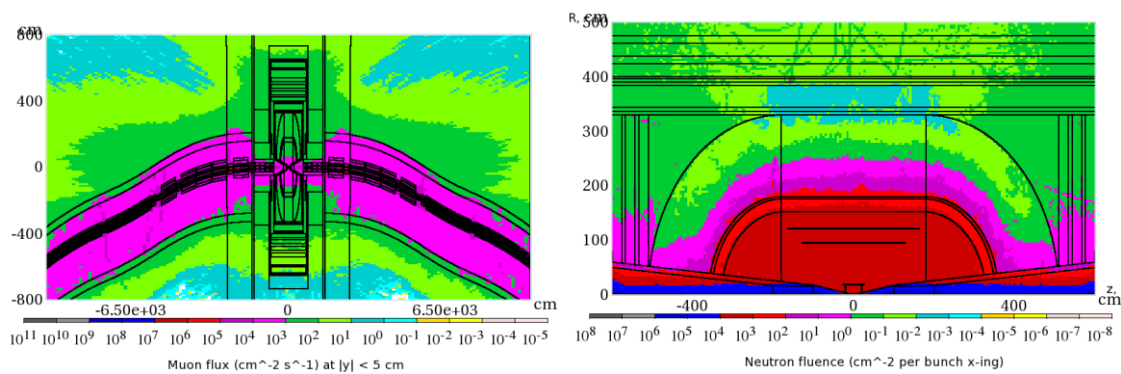
Figure 5: Muon isofluxes in IR (left) and neutron isofluences in the detector (right).

Realistic simulations of detector performance in the presence of these backgrounds have started and revealed that background loads are manageable thanks to all the measures implemented into the MDI design. It was found that with fast (< 0.5 ns) vertex and tracker Si detectors and a time gate of 2–3 ns, a further substantial reduction in the number of background-induced hits is achievable.

Acknowledgments to my collaborators Y.I. Alexahin, V.V. Kashikhin, S.I. Striganov, N.K. Terentiev and A.V. Zlobin.

3.3.7   References

1. Y.I. Alexahin, E. Gianfelice-Wendt, V. V. Kashikhin, N.V. Mokhov, A.V. Zlobin, PRSTAB (2011).
2. I. Novitski, V.V. Kashikhin, N.V. Mokhov, A.V. Zlobin, ASC2010, Fermilab-Conf-10-277-APC-TD (2010).
3. C.J. Johnstone, N.V. Mokhov, in Proc. Snowmass 1996, pp. 226-229 (1996).
4. C.J. Johnstone, N.V. Mokhov, in Proc. PAC97, pp. 414-416 (1997).
5. N.V. Mokhov, Y.I. Alexahin, V.V. Kashikhin, S.I. Striganov, A.V. Zlobin, "Muon Collider Interaction Region and Machine-Detector Interface Design", MOODN6, PAC2011, Fermilab-Conf-11-094-APC-TD (2011).
6. N.V. Mokhov, "Muon Collider Machine-Detector Interface and Detector Backgrounds", Plenary talk at the Muon Collider 2011 Workshop, Telluride, Colorado, June 27 – July 1, 2011

7. N.V. Mokhov, V.V. Kashikhin, I. Novitski, A.V. Zlobin, "Radiation Effects in a Muon Collider Ring and Dipole Magnet Protection", THP085, PAC2011, Fermilab-Conf-11-095-APC-TD (2011).
8. N.V. Mokhov, http://ww-ap.fnal.gov/MARS/.
9. http://www.4thconcept.org/4LoI.pdf
10. G.W. Foster, N.V. Mokhov, AIP Conf. Proc. 352, Sausalito (1994), pp. 178-190.

3.4 The MICE Program

Daniel M. Kaplan
Illinois Institute of Technology, Chicago, IL, USA
Mail to: Kaplan@iit.edu

3.4.1 Introduction

The Muon Ionization Cooling Experiment (MICE) [1], which is hosted at Rutherford Appleton Laboratory in the UK, has been designed and is being constructed, commissioned, and operated by an international collaboration. The purpose of MICE is to demonstrate and characterize the performance of muon ionization cooling and thereby validate the simulations that are used to design cooling channels for future neutrino factories (NF) and Muon Colliders (MC).

3.4.2 The MICE Experimental Program

The goals of MICE are to:
- engineer and build a section of cooling channel (of a design that can give the desired performance for a Neutrino Factory) that is long enough to provide a measurable ($\approx 10\%$) cooling effect, but short enough to be moderate in cost;
- use particle detectors to measure the cooling effect with an absolute emittance accuracy of 0.1% or better;
- perform these measurements with muon beams having momenta in the range 140–240 MeV/c, in which particles can be tracked individually, one particle every 100 ns or more.

3.4.2.1 *MICE Overview*

The MICE apparatus is shown schematically in Fig. 1. It consists of an upstream instrumentation section to precisely measure incoming muons, a short cooling channel section consisting of absorbers and RF cavities in a solenoid lattice, and a downstream instrumentation section to precisely measure the outgoing muons. The MICE apparatus can be viewed as a quite general test-bed for ionization cooling ideas. The ionization-cooling lattice cell comprises eight superconducting coils that can be variously powered to create "super-FOFO" [2] (field direction alternating each half-cell) or solenoid-type (field direction constant) optics, and the currents can be tuned to characterize cooling performance with a variety of beta functions. The MICE goals require that this be done in order to validate the Monte Carlo simulations that are used to design such cooling channels.

MICE is located in a new purpose-built muon beam at the ISIS 800 MeV proton synchrotron. Preparing for MICE has required the development and installation of a

target that can be dipped into the ISIS beam on demand as well as a tunable pion/muon beam line. These are now in place, and the process of installing and commissioning the beam and particle-identification instrumentation is nearly complete. The MICE cooling channel is under construction. As discussed further below, we anticipate that MICE will carry out a first measurement of ionization cooling in 2012; the full suite of measurements will be completed by about 2016. At that time, a transverse cooling channel suitable for a NF or MC would have been demonstrated. Beyond this initial MICE program, there is the possibility of using the MICE apparatus to begin to explore some aspects of 6D cooling that are relevant to the design of MC cooling channels, and that can inform the Muon Accelerator Program [3] design studies.
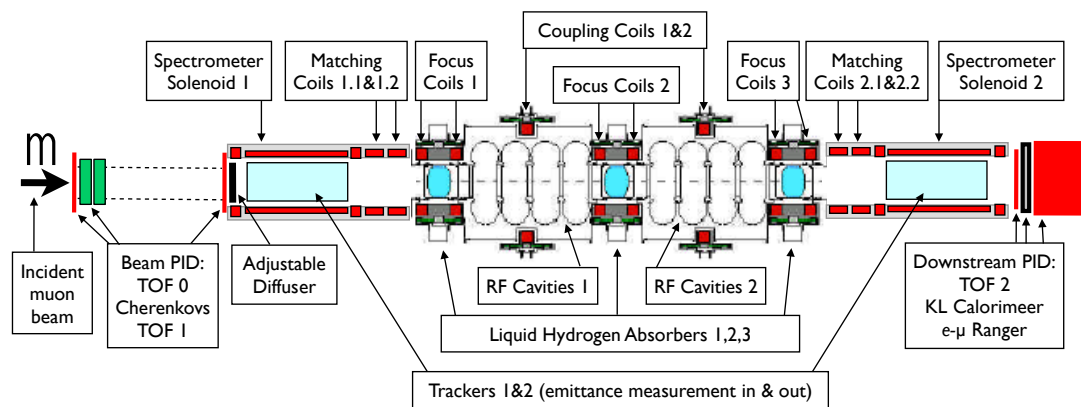
Figure 1: Schematic drawing of MICE apparatus, comprising a muon beam line at left (not shown), particle-identification systems, and input and output spectrometers surrounding a single ionization-cooling lattice cell.

A simple test of the six-dimensional ionization-cooling concept can be made by inserting a wedge absorber (composed, e.g., of LiH) into a beam having suitable dispersion, and measuring its effect on the beam. This can be done in MICE either by tuning the incoming beam so as to produce the desired dispersion or by selecting out of the distribution of incoming muons an ensemble that has dispersion matched to the configuration of the wedge absorber. This concept has been studied in sufficient detail that a LiH wedge absorber has been ordered for use in MICE Step IV (see below). Further study is needed to evaluate the degree to which it could constitute an incisive demonstration of six-dimensional cooling, perhaps obviating the need for a more elaborate demonstration.

3.4.2.2 *MICE Apparatus*

The MICE muon beam is produced by dipping a target consisting of a thin-walled titanium tube into the ISIS proton beam towards the end of the acceleration cycle (Fig. 2). Since ISIS cycles at 50 Hz, for the target to intercept only one ISIS beam pulse requires an acceleration of 80*g*, produced by means of a linear magnetic drive. A Luminosity Monitor telescope of thin scintillators (Fig. 3) monitors the interaction rate in the target.

The resulting pions are focused and momentum-analyzed by the beam line shown in Figs. 4–7. Pions decaying within the 5-T superconducting (SC) Decay Solenoid (Fig. 6)

produce muons, which are then momentum-analyzed and focused onto the variable-thickness Diffuser in order to produce beams of the desired momenta and emittances for input to the cooling cell. The input beam is tunable from 3 to 10π mm·rad transverse emittance. Particle identification using time of flight (TOF) and two aerogel Cherenkov counters (Fig. 8) ensures better than 99.9% muon purity.
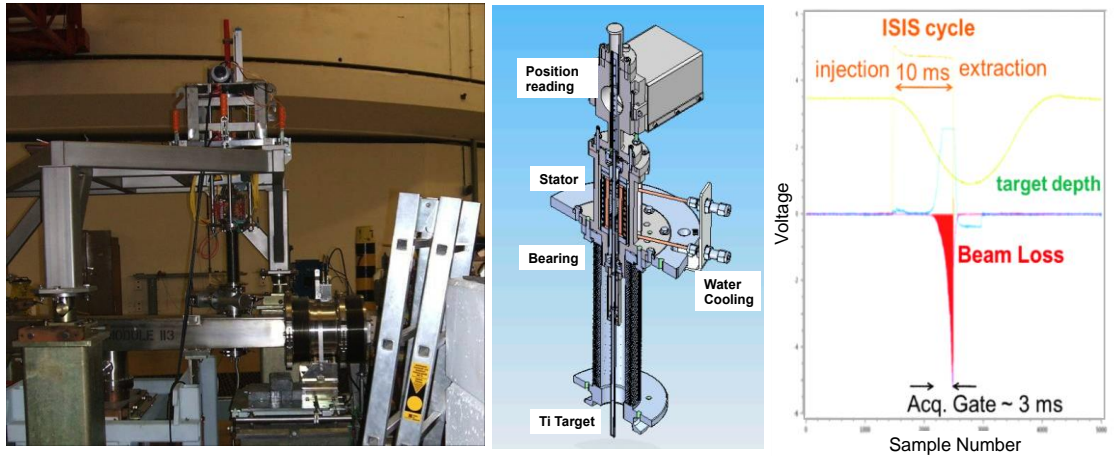
Figure 2: MICE target apparatus, with target dip cycle illustrated at right.
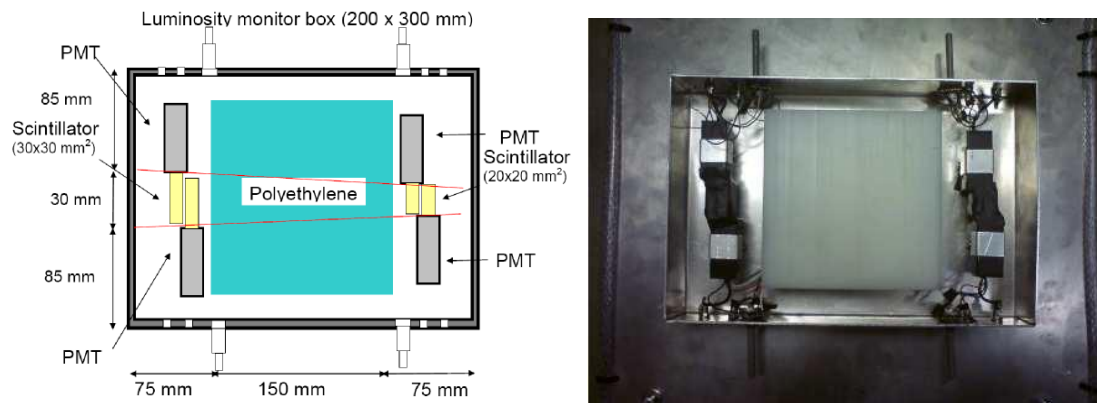
Figure 3: Schematic and photo of MICE Luminosity Monitor.
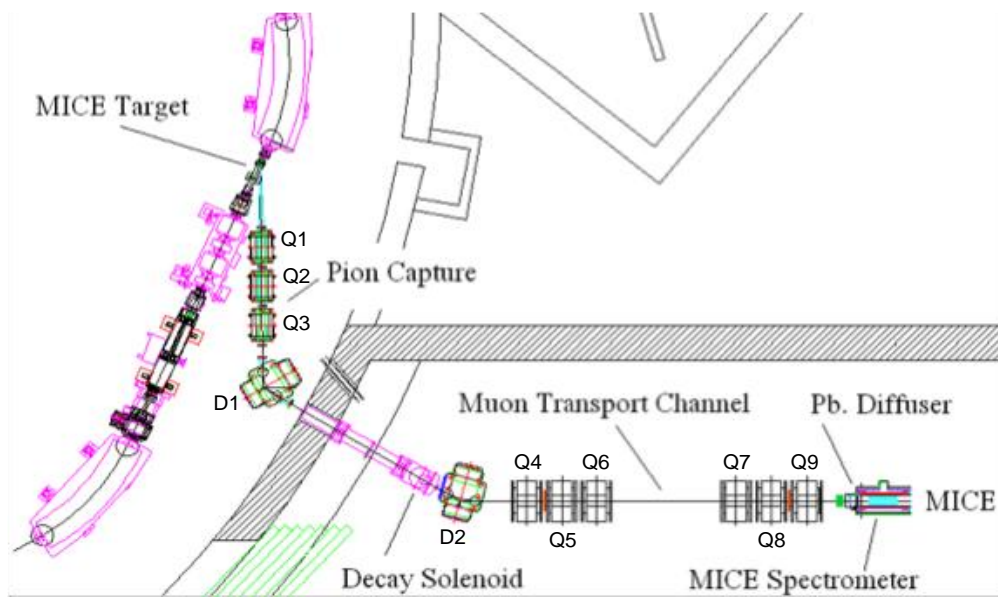
Figure 4: The MICE muon beam line, with a portion of the ISIS synchrotron at left.
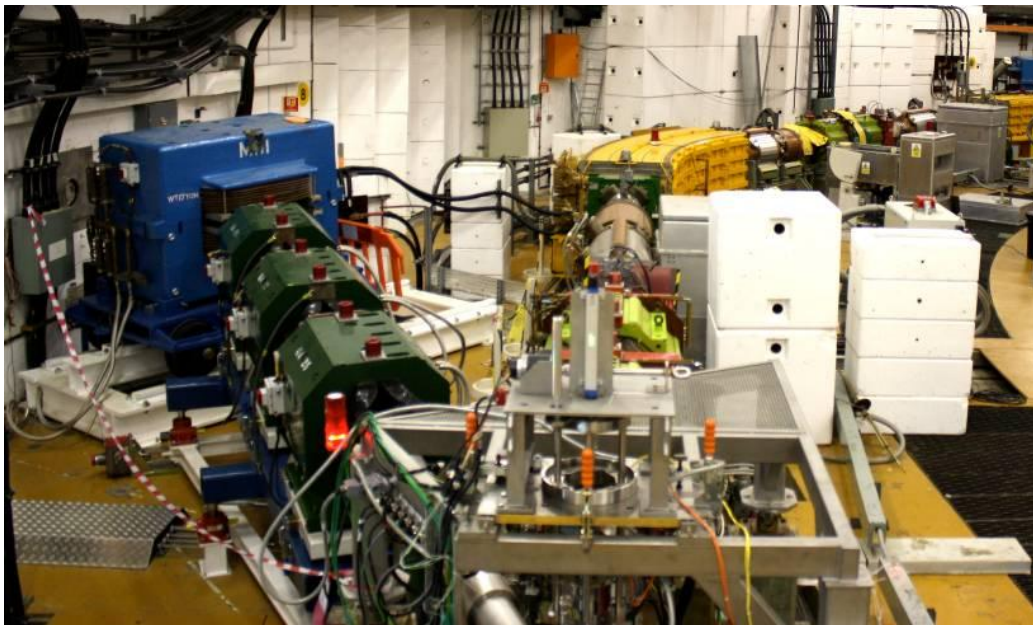
Figure 5: Photo of MICE target and of those beam-line elements located within the ISIS vault (Q1, Q2, Q3 and D1).

Figure 6: Photo of Decay Solenoid prior to its installation into the ISIS-vault shielding wall.

Figure 7: Photo of elements downstream of Decay Solenoid Area: Q7, Q8, Q9, TOF1, TOF2, KL, and part of EMR.
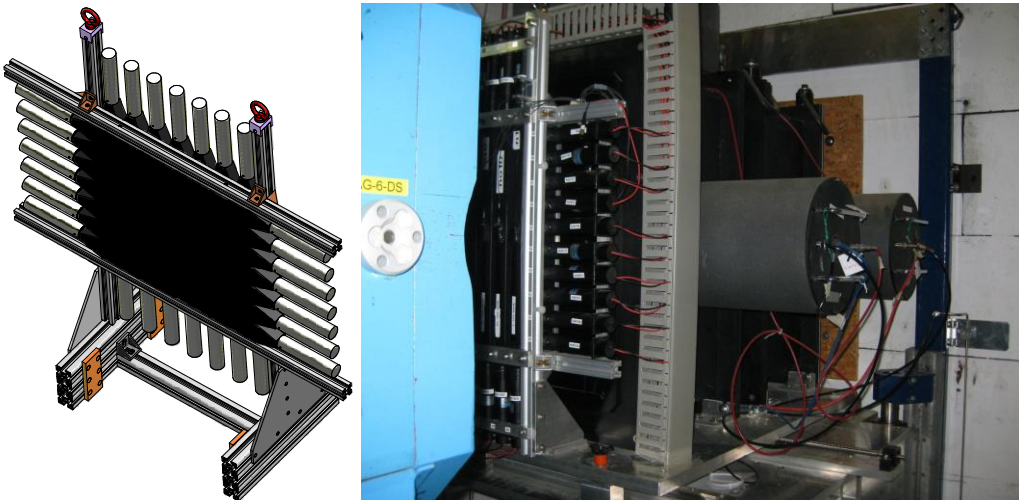
Figure 8: TOF (left) and Cherenkov (right) counters.

The input 6D emittance is measured particle-by-particle in a magnetic spectrometer comprising a five-station scintillating-fiber tracker [4] (Fig. 9) mounted within a 4-T SC solenoid. The tracker determines x, x', y, y', and particle energy, and the TOF counters measure the sixth phase-space coordinate, t. The cooling cell consists of low-Z absorbers and normal-conducting (NC) RF cavities, with SC coils providing strong focusing. The final emittance is measured in a second spectrometer system identical to the first one. Muon-decay electrons, which would bias the emittance measurement, are eliminated via calorimetry (Fig. 10).
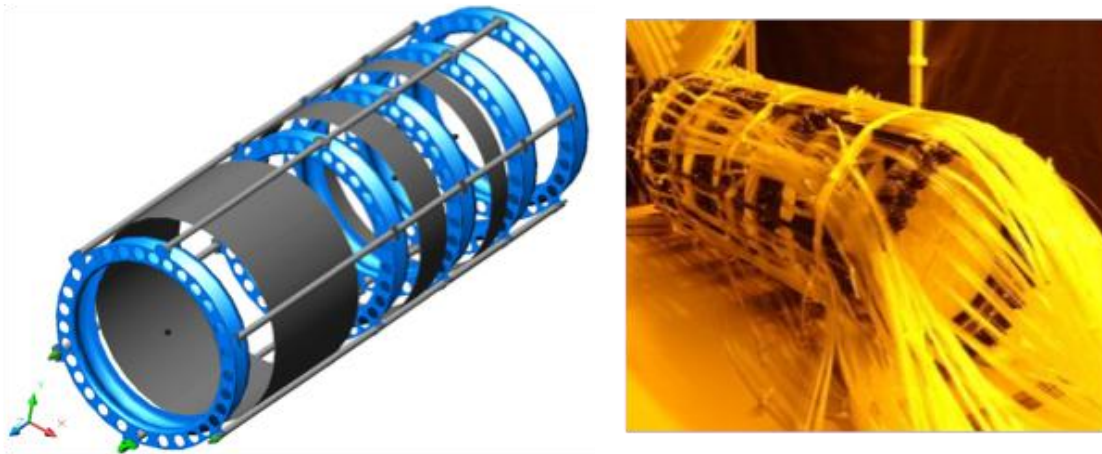
Figure 9: Scintillating-fiber tracker schematic and photo.
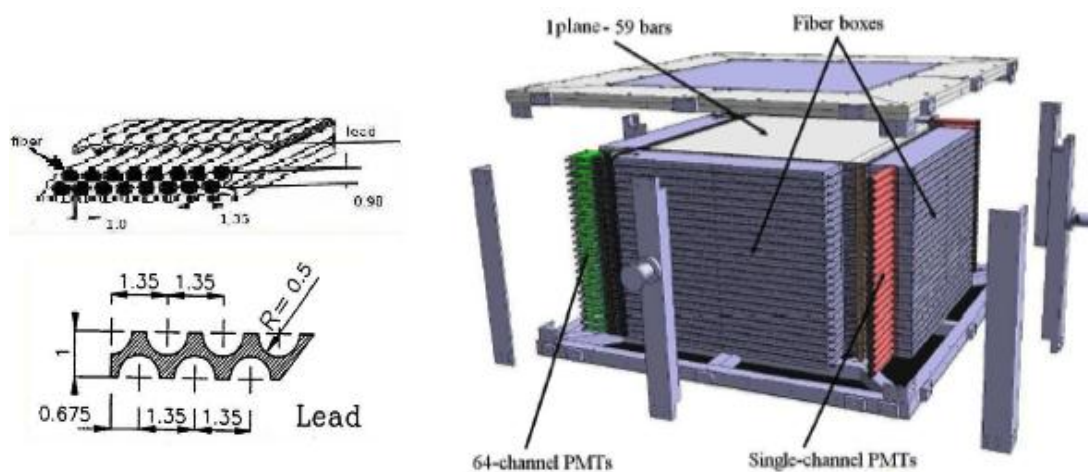
Figure 10: (left) KL Pb–scintillating fiber calorimeter layer, with detail of Pb extrusion shown; (right) totally active scintillator EMR calorimeter.

3.4.2.3   *MICE Status and Schedule*

The MICE beam line and all but one of the detectors have been installed and commissioned, thus completing "Step I" of the experiment. The final detector, the Electron-Muon Ranger (EMR), has been partially installed and its completion is imminent. Construction of the cooling-channel components is in progress. The

spectrometer solenoids have been built but difficulties in their training have necessitated a retrofit, which is in progress. The estimated schedule for completion of MICE Step IV is given in Fig. 11, along with a goal for Step V.
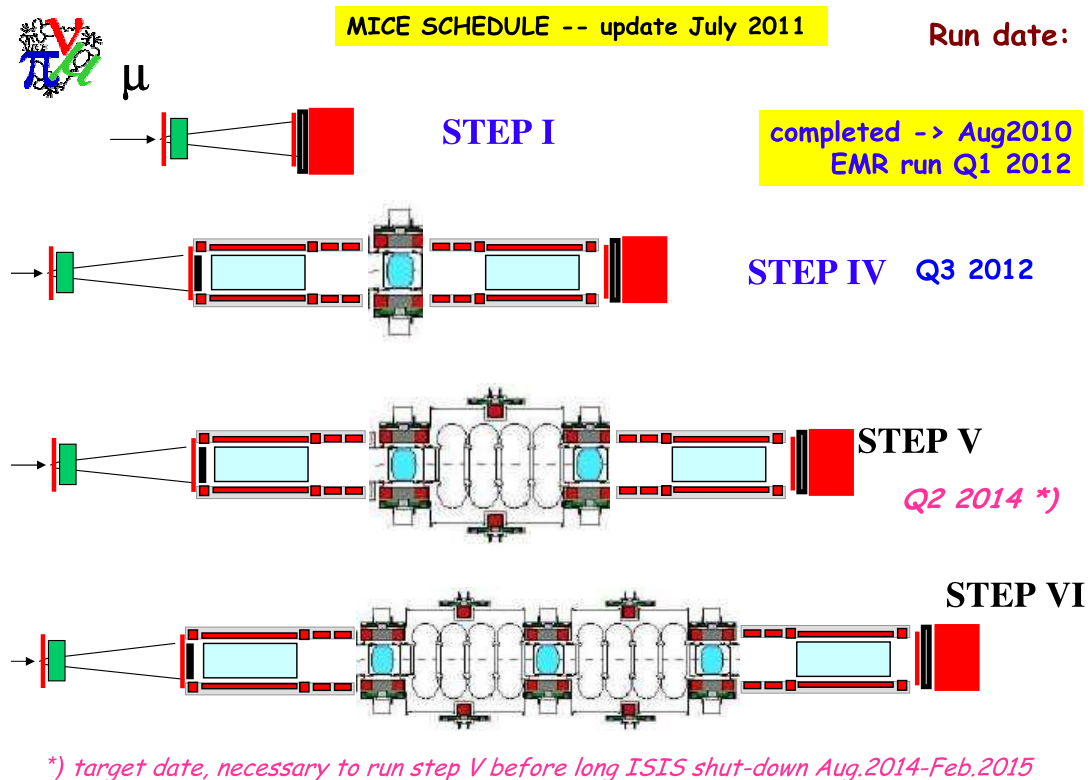
Figure 11: MICE schedule (the former Steps II and III have now been incorporated into Step IV).

3.4.2.4   *Results from Step I*

The TOF counters allow a rather thorough characterization and calibration of the beam (Fig. 12). Employing fast, 5-cm-thick scintillator, fast photomultiplier tubes, and temperature-compensated signal cable, they were designed for 50 ps resolution. TOF0 and TOF2 have been shown to meet this specification, while the demonstrated TOF1 resolution is 58 ps. Several of the TOF1 phototube assemblies have recently been replaced or refurbished by their manufacturer (Hamamatsu), and we expect the TOF1 resolution to match that of the other counters in future data-taking. In any case, the achieved resolution suffices to determine both the beam momentum and emittance (Fig. 13).
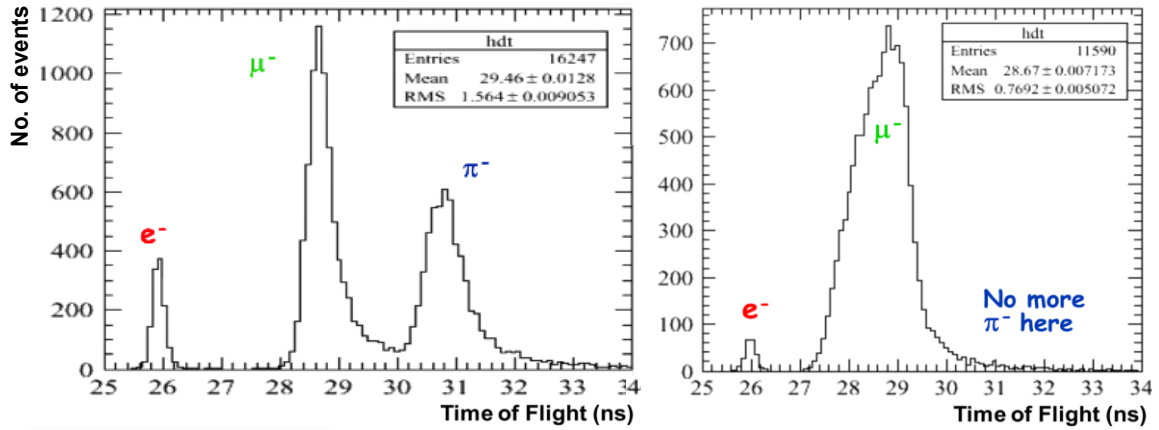
Figure 12: Time of flight of beam particles between TOF0 and TOF1 when the two beam-line dipoles are set to (left) equal momenta; (right) second dipole momentum equals half of first, selecting muons from backwards pion decays.
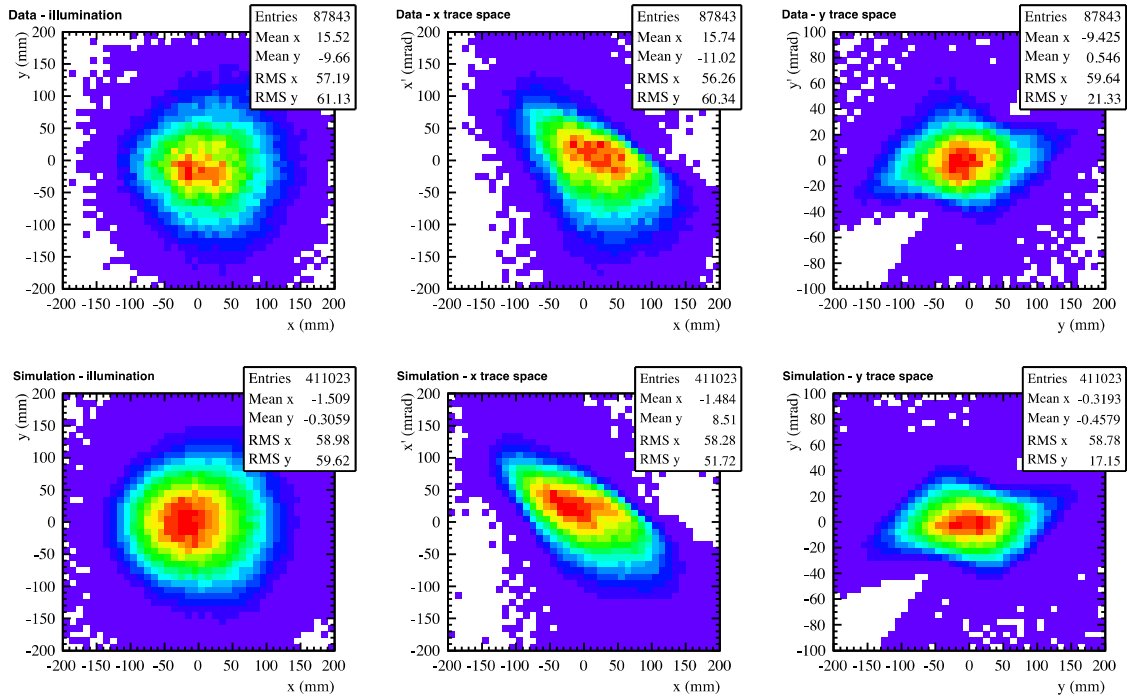
Figure 13: Comparison of muon-beam emittance predicted in simulation (top) and measured using TOF counters (bottom). Columns are y vs x, x' vs x, and y' vs y.

3.4.3   Conclusions

By Step IV, MICE will have demonstrated the principle of ionization cooling: reduction of normalized transverse emittance via dE/dx loss in low-Z material. We also anticipate demonstrating the principle of six-dimensional (6D) ionization cooling via emittance exchange in a wedge absorber. Step V will show the feasibility and performance of "sustainable" cooling: cooling by energy loss followed by longitudinal-

momentum restoration, as required in order for the cooling process to be iterated. In Step VI a wide range of cooling-lattice optics variations will be tested, validating muon-cooling Monte Carlo codes such that a long cooling channel can be designed with confidence. A MICE follow-on experiment to test a section of a realistic 6D cooling lattice has also been considered but is not yet proposed. The suite of MICE measurements will set the stage for Muon Collider and Neutrino Factory proposals with reliable performance benchmarks.

3.4.4   References

1. See http://mice.iit.edu/ and references therein.
2. *Feasibility Study-II of a Muon Based Neutrino Source*, S. Ozaki, R. B. Palmer, M. S. Zisman, eds., Report BNL-52623 (2001), available from http://www.cap.bnl.gov/mumu/studyii/FS2-report.html.
3. See Muon Accelerator Program website, http://map.fnal.gov and links therefrom.
4. M. Ellis et al., "The design, construction and performance of the MICE scintillating fibre trackers," to appear in Nucl. Instrum. Meth. Phys. Res. A (2011); arXiv:1005.3491v2 [physics.ins-det].

3.5   The EMMA Non-Scaling FFAG Experiment

J. Scott Berg
Brookhaven National Laboratory, P.O. Box 5000, Upton NY 11973-5000, USA
Mail to: jsberg@bnl.gov

3.5.1   Motivation and Introduction to the Experiment

Fixed field alternating gradient (FFAG) accelerators are of interest as muon accelerators because they can allow us to take advantage of the ability to bend high-energy muons without significant synchrotron radiation loss by making a large number of passes through RF cavities. The highest energy acceleration stage of the IDS-NF Neutrino Factory design uses an FFAG, and one could contemplate their use for a subsequent stage in a Muon Collider. The NuFACTJ Neutrino Factory design [1] used a number of FFAG stages based on a traditional "scaling" design, but examination of those designs revealed that they required superconducting magnets with extremely large apertures, calling into question the cost-effectiveness of this solution. To reduce the magnet apertures, one can instead use a non-scaling design [2,3], which was adopted for the IDS-NF design.

No such non-scaling FFAG had ever been built, so a collaboration was formed to build a linear non-scaling FFAG to study its beam dynamics. The result (see Figs. 1 and 2) is the Electron Model for Many Applications, EMMA [4].
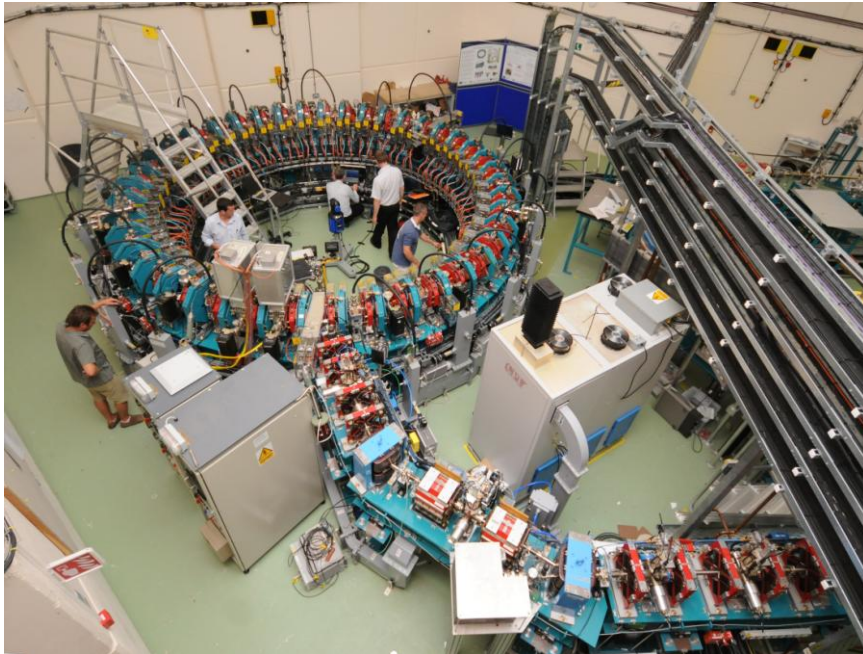
Figure 1: Overhead view showing the EMMA ring (top left) and the injection line from ALICE (coming from the bottom right). The beam circulates clockwise in the ring. To the right of the injection line, the large box is the RF power supply. To the lower left of the ring are the kicker and septum supplies. The single RF supply powers 19 cavities almost evenly distributed around the ring (nearly every other cell) using the grey waveguide that can be seen outside and below the perimeter of the ring. The cavity locations are easily identified from the heavy black cables transferring power from the waveguide to the cavity.
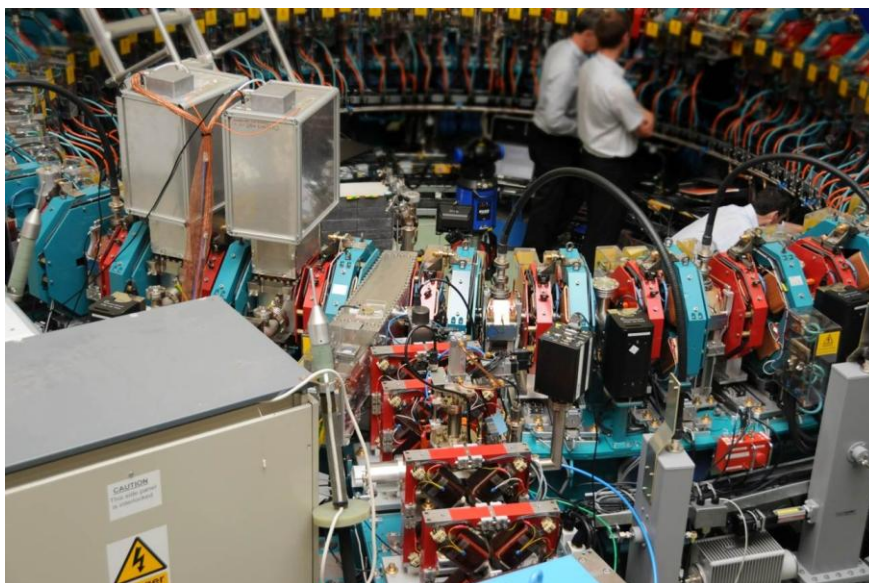
Figure 2: Close-up view of the EMMA ring where the injection line enters. In the ring, red magnets are focusing quadrupoles and blue magnets are defocusing quadrupoles. Nearly every other cell contains an RF cavity, which can be identified here by the heavy black cable supplying RF power from above. The injection septum enclosure is the silver box where the injection line enters the ring and the two kickers can be seen in the cells that immediately follow it (silver boxes supported over the kickers themselves).

The EMMA experiment was designed to have a number of capabilities:

- It can accelerate electrons from 10 MeV to 20 MeV kinetic energy using 1.3 GHz RF. The acceleration mode, which we refer to as "serpentine acceleration," is identical to the one that would be used to accelerate muons.
- To be able to study beam dynamics of the machine at fixed energies, and to be able to examine the beam throughout the acceleration cycle, one can inject into and extract from the machine at any energy over the machine's acceleration range.
- The transverse normalized acceptance of the machine is at least 3 mm, which is comparable, after scaling, to what is needed to accelerate the Neutrino Factory muon beam. The injection system is capable of scanning that entire acceptance with a small emittance beam.
- There are extensive capabilities to adjust the fields and gradients of the main ring magnets, so as to be able to study the behavior of the machine as a function of the lattice design parameters.
- The machine has extensive diagnostics, including two BPMs in almost every cell.

The main ring for the machine consists of 42 identical doublets, using displaced quadrupoles to create combined-function magnets. The quadrupoles in the doublet can move transversely to vary the dipole component of the field. The design drift length between the doublets is 21 cm, though the physical space ends up being significantly less than that. The resulting ring circumference is about 16.6 m. We use the ALICE machine [5] as our variable-energy injector.

3.5.2   Achievements Thus Far

We have made extensive measurements in the machine, and have thus far achieved a number of milestones:

- We have injected beam into the ring and have stored it for hundreds of turns at fixed energy.
- We have measured the closed orbit, tune, and the time of flight for a number of different fixed energies. To simplify the studies, this was done for fixed injection energy, and the main ring magnet fields were scaled to simulate different momenta. The energy dependence of the tune and time of flight were what one expects for a linear non-scaling FFAG lattice.
- We have successfully accelerated the beam from approximately 12 MeV/c to 18 MeV/c. Using the fixed-energy measurements of tune and closed orbit position, we were able to reconstruct the energy variation of the beam during acceleration. This allowed us to reconstruct a picture of the longitudinal phase space, which is consistent with the serpentine acceleration mode that one expects.
- We have extracted the beam, and confirmed an energy gain during the acceleration process.

3.5.3 Challenges Faced

Probably the greatest problem we have faced is a large closed-orbit distortion. The machine consists of 42 identical doublets, and the closed orbit should be identical in each cell. Every cell has one BPM in the middle of the doublet, and for a perfect lattice we should therefore see identical closed-orbit positions at each of these BPMs. In practice we have closed-orbit distortion of several mm in each plane (see Fig. 3 for an example); we expect more like 1 mm from alignment errors. It appears that a significant portion of the closed orbit distortion arises from the leakage field of the septum. However, this cannot explain all of the observed closed orbit distortion (in particular for the vertical), and we have yet to identify the other sources.
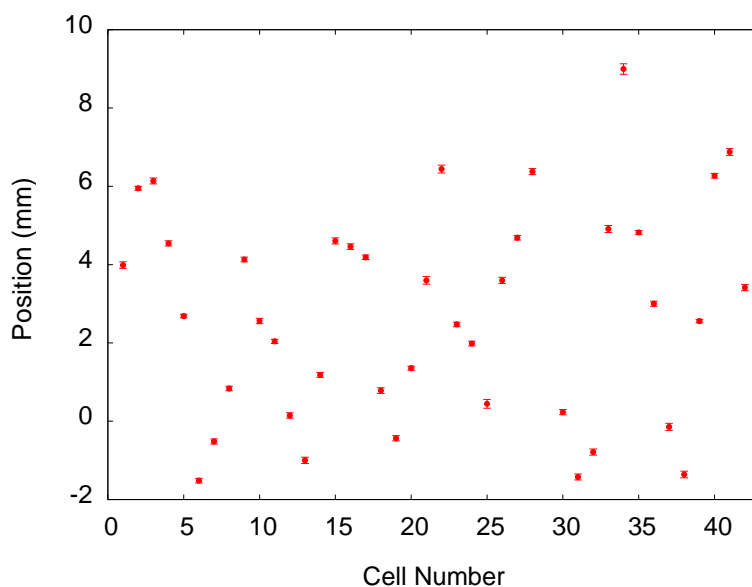
Figure 3: Horizontal closed orbit at one particular energy in EMMA. If all cells were identical as desired, the closed orbit would be at the same position in each cell. Error bars are estimates based on turn-by-turn fluctuations in the closed measured orbit position.

Despite this large orbit distortion, we have successfully accelerated the beam. We have also been able to inject the beam at a number of different energies. This is due in no small part to the very large dynamic aperture of a linear non-scaling FFAG, and is a testament to the robustness of this type of machine.

Injection has been very challenging for a number of reasons. A large strength is required for the septum and kickers (the septum must bend nearly 90 degrees), and very little drift length is available for them in the cells. The relatively short circumference of the ring (16.6 m) requires very short kicker pulse rise and fall times. The septum was required to be movable to permit a large range of injection trajectories.

In practice we have fallen short on some of these goals. As pointed out earlier, septum leakage fields give a major contribution to closed-orbit distortion. The injection kicker fields are not negligible by the time the beam comes back to the kicker. Spatial constraints have prevented the septum from moving as much as we would like (see Fig. 4). Finally it has been difficult to shield the diagnostics from the powerful pulses

required for these magnets. Nonetheless, we have succeeded in injecting, storing, and accelerating the beam. We have successfully filtered the kicker noise from our diagnostic signals while simultaneously improving the shielding.

Measurement of parameters such as tune is challenging due to the lack of chromaticity correction in the machine (which is, by design, to achieve large transverse dynamic aperture): signals from betatron oscillations quickly de-cohere due to the nonzero energy spread in the beam. We have nonetheless been able to make reasonably accurate tune measurements by taking advantage of the large number BPMs in the ring and the symmetry in the ring design.
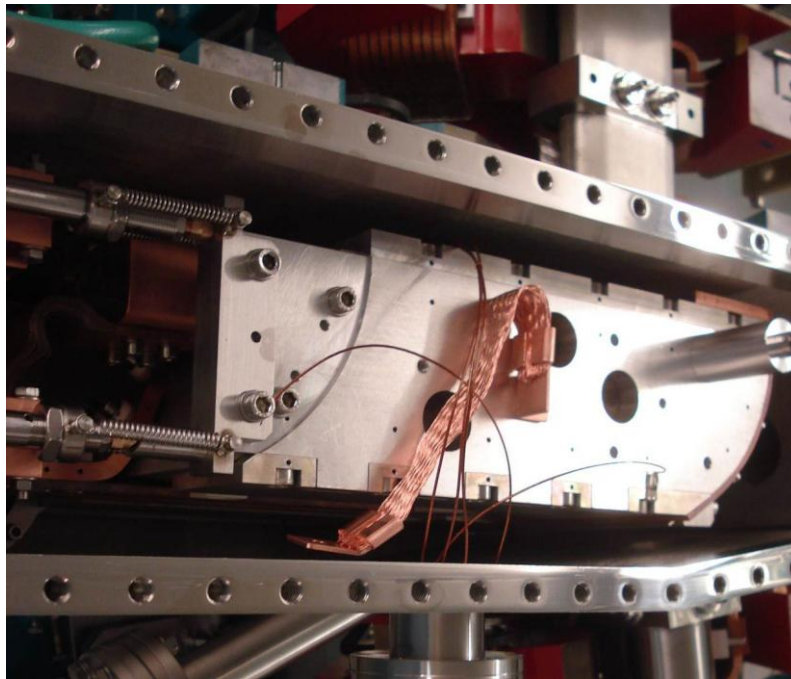
Figure 4: Injection septum in its enclosure. Beam is injected from the bottom left, and enters the ring moving upward at the right of the figure. The septum can translate horizontally in this picture, and rotate about a pivot near the lower left point of the septum.

3.5.4   Future Plans

We have an extensive program for EMMA, only a portion of which has direct implications for muon acceleration. Here we will focus on the parts of the program that are relevant for muon acceleration.

Our first goal in this regard will be to show acceleration over a factor of two in momentum, which will require us to inject at lower momentum than we have thus far. This will be made more challenging by the closed-orbit distortion (since the tune varies more rapidly at lower momentum, making it more difficult to stay clear of integer resonances where the closed-orbit distortion is amplified, and the injected orbits are closer to the beam pipe walls), and we may therefore need to address the closed orbit distortion. It will also require us to set our injection system differently than we have

thus far (with the two kickers having opposite polarity, and probably a different trajectory coming out of the septum).

We will then need to demonstrate that we have the expected large transverse acceptance. This will require us to scan the transverse phase space and measure the results of doing so, and will thus require more control of the injection process and the ALICE beam than we have thus far achieved. It will also require extraction of the beam and measurement of its properties, which will be challenging due to the somewhat arbitrary phase space coordinates that the beam will have at extraction, requiring a precise method for relating measured beam properties in the ring to extraction system settings. The nonzero chromaticity in the ring and nonzero energy spread in the beam will also lead to an increase in the projected beam size at extraction.

We will also want to see how the machine performance depends on the parameters of the ring. In particular, we will want to set the ring parameters to values closer to what one would use for a muon accelerator. We will also want to scan over some values of the machine parameters (voltage, frequency, quadrupole and dipole strengths) to ensure that we do understand the behavior of the ring.

Finally, in the long term, we may wish to use EMMA to look at slower acceleration. While this does not have direct implication for muon acceleration, it could be of interest for proton drivers, for which non-scaling FFAGs have been contemplated [6,7]. Such studies would help us understand the limitations on the acceleration rate for a machine which has a varying tune. But we would first need to reduce sources of asymmetries that lead to our large closed-orbit distortion, and to replace the RF system (one proposal for doing so is outlined in [8,9]).

3.5.5   Implications for Muon Accelerator Design

While large differences in size and energy between this electron model and a muon accelerator make direct comparisons of hardware issues impossible, we can draw some general conclusions from our experience.

First of all, despite thus far falling short on some of our goals for the hardware parameters, the fact that 1) the energy dependent parameters of the beam are what we expect, and 2) we have accelerated the beam, indicate that a linear non-scaling FFAG can be used to accelerate a muon beam. We have yet to truly demonstrate that we can accelerate over the full energy range desired and that we have the required transverse dynamic aperture, but we are only at the beginning of our studies.

The challenges in EMMA also remind us what we need to focus on in the design and engineering of a muon FFAG. Ensuring that the magnets produce identical fields in each cell will be important to limit closed orbit distortion and to insure that we can inject at our desired energy. It will therefore be important to account for all sources of magnetic field errors in our design. In particular we must understand asymmetries in the magnet design. Simply ensuring that all magnets have identical integrated multipole strengths may not be sufficient.

The injection system will be challenging as it was in EMMA. Though the required technologies may be different, the concerns will be the same: ensuring that septum leakage fields are sufficiently low and kicker rise and fall times are sufficiently short. This will have implications for the amount of space allocated to drifts, and will lead to a tradeoff: shorter drifts improve acceleration performance [10], but longer drifts may be needed for injection and extraction hardware.

Careful modeling of the magnet fields in a suitable tracking code will be essential. One example, in particular, is that, despite showing the expected dependence on energy, the time of flight in EMMA has been somewhat shorter than expected based on hard-edge field models; this discrepancy is likely due to a significant deviation of the actual magnet fields from our original models.

3.5.6   References

1. Yoshitaka Kuno, Yoshiharu Mori, Yoshihisa Iwashita, Shinji Machida, Joe Sato, Osamu Yasuda, and Takeichiro Yokoi, "A Feasibility Study of A Neutrino Factory in Japan," http://www-prism.kek.jp/nufactj/ (2001).
2. C. Johnstone, W. Wan, and A. Garren, "Fixed Field Circular Accelerator Designs," in *Proceedings of the 1999 Particle Accelerator Conference, New York, 1999*, edited by A. Luccio and W. MacKay (IEEE, Piscataway, NJ, 1999), p. 3068.
3. F. E. Mills and C. Johnstone, "Linear Orbit Recirculators," in *4th International Conference on Physics Potential & Development of $\mu^+ \mu^-$ Colliders, December 10-12, 1997, San Francisco, California: Transparency Book*, pp. 693–698.
4. R. Barlow *et al.*, "EMMA—The world's first non-scaling FFAG," Nucl. Instrum. Methods A **624** (2010) 1–19.
5. D. J. Holder, N. Bliss, A. R. Goulden, P. A. McIntosh, and S. L. Smith, "The Status of ALICE, the Daresbury Energy Recovery Linac Prototype," in *Proceedings of EPAC08, Genoa, Italy* (EPAC/European Physical Society Accelerator Group, 2008), p. 1001.
6. G. H. Rees, "FFAG Studies for Neutrino Factory Accelerators," Nucl. Phys. B (Proc. Suppl.) **155** (2006) 301–304.
7. Alessandro G. Ruggiero, "FFAG Accelerator Proton Driver for Neutrino Factory," Nucl. Phys. B (Proc. Suppl.) **155** (2006) 315–317.
8. Chihiro Ohmori and J. Scott Berg, "Upgrading EMMA to use Low-Frequency RF Cavities," Int. J. Mod. Phys. A **26** (2011) 1822–1832.
9. C. Ohmori and J. Scott Berg, "A Magnetic Alloy Loaded RF Cavity System for EMMA," in *Proceedings of IPAC'10, Kyoto, Japan* (IPAC'10/ACFA, 2010) p. 3714.
10. J. Scott Berg and Carol Johnstone, "Designs of FFAGs Based on a FODO Lattice," in *Proceedings of the 2003 Particle Accelerator Conference*, edited by Joe Chew, Peter Lucas, and Sara Webber (IEEE, Piscataway, NJ, 2003), p. 2216.

3.6   The Muon Collider Target System

Harold G. Kirk, Brookhaven National Laboratory, Upton, NY 11973
Mail to: kirk@bnl.gov

Kirk T. McDonald, Princeton University, Princeton, NJ 08544
Mail to: kirkmcd@princeton.edu

3.6.1   Introduction

The target system consists of a free liquid mercury jet immersed in a high-field solenoid magnet capture system that also incorporates the proton beam dump.

The requirements for a Muon Collider/Neutrino Factory [1] (some of which are summarized in Table 1) call for a target capable of intercepting and surviving a 4-MW, 15-Hz pulsed proton beam.

Table 1: Assumed proton beam parameters.

Proton-beam energy [GeV]	8
Rep rate [Hz]	15
Bunch length [ns]	2 ± 1
Beam radius, rms [mm]	1.2
Beam power [MW; p/s]	4; 3.125×10^{15}

A $\mu^+\mu^-$ collider requires simultaneous production/capture of charged pions of both signs, which mandates the use of solenoid magnets in the target system. The target-system concept is illustrated in Fig. 1, in a version slightly modified from Neutrino Factory Study 2 [2]. The target, the proton beam dump, and a shield/heat exchanger will be located inside a channel of superconducting solenoid magnets that capture, confine and transport secondary pions and their decay muons, of energy 100–400 MeV, to the bunching, phase-rotation, cooling and acceleration sections downstream. Most of the 4-MW beam power will be dissipated within a few meters, inside the solenoid channel, which presents a severe challenge. The present baseline target system includes considerably more shielding of the superconducting magnet near the target, as indicated in the upper part of Fig. 2. Studies of the tradeoffs between capital and operational costs, including frequency of replacement of irradiated components, are ongoing, and the baseline configuration is expected to continue to evolve in the near future.
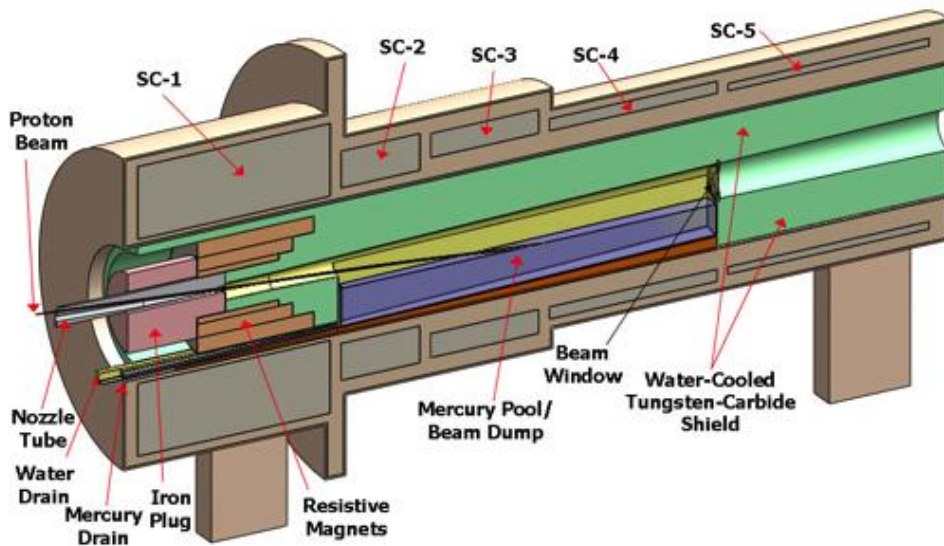
Figure 1: Target-system concept, with small changes from Neutrino Factory Study II [2].
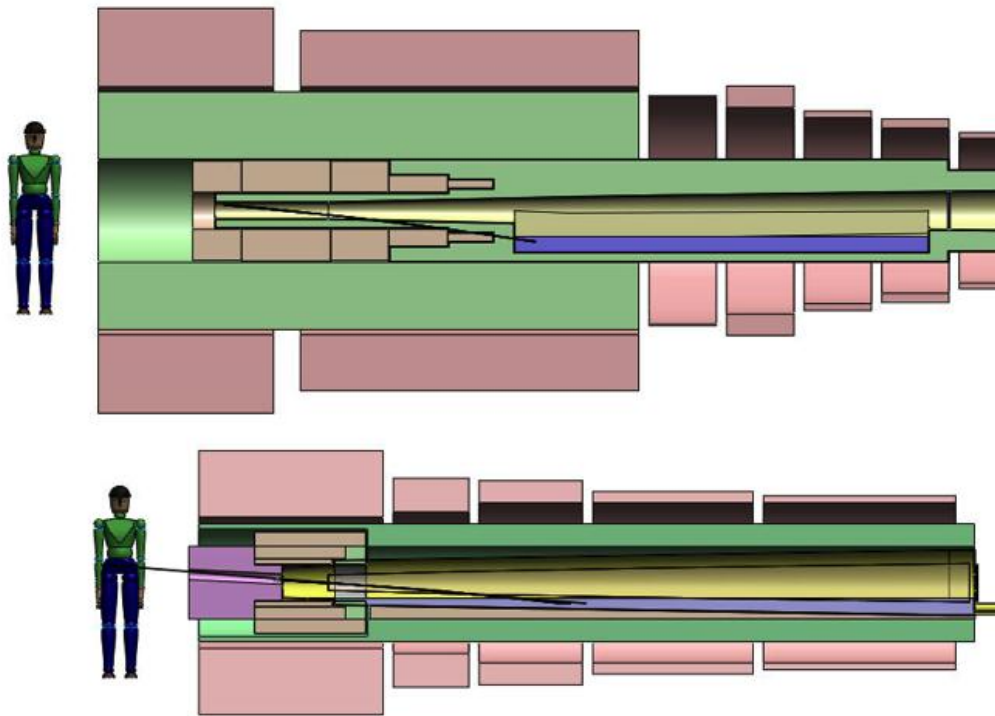
Figure 2: Comparison of present vision of the target system (top) with that of Neutrino Factory Study II (bottom).

Maximal production of low-energy pions is obtained with a proton beam of 1–2 mm (rms) radius and a target of radius 2.5 times this, such that the secondaries exit the side of the target rather than its end [3]. The resulting high density of energy deposition in the target makes it questionable whether any passive solid target could survive at 4-MW beam power. Schemes for a set of moving solid targets are not easily compatible with the surrounding solenoid magnets. Hence, the baseline target concept is for a free liquid jet target,[1] in particular mercury. The present baseline parameters of the target are summarized in Table 2.

Table 2: Baseline target-system parameters

Target type	Free mercury jet
Jet diameter [mm]	8
Jet velocity [m/s]	20
Jet/solenoid-axis angle [mrad]	96
Proton-beam/solenoid-axis angle [mrad]	96
Proton-beam/jet angle [mrad]	27
Capture solenoid field strength [T]	20
Front-end π/μ transport channel field strength [T]	1.5
Length of transition between 20 T and 1.5 T [m]	15

---

[1] A free-liquid jet is chosen because the intense pressure waves in a liquid target due to a pulsed beam lead to damage/failure of any pipe that contains the liquid in the interaction region.

The target itself is a free liquid mercury jet ($Z = 80$, $A = 200.6$, density $\rho = 13.5$ g/cm^3, $\lambda_I \approx 15$ cm) of diameter $d = 8$ mm, flowing at $v = 20$ m/s. The volume flow rate is 1 L/s, and the mechanical power in the flowing jet is 2.7 kW. The flow speed of 20 m/s ensures that the gravitational curvature of the jet over 2 interaction lengths (30 cm) is negligible compared with its diameter, and that more than 2 interaction lengths of new target material are presented to the beam every cycle of 20 ms (at 50 Hz[2]).

This target concept has been validated by R&D over the past decade, culminating in the so-called MERIT experiment [4] that ran in the Fall of 2007 at the CERN PS. The experiment benefited from the intensity of the beam pulses (up to 30×10^{12} ppp) and the flexible beam structure available for the extracted PS proton beam. Key experimental results include demonstration that [5]:

- The magnetic field of the solenoid greatly mitigates both the extent of the disruption of the mercury and the velocity of the ejected mercury after interception of the proton beam. The disruption (see Fig. 3) of a 20-m/s mercury jet in a 20-T field is sufficiently limited that operation up to 70 Hz should be feasible without loss of secondary particle production.
- Individual beam pulses with energies up to 115 kJ can be safely accommodated.
- Subsequent proton beam pulses separated by up to 350 μs have the same efficiency for secondary particle production as does the initial pulse.
- Two beam pulses separated by more than 6 μs disrupt the mercury independently.
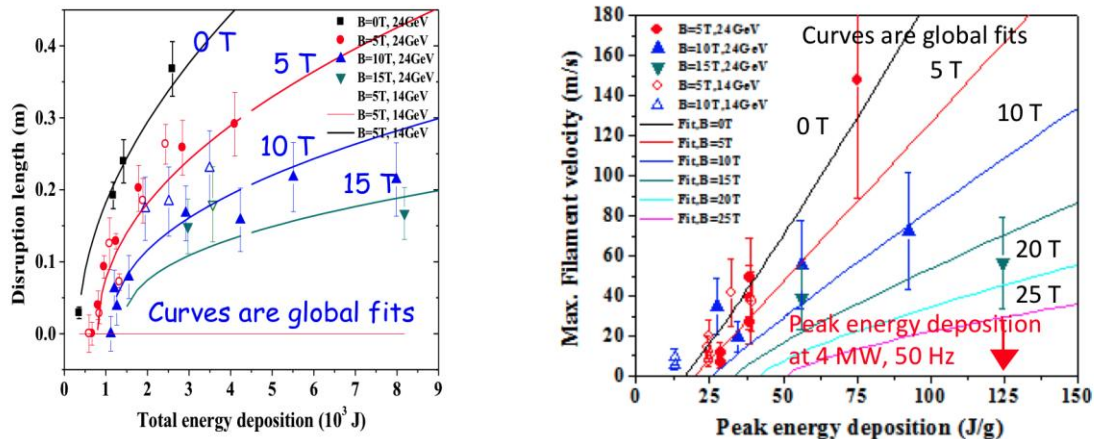
Figure 3: Disruption length vs. total energy position (left) and filament velocity vs. peak energy deposition as observed in a free mercury jet in the MERIT experiment.

As illustrated in Fig. 1, the mercury jet is collected in a pool inside the solenoid magnet channel that also serves as the proton beam dump. Disruption of this pool by the mercury jet (whose mechanical power is 2.7 kW) and by the noninteracting part of the proton beam is nontrivial, and needs further study.

The superconducting magnets of the target system must be shielded against the heat and the radiation damage caused by secondary particles from the target (and beam dump). A high-density shield is favored to minimize the inner radii of the magnets.

---

[2] The higher repetition rate specified here is to maintain compatibility with Neutrino Factory parameters.

102

The baseline shield concept is for water-cooled tungsten-carbide beads inside a stainless steel vessel (of complex shape, as sketched in Fig. 2).

The magnets of the target system vary in strength from 20 T down to 1.5 T in the subsequent constant-field transport channel,[3] with a corresponding increase in the radius of the capture channel from 7.5 cm to 30 cm.

A 20-T field is beyond the capability of Nb_3Sn, so the 20-T coil set is proposed as a hybrid of a 15-T superconducting coil outsert with a 5-T hollow-core copper solenoid insert. A 45-T solenoid with this type of construction has been operational since 2000 at the National High Magnetic Field Laboratory [6], and a 19-T magnet of this type, with 16-cm-diameter bore, exists at the Grenoble High Magnetic Field Laboratory [7] (and was used in an earlier phase [8] of our R&D program). A topic for further study is possible fabrication of the 20-T magnet with high-T_C superconductor and no copper solenoid insert, which could provide more space for internal shielding of the superconducting coils and/or permit operation at a higher field for improved capture of the initial beam.

The target system (and also the subsequent π/μ solenoid transport channel) will be subject to considerable activation, such that once beam has arrived on target all subsequent maintenance must be performed by remote-handling equipment. The infrastructure associated with the target hall, its remote-handling equipment, and hot-cells for eventual processing of activated materials, may well be the dominant cost of the target system.

3.6.2 References

1. M.M. Alsharo'a *et al., Status of Neutrino Factory and Muon Collider Research and Development and Future Plans*, Phys. Rev. ST Accel. Beams **6**, 081001 (2003), http://puhep1.princeton.edu/~mcdonald/examples/accel/alsharoa_prstab_6_081001_03.pdf.
2. S. Ozaki *et al.*, *Feasibility Study II of a Muon-Based Neutrino Source* (June 14, 2001), http://www.cap.bnl.gov/mumu/studyii/FS2-report.html.
3. X. Ding *et al., A Pion Production and Capture System for a 4 MW Target Station*, IPAC10, http://www.hep.princeton.edu/~mcdonald/mumu/target/ipac10/thpec092.pdf.
4. J.R.J. Bennett *et al., Studies of a Target System for a 4-MW, 24 GeV Proton Beam, proposal to the ISOLDE and Neutron Time-of-Flight Experiments Committee*, CERN-INTC-P-186 (April 26, 2004), http://www.hep.princeton.edu/~mcdonald/mumu/target/cern_proposal.pdf.
5. K.T. McDonald *et al., The MERIT High-Power Target Experiment at the CERN PS*, PAC09, http://www.hep.princeton.edu/~mcdonald/mumu/target/pac09/tu4gri03.pdf.
6. 45-T Hybrid, NHMFL, http://www.magnet.fsu.edu/mediacenter/features/meetthemagnets/hybrid.html.
7. Magnet M8, GHMFL, http://ghmfl.grenoble.cnrs.fr/spip.php?rubrique77&lang=en.
8. A. Fabich, *High Power Proton Beam Shocks and Magnetohydrodynamics in a Mercury Jet Target for a Neutrino Factory,* Ph.D. thesis (U. Vienna, Nov. 2002), http://www.hep.princeton.edu/~mcdonald/mumu/target/thesis-2002-038.pdf.

---

[3] The target system is defined to end where the subsequent constant-field capture channel begins, at $z = 15$ m downstream of the downstream end of the beam-jet interaction region ($z = 0$).

3.7   MuCool R&D

Y. Torun[#], D. Huang, IIT, Chicago, IL
J. Norem, ANL, Argonne, IL
Robert B. Palmer, Diktys Stratakis, BNL, Upton, NY
A. Bross, M. Chung, A. Jansson, A. Moretti, K. Yonehara, Fermilab, Batavia, IL
D. Li, LBNL, Berkeley, California
R. Rimmer, TJNL, Newport News, Virginia

[#]Mail to: torun@iit.edu

3.7.1   Introduction

MuCool is an R&D program at Fermilab to develop ionization cooling components. A crucial challenge for the design of Neutrino Factory and Muon Collider front end and cooling channels is the operation of high-gradient normal-conducting RF (NCRF) cavities in the presence of high magnetic fields which are used for focusing the muon beams. This problem has been the focus of the MuCool program [1]. It was found that the safe operating gradient limit degrades significantly [2] when a NCRF cavity is operated in an external magnetic field, dropping by as much as a factor of two at 2 T (typical of the magnetic field strength in a cooling channel lattice). This effect is believed to be linked to field emission from the cavity surface due to field enhancement around sharp features [3].

In order to address this problem, four approaches are being investigated in the MuCool program. The first is to suppress field emission by processing the NCRF copper cavities using superconducting RF (SCRF) or more advanced techniques. This has been done in MuCool for a 201 MHz copper cavity with promising results [4]. A new concept in processing for SCRF that can, in principle, also be applied to NCRF is Atomic Layer Deposition (ALD) [5]. Initial tests of a superconducting cavity coated with 5 nm of ZrO_2 plus 30 nm of Pt were performed at Jlab. The ALD treatment greatly reduced the dark current while maintaining the achievable cavity gradient. The next step will be to operate a similarly treated normal conducting cavity in a magnetic field in order to evaluate its resistance to breakdown. The second approach is to investigate materials other than copper for the construction of the cavity. Materials such as Be [6] may be less susceptible to the otherwise damaging breakdown events seen when copper cavities are operated in magnetic field.

The third approach for abating the magnetic field effect is to avoid the magnetic focusing. In this case, an open-cell geometry is required and additional coils are used in the lattice to modify the *B* field direction at the cavities and thus eliminate the *B* field focusing effect. However, the open-cell structure does mean that roughly twice the power is needed to reach the same on-axis accelerating gradient.

The fourth approach to dealing with the magnetic field effect is to operate RF cavities filled with high-pressure H_2 gas [7, 8]. Initial tests of this concept [9] are encouraging, and such a cavity has recently been operated with beam. In pure hydrogen, ionization electrons will remain in the gas for a significant portion of the RF pulse, being accelerated back and forth by the RF fields. This process can then transfer the electromagnetic energy stored in the cavity to the gas through collisions.

3.7.2 The MuCool Test Area

The MuCool Test Area (MTA) is a dedicated facility built at Fermilab to support technology development for muon ionization cooling channels. The facility is shown schematically in Fig. 1, where the service building (cryogenics plant) is in the lower center, the access pit center right and the MTA hall in the upper right. The facility now provides the following resources:

- 20' x 40' experimental hall with radiation protection (for component x-ray emission and beam experiments)
- 201 MHz (4.5 MW) and 805 MHz (12 MW) RF power
- LHe plant with 385 W capacity and a distribution system for both LHe and LN_2
- H_2 safety systems for the operation of both high-pressure gaseous devices and LH_2 storage vessels for absorber studies
- 400 MeV high-intensity proton beam from the Fermilab linac
- Radiation detectors consisting of ionization counters, plastic scintillation counters and a crystal scintillation counter
- A class 100 (or better) clean room [Note: The MTA hall itself is kept at better than class 2000 with HEPA filtered make-up air.]
- Additional diagnostics including vacuum instrumentation and optical fiber probes with spectroscopic analysis capability.

A recent photograph of the MTA hall is shown in Fig. 2. In this picture, you can see the 5 T superconducting magnet, the 805 MHz waveguide power feed into the box cavity (see below) that is inserted into the magnet and then downstream of the magnet, the 201 MHz cavity on its platform inside the clean room.
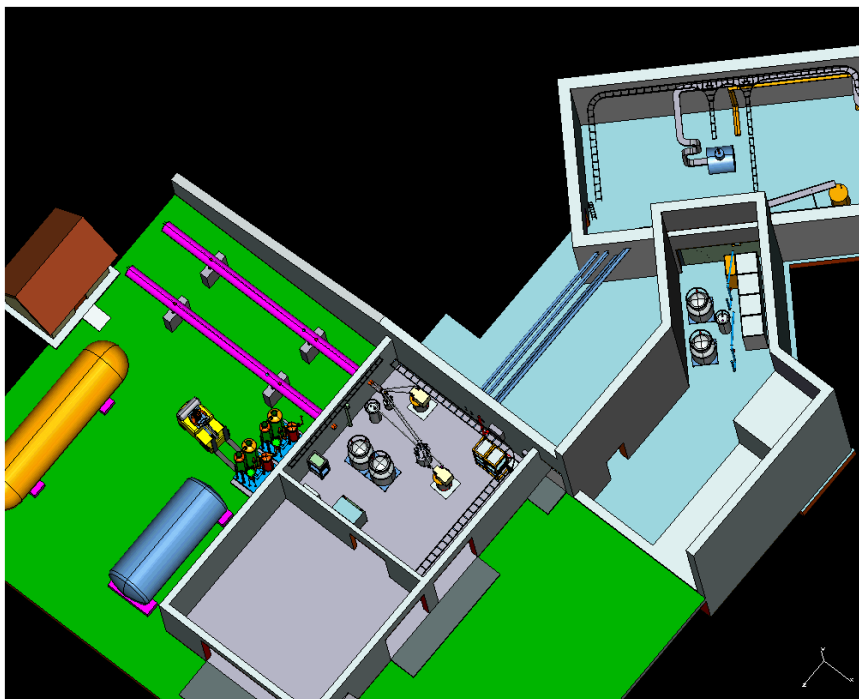
Figure 1: Schematic of the MuCool Test Area.
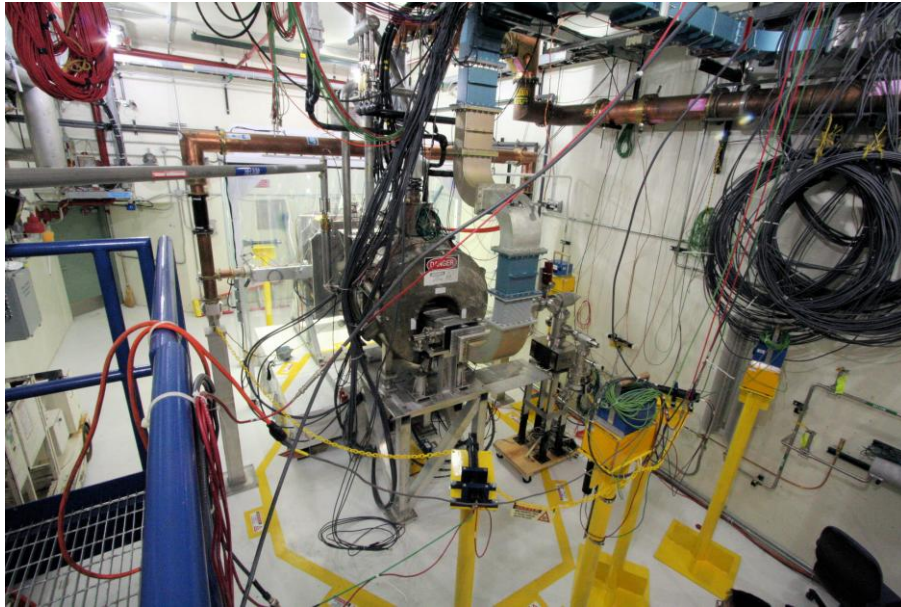
Figure 2: A recent snapshot of the MTA hall.

3.7.2.1 *MTA Cryogenics Plant*

The cryogenics plant [10] for the MTA is needed to supply cryogens for supporting operation of the superconducting magnets in the experiment hall, and enables testing of various types of liquid-hydrogen absorbers. Two Sullair compressors have been commissioned (with one used as backup for additional reliability of the system) as well as a 385 W LHe refrigerator, which provides a fill capacity of 72 L/hr. Eventually, a second LHe refrigerator can be added to increase the cooling capacity for the needs of future experiments. Figure 3 shows the MTA refrigerator room. Since March 2010, the plant has been used successfully to operate the 5 T superconducting solenoid. In the past, this magnet has only been run in "batch-mode" off LHe dewars.

Figure 3: MTA refrigerator room.

Figure 4 shows a schematic of the MTA hall that includes the cryogen valve/distribution box (pink) in relation to the 5 T solenoid (blue). In white is shown the eventual location of the 2.5 T large-bore solenoid [11] that will be used for future studies of a 201 MHz cavity in high magnetic field. This magnet is expected to be delivered to Fermilab in fiscal year 2013.
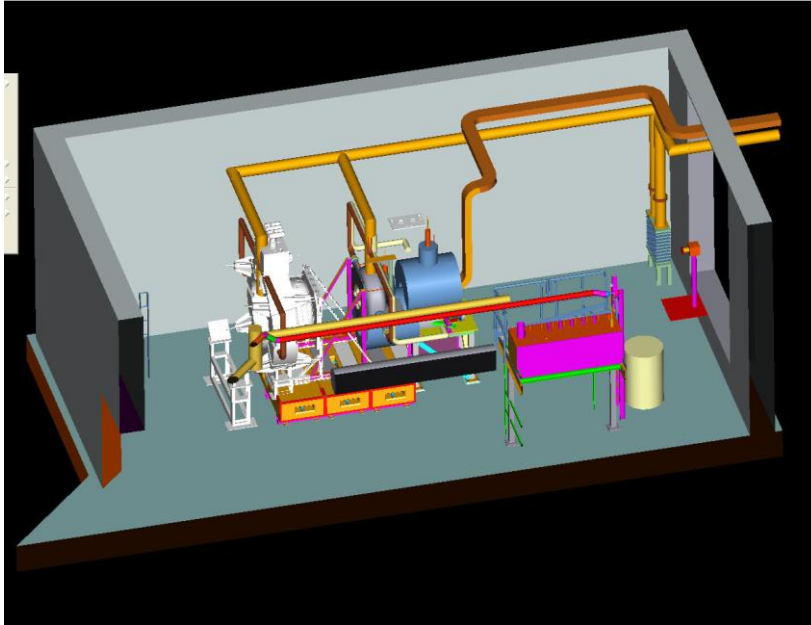
Figure 4: Schematic of MTA hall.

3.7.2.2 *MTA Beam Line*

The beam line coming into the MTA uses a primary, 400 MeV H^- beam extracted directly from the Fermilab Linac [12]. The MTA was envisioned to accept the full linac beam intensity (1.6×10^{13} protons @ 15 Hz). However, in order to meet radiological limits, initial experiments will use much lower integrated intensity. This is driven by the current state of the shielding and certain control issues. Installation and commissioning of the beam line is complete. In addition to providing beam to experiments in the MTA, this beam line will also allow for a measurement of the emittance of the Linac beam. Instrumentation for this purpose has been installed in the section of the beam line that is in the tunnel stub leading into the MTA hall (see Fig. 5). The first experiment with the beam was for testing an H_2-filled RF cavity.
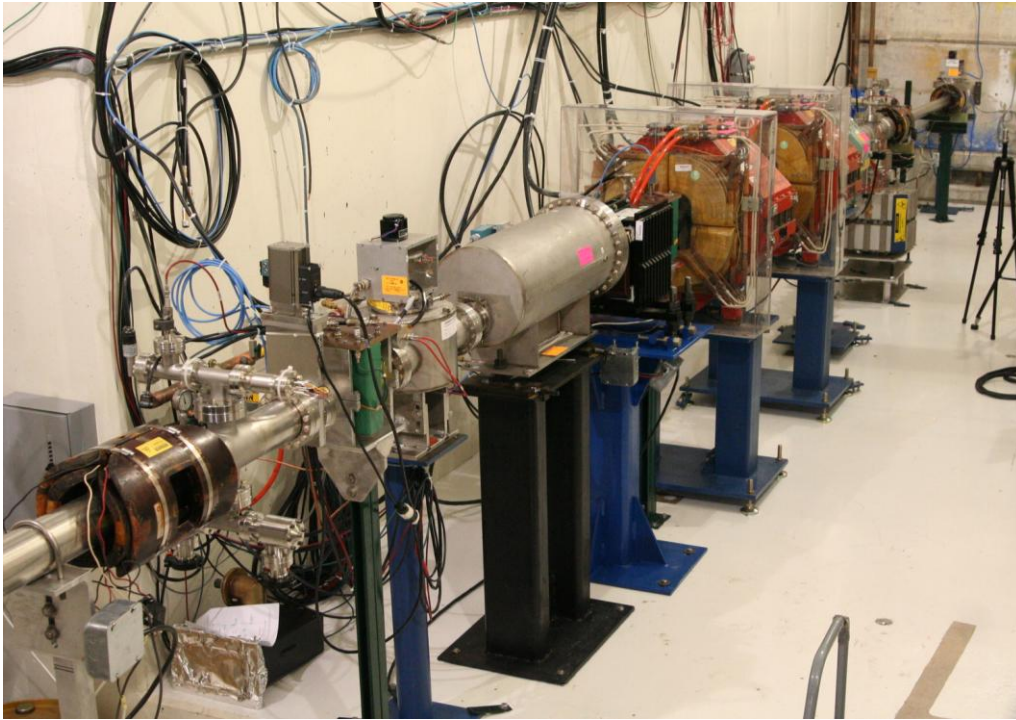
Figure 5: MTA beam line section in MTA hall stub.

3.7.3   The RF Program

As mentioned in the introduction, the MuCool RF program seeks to mitigate the deleterious effects of operating NCRF cavities in a magnetic field. External magnetic fields can significantly modify the performance of RF cavities by deflecting and focusing electrons coming off the surface at field-emission sites or changing the dynamics of plasma spots that might form near the surface:

- When the external magnetic field, B_{ext} is parallel to the RF electric field, E_{RF}, electrons can ride the magnetic field lines in the accelerating gap and cause damage on the surface due to the focused current density
- When $B_{ext} \perp E_{RF}$ electrons can be deflected into grazing angles to the surface before they can be accelerated by the electric field [13]

The MuCool program is studying four approaches to mitigate the B field problem:

1. Surface processing utilizing SCRF techniques and/or Atomic Layer Deposition (ALD)
2. Material studies
3. Magnetic Insulation
4. Operation of cavities with high-pressure H_2 gas

Work continues in all these areas but in the following sections, we will elaborate only on our recent work on magnetic insulation and high-pressure H_2-gas-filled cavities [14, 15].

3.7.3.1   *Magnetic Insulation*

A first round of tests on magnetic insulation using an 805 MHz rectangular box cavity [15] has been performed and operation at about 33 MV/m was demonstrated in a 3 T field.

3.7.3.1.1 Cavity Geometry

A rectangular geometry was chosen for the test cavity to allow for fast fabrication and to simplify analysis. The cavity assembly is shown in Fig. 6. The interior dimensions are $276.5 \times 250 \times 123.8$ mm. The cavity was made of 101 OFE copper plates, 25.4-mm thick top and bottom (horizontal), 19-mm thick on 3 of the vertical sides and 12.7-mm thick on the fourth (the one with the coupling aperture). The plates were electropolished for a very smooth finish. A rectangular coupling aperture with rounded edges was machined into one of the vertical side plates and a coupling cell was built to match the power coupler to a WR975 waveguide. The peak field at the aperture is about a quarter of that in the cavity. Interior parts and the aperture were machined to a 32 μ-inch finish. Two hydrogen brazing cycles were required to complete the fabrication. A special compound curved waveguide vacuum tin seal was designed to attach the cavity to the waveguide coupler. At the design gradient of 50 MV/m with 4 MW of peak power, the average power dissipation is expected to be 5 kW, about half of it split equally across the top and bottom plates and the other half distributed equally among the four vertical sides. Cooling tubes were drilled into the top and bottom plates and connected to a chilled de-ionized water system. Three CF flange tubes were installed on the vertical side opposite the coupling aperture for RF pickups and optical diagnostics.

3.7.3.1.2 Operation

The resonant frequency and Q of the cavity were measured as 805.34 MHz and 2.74×10^4, respectively. The coupling factor is 0.96. The cavity was powered with 20-μs pulses at 15 Hz. Vacuum pressure was steady below 10^{-8} Torr during normal operation. A LabView based program [16] developed for use at the MuCool Test Area was used to automate the operation, although some manual intervention was required. The program monitored RF pickup and reflected power, vacuum and cavity light signals to detect breakdown, and based on these could adjust the RF power and frequency.
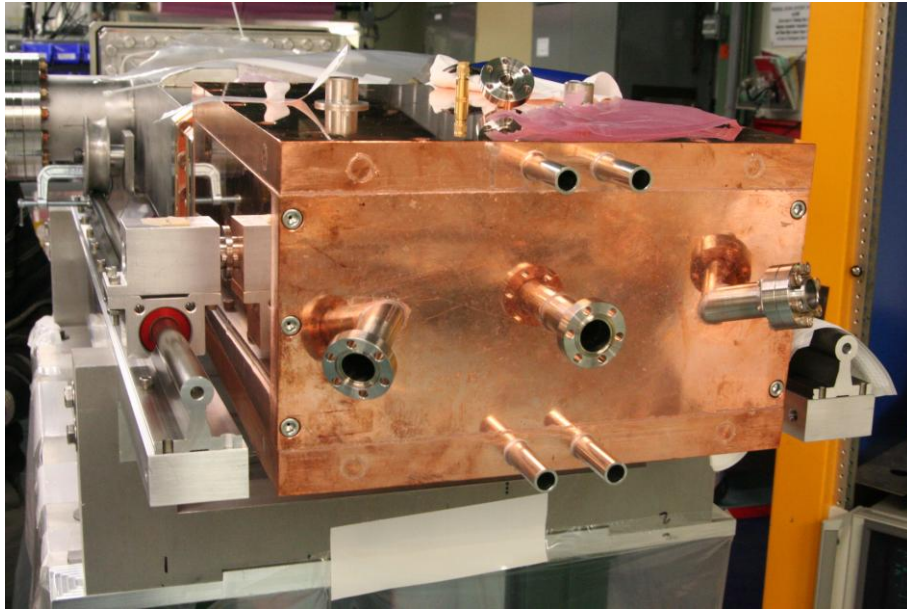
Figure 6: 805 MHz box cavity for magnetic insulation tests.

3.7.3.1.3 Results

The box cavity was first conditioned with no external magnetic field to 23 MV/m. This level was chosen to be significantly higher than the limit of stable operation observed at $B = 3$ T in the past with the 805-MHz cylindrical pillbox cavity (16 MV/m) but still quite low for $B = 0$, in order to minimize the risk of any initial damage to cavity surfaces. Next, the magnetic field was set to $B = 3$ T with the cavity in the nominal ($E_{RF} \perp B_{ext}$) configuration, the cavity was conditioned to 32.6 MV/m and operated at that level for more than 10^7 pulses. This gradient was also chosen to limit possible spark damage because of the large stored energy (over 15 J at 32.6 MV/m) before other angles were measured. The cavity can be rotated up to 12° (Fig. 7) relative to the B field axis, where modeling indicates that at this angle (12°) and at 3 T magnetic field, damage can occur for gradients as low as 15 MV/m**.**

We initially operated the cavity in a horizontal orientation in the magnet such that the electric and magnetic fields are perpendicular (90°). In this orientation, the magnetic insulation should be perfect. Afterward, a series of runs was taken with the angle set to 87, 89, 86 and 91° at $B = 3$ T, with periods of $B = 0$ conditioning to 33 MV/m in between. The maximum operating gradient with a sparking rate of less than 1 in 10^5 pulses was found to be 33 MV/m at 89, 90 and 91°, 25 MV/m at 87°, and 22.5 MV/m at 86° (all these have an uncertainty of about ±1 MV/m). These preliminary results show that magnetic insulation works to some extent, but the effect is reduced quickly away from 90°.

110
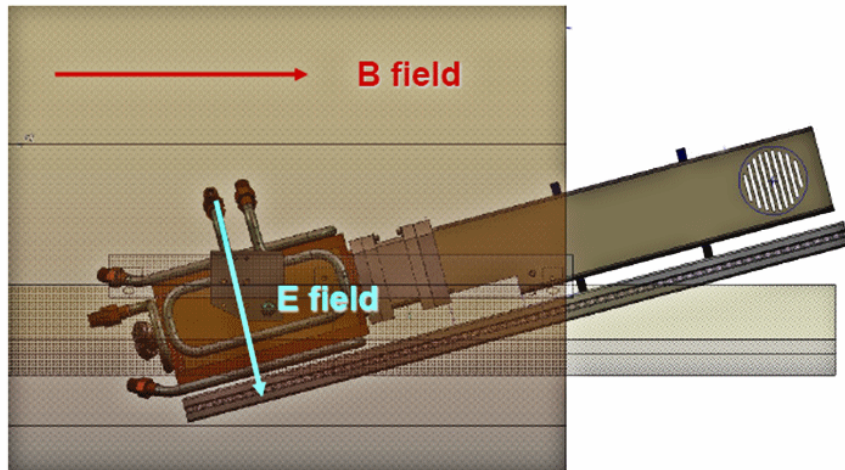
Figure 7: Box cavity set at angle to B field.

3.7.3.2   *High-Pressure H$_2$-Filled Cavity*

Since the maximum field gradient of a pressurized cavity is not affected by the external magnetic field (due to Paschen's law), the High Pressure RF (HPRF) cavity concept can provide a very compact and effective solution for the cooling channel design. One potential problem for the HPRF cavity, however, is the dissipation of significant RF power through the electrons generated from the beam-induced ionization of the insulating gas [17]. Therefore, a conclusive demonstration of the feasibility of the HPRF cavity with beam is a critical step in the Muon Collider R&D program.

3.7.3.2.1 Experimental Setup

For precise measurements of the loading effects in the HPRF cavity, it is necessary to reduce the intensity of the Fermilab linac beam by about a factor of 10. Too much beam will essentially short the cavity, making any measurements of the transient effects impossible. The beam intensity going through the cavity can be controlled by inserting a collimator in front of the cavity and changing the spot size of the beam itself and the hole size of the collimator. The beam spot size is adjusted by changing the focusing strength of the final quadrupole triplet in the MTA beam line, and the collimators with different hole size (1, 2, and 3 mm in radius) can be swapped in. The collimator used for this test is composed of two 6-inch diameter cylindrical pieces of steel that are arranged to sit inside the support system that, in turn, sits on the two parallel rails (see Fig. 8). The support system has several set screws for accurate alignment. The front cylinder is 10 cm thick and has a 1-cm-radius hole in the center. This front piece will catch the back splash from the actual collimator behind. The second piece is 20 cm thick and has a hole in the center that does the actual collimation. Moreover, there is a hook structure welded on each of these pieces so that they can be easily lifted out and handled remotely. Since some of the full-energy protons may pass through the cavity, it is necessary to have a beam stop behind the cavity. The beam stop is essentially a 6-inch diameter cylindrical piece of steel, but was modified to accommodate a coaxial pipe that feeds the RF power from the waveguide. To minimize further scattering of the beam in the cavity wall and the electrode, the cavity was modified to remove unnecessary

materials along the beam path. Since no electrically-powered beam diagnostics are allowed within 15-ft from the HPRF cavity (due to the hydrogen safety requirements), a scintillation screen was used for aligning the beam to the collimator center (see the 5 cm ×5 cm screen mount indicated in Fig. 8). A thin plate (1 mm) of Chromox[1] was used, which is made of Al_2O_3 powder with Cr doping. The scintillation is due to the Cr activator, and the light emitted is red (> 600 nm) with a decay time of ~100 ms. A CCD camera located 15 ft away from the screen was used to detect the light intensity. It was equipped with a telephoto lens having a focal length of 200 mm and a neutral density filter to attenuate the signal (reduce the light output from the screen) to within the dynamic range of the camera.
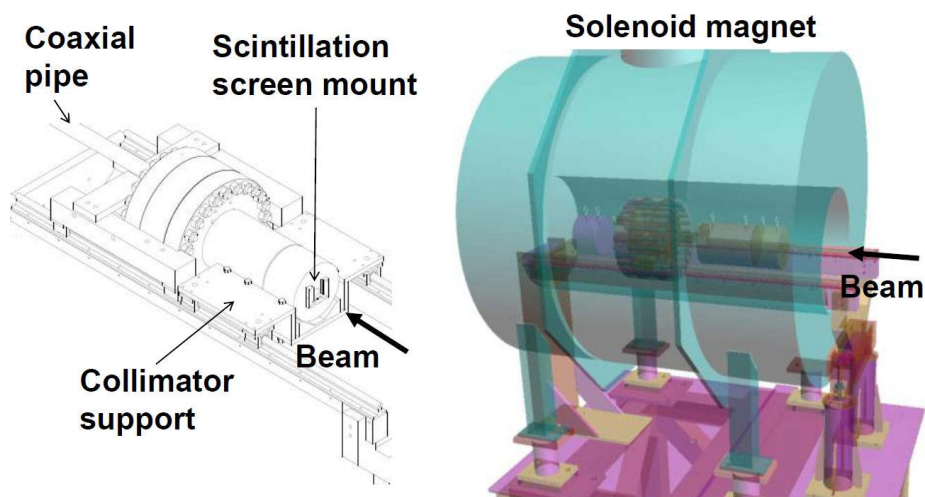
Figure 8: A CAD drawing of the collimator-cavity assembly (left) and a 3D illustration of its installation inside the magnet (right).

3.7.3.2.2 Operation

The main scanning parameters for the beam test include the field gradient (E_0), gas pressure (P), and beam intensity. The beam intensity determines the electron generation rate, whereas the ratio E_0/P determines the equilibrium electron temperature, which in turn affects the recombination and attachment rates for electron evolution. The cavity was recently (July-August 2011) exposed to beam and data were taken in a variety of settings to explore RF gradient (0–30 MV/m), gas pressure (500–950 psi) and beam intensity dependence as well as the effect of dopants (NH_3 and SF_6). The main diagnostics for the beam test were the RF signals including forward and reflected waveforms and a field pickup inside the cavity. A circulator with a matched load was used in the waveguide in order to reduce spurious reflections. The low-level RF system was triggered by the linac clock and the timing delay adjusted such that the beam pulse would arrive after the maximum RF amplitude was reached in the cavity. Since the resonance frequency of the HPRF cavity depends on the gas pressure, and thus generally differs from the linac klystron frequency, the klystron cannot be phase locked to the beam. Most of the data were taken using an 8-μs beam pulse within a 40-μs RF

---

[1] The Chromox screen is one of the most widely used screens in proton machines because of its mechanical robustness, reasonable sensitivity and spatial resolution (~100 μm), and fairly long lifetime.

pulse; longer beam and RF pulses were also explored. Light from inside the cavity was brought out through optical fiber feed-throughs, detected by photomultiplier tubes, and analyzed by a spectrometer.

3.7.3.2.3 Results

A sample set of waveforms is shown in Fig. 9. Detailed analysis of the data is in progress but the following preliminary observations are supported. No beam-induced breakdown in the cavity was seen, the field in the cavity started to recover right after the beam passed and was fully restored by the next RF pulse (while running at a rep rate of 15 Hz). The ratio of equilibrium beam-on to beam-off amplitude decreased at higher beam intensity and increased at higher pressure and with doping. These features suggest various potential ways to overcome the effect of cavity loading due to beam-induced ionization and a follow-up experiment is already being planned.
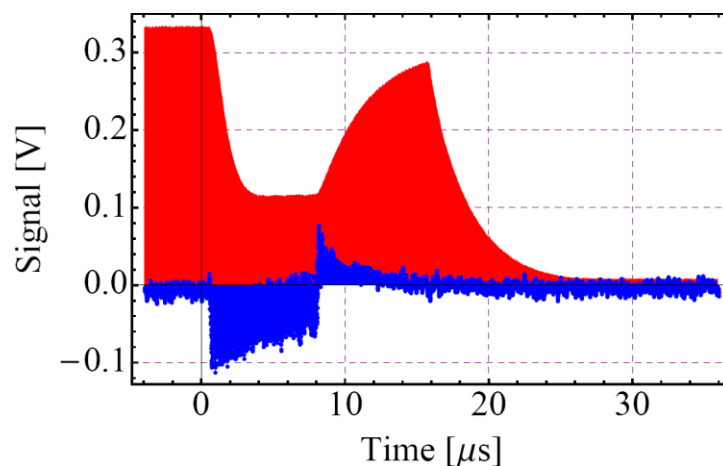
Figure 9: A snapshot showing the toroid (blue) and RF pickup (red) signal envelopes. Note the drop in RF field amplitude due to loading during the beam pulse and recovery after the beam is off.

3.7.4 Outlook

Several other upcoming tests are not covered here. The 805-MHz pillbox cavity that was used for studying magnetic field dependence, thin curved windows, and materials, will soon be operated with Be inserts in the MTA solenoid. Another 805-MHz pillbox cavity that was designed with flat endplates and for operation both under vacuum and with high-pressure gas [18] was recently powered under vacuum up to about 16 MV/m and will be commissioned to 25 MV/m. Further tests are envisioned using Be end walls and in magnetic field. The 201-MHz pillbox cavity has been partially disassembled and some damage was observed in the power couplers. New couplers with improved design will be built and tested.

A rich experimental R&D program is being carried out at the Fermilab MuCool Test Area to explore potential solutions to RF cavity operation in magnetic fields. This effort is expected to lead to a practical technology for muon ionization cooling in the near future.

3.7.5   References

1. J. Norem, *et al.,* "Recent RF Results from the MuCool Test Area", Proceedings of PAC07, Albuquerque, USA, Jun. 2007, WEPMN090, pg. 2239.
2. A. Moretti, *et al.,* "Effects of High Solenoidal Magnetic Fields on RF Accelerating cavities", Phys. Rev. ST Accel. Beams 8, 072001 (2005).
3. J. Norem, *et al.,* "Dark Current, Breakdown and Magnetic Field Effects in a Multicell 805 MHz Cavity", Phys. Rev. ST Accel. Beams 6, 072001 (2003).
4. D. Huang *et al.,* "RF Studies at Fermilab MuCool Test Area," Proc. PAC09, Vancouver, Canada, May 2009, TU5PFP032, pg. 888.
5. J. Norem *et al.,* "Results from Atomic Layer Deposition and Tunneling Spectroscopy for Superconducting RF Cavities," in the Proceedings of 11th European Particle Accelerator Conference (EPAC 08), Magazzini del Cotone, Genoa, Italy, 23-27 Jun 2008, pp WEPP099.
6. R. Palmer *et al.,* "RF breakdown with external magnetic fields in 201 and 805 MHz cavities", Phys. Rev. ST Accel. Beams 12, 031002 (2009).
7. P. Hanlet *et al.,* "High Pressure RF Cavities in Magnetic Fields," Proceedings of EPAC 2006, Edinburgh, Scotland.
8. M. Zisman *et al.,* "Alternative Muon Front-End for the International Design Study (IDS)," Proceedings of IPAC'10, Kyoto, Japan, May 2010, WEPE050, pg. 3457.
9. M. BastaniNejad *et al.,* "RF Breakdown of Metallic Surfaces in Hydrogen", Presented at Particle Accelerator Conference (PAC 09), Vancouver, Canada, May 2009, WE5PFP008, pg. 2000.
10. M. Geynisman, "Commissioning Report of the MuCool 5 Tesla Solenoid Coupled with the Helium Refrigerator", FERMILAB-TM-2462-AD, April 2010.
11. L. Wang *et al.,* "Magnetic and Cryogenic Design of the MICE Coupling Solenoid Magnet System", IEEE Trans. Appl. Supercond. 19, 1344-1347, 2009.
12. C. Johnstone *et al.*, "MuCool Test Area at Fermilab," PAC'05, Knoxville, May 2005, p. 3482.
13. R. Palmer *et al.,* "RF breakdown with external magnetic fields in 201 and 805 MHz cavities," Phys. Rev. ST Accel. Beams 12, 031002 (2009).
14. K. Yonehara *et al.,* "Study of Electron Swarm in High-Pressure Hydrogen Gas Filled RF Cavities," Proceedings of IPAC'10, Kyoto, Japan, WEPE069, pg. 3503.
15. Y. Torun *et al.,* "Rectangular Box Cavity Tests in Magnetic Field for Muon Cooling," Proceedings of IPAC'10, Kyoto, Japan, THPEA054, pg. 3795.
16. A. Kurup, Manual for the MTA 805MHz Automated Conditioning Program.
17. M. Chung *et al.,* "Beam-Induced Electron Loading Effects in High-Pressure Cavities for a Muon Collider," Proceedings of IPAC'10, Kyoto, Japan, WEPE067, pg. 3497.
18. G. Kazakevich *et al.,* "Multi-purpose 805 MHz Pillbox RF Cavity for Muon Acceleration Studies", Proceedings of PAC'11, New York, USA, TUP092.

3.8   Neutrino Factory and Muon Collider Magnets

John C. Tompkins, Fermilab, Batavia, IL 60510
Mail to: jct@fnal.gov

3.8.1   Introduction

The Neutrino Factory (NF) and Muon Collider (MC) accelerator complexes require magnets with quite challenging parameters. In particular, the cooling channel performance will be determined in part by the fields that can be reasonably delivered in

the high-field solenoids at the end of the cooling channel. The ongoing MAP magnet R&D program has been addressing:

(i) **_HTS solenoid R&D_** to assess the parameters that are likely to be achieved, including evaluation of both Bi2212 (strand/cable) and YBCO (tape) superconductors and their suitability for accelerator magnets. This work is being carried out in cooperation with VHFSMC[1], and SBIR efforts such as Muons, Inc.[2] working with Fermilab on HTS coils, and the PBL/BNL[3] YBCO solenoid development effort;

(ii) **_HCC magnet R&D_** to assess the feasibility of this type of cooling channel and possibly to build a demonstration magnet for an HCC test section;

(iii) **_Very fast ramping normal-conducting magnets_** for the later stages of acceleration;

(iv) **_Design studies for collider ring magnets_** to evaluate different solutions accommodating the large decay $e^{\pm}$ flux while maintaining field quality and structural support and, in particular, machine-detector interface requirements.

3.8.2   *High-Field Solenoids for the Cooling Channel*

Very high field solenoids with on-axis fields in excess of 30 T and apertures on the order of 50 mm are part of the initial design configuration for the MC final cooling channel. The HTS technology for such magnets has been demonstrated in the 20 T regime, but it needs to be extended to higher fields with good field quality, and with reliable construction at a reasonable cost. Thus, the goals for the HTS magnet R&D program include:

1. establish the R&D issues that must be addressed before high-field ($B > 30$ T) HTS solenoids can be built that are suitable for the low-emittance sections of a muon cooling channel, and hence

2. assess the likelihood that suitable high-field HTS solenoids will be available within the next several years and, if so, provide estimates of their likely cost and performance.

3.8.2.1   *Current Status of the R&D*

A helical cooling channel (HCC) is based on a continuous absorber and RF cavities imbedded into superconducting magnets that create solenoid, helical dipole and helical gradient field components. The HCC for the MC is divided into several sections, each with progressively stronger fields, smaller aperture and shorter helix to achieve the optimal muon cooling rate.

In FY11, a double pancake coil of 19 mm ID and 62 mm OD wound from ~30 m of 4-mm wide YBCO ($YBa_2Cu_3O_{7-x}$) tape spiral-wrapped with Kapton produced a maximum field of 18.2 T at 4.2 K in a background of 13.5 T. This corresponds to a peak current of 100% of the short-sample limit. Later, a coil made of four double pancakes was assembled. A maximum field of 21.5 T (21.2 T in the bore) was produced at 4.2 K by testing the coil package in a 14 T background field. This

---

[1]   The Very High Field Superconducting Magnet Collaboration – BNL, FSU/NHMFL-ASC, Fermilab, LANL, LBNL, NIST, NCSU, & TAMU – a DOE/ARRA funded conductor R&D program.

[2]   Muons, Inc. is an SBIR company.

[3]   PBL is Photons Beams Lasers and is an SBIR-funded company; BNL is Brookhaven National Laboratory.

corresponds to a coil self-field of ~9 T and roughly 92% of the expected short-sample limit

Double pancake sections of the HTS Helical Solenoid (HS) model made of 12 mm YBCO tape have also been tested at 77 K and 4.2 K in the SC R&D lab. Figures 1 and 2 show details of the coils and winding technique, as well as a short model assembly. Three helical double pancakes made of 12-mm-wide YBCO tape were fabricated and successfully tested at 77 K and 4.2 K, demonstrating low I_c degradation. To perform these tests, a quench detection system based on a low-noise measurement technique was developed and a quench protection system is under development.
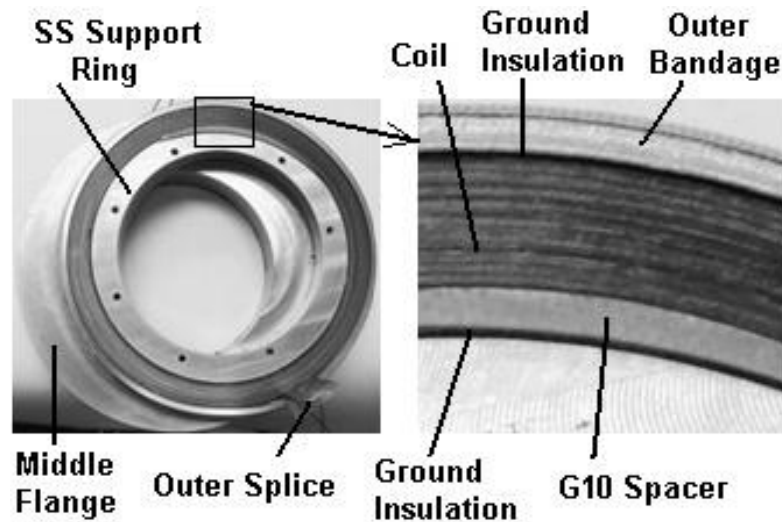
Figure 1: Side view of one coil in a pancake model.
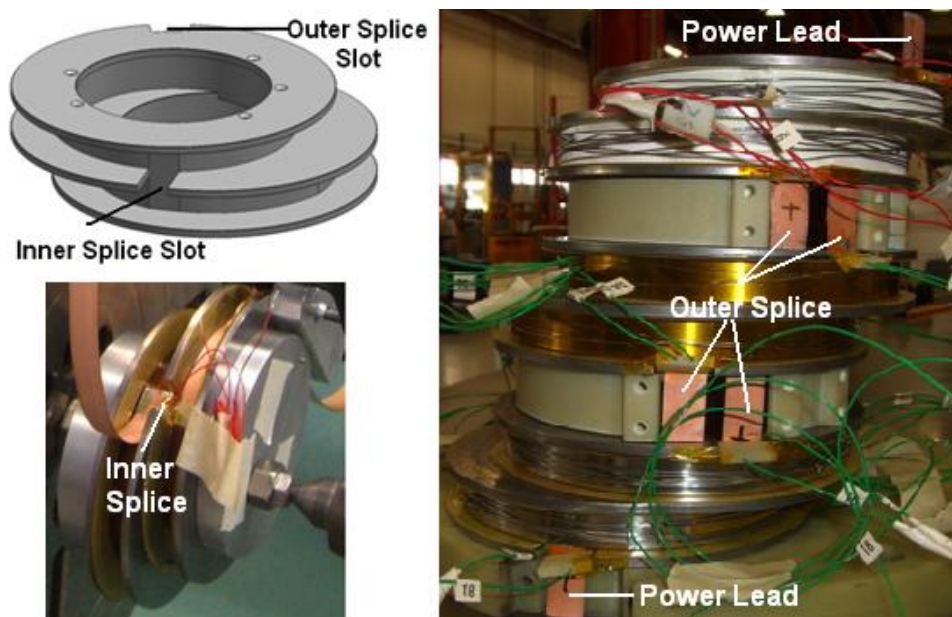
Figure 2: Left: Fabrication of a double-pancake model; Right: Short HS Model.

For the high-field section, the double-pancake unit model for a helical solenoid was designed using YBCO tape, a high temperature superconductor. Three such models were fabricated and tested at 77 K and 4.2 K. A short HS, combining three double-pancake models and two dummy cavities, was assembled and tested at 77 K [1]. The bridge joint, a critical element in the model connecting each adjacent coil, was also studied [2].

The MAP magnet program will also work closely with the ongoing YBCO-based solenoid development being carried out by PBL (an SBIR company) in collaboration with BNL and UCLA. A 'fast track' approach to a >20 T insert assembly is being pursued. A number of issues will need to be investigated, including quench protection and splice optimization; these will require additional support.

3.8.2.2   *Recent Progress of the Very High Field Superconducting Magnet Collaboration (VHFSMC)*

The MAP magnet program is working with the DOE VHFSMC program, which shares a complementary goal of developing HTS material suitable for high-field accelerator magnets. The present focus of VHFSMC is Bi2212 ($Bi_2Sr_2CaCu_2O_x$) conductor, which has several attractive features for high-field solenoids: it is made in wires that can be made into cables providing lower inductance, similar to the LTS conductors NbTi, and Nb_3Sn. We report briefly on some of the achievements of VHFSMC that have direct applicability to the MAP magnet program.

In the second year of a two-year program, VHFSMC has demonstrated success in deciphering the thermal processing ('heat treatment') of the wires and doubling the engineering current density, J_E, of Bi2212 using two industrial-scalable approaches.

Very high engineering current densities: J_E >300 A/mm^2 are require to generate the required 20–50 T fields needed for the cooling channel solenoids. A benchmark of J_E(4.2 K, 20 T) of 480 A/mm^2 was demonstrated by Oxford Superconductor in a 1 m long sample in 2004, however, more recent studies with ten VHFSMC qualification batches (2010) showed a J_E that varied from 200 to 720 A/mm^2 at 4.2 K, 5 T.

A significant effort was devoted to understanding the complex thermal process involved in reacting the wire to form the superconductor. Detailed electron microscopy studies performed on these samples revealed several key processing-property–microstructure relationships and reasons that wire property strongly varied in the qualification batches.

- Upon being heated above its peritectic temperature, Bi2212 powders melt. After melting, porosity in filaments accumulates into large bubbles that are ~20 μm in diameter and hundreds of μm long. These bubbles divide filaments into segments, despite the fact that there may be a thin Bi2212 liquid that coats the bubble [3, 4].
- The bubbles don't disappear even after Bi2212 grains start to form from the melt. They are partially filled with Bi2212 but remain as a strong critical-current-limiting mechanism [3, 4, 5].
- The J_E variation in the ten industrial VHFSMC batches was found to strongly correlate with the observed bubble density deduced from the samples quenched from the melt

A number of subsequent experiments confirmed the negative effect of bubbles on J_E. Jiang *et al*. [5] used two different approaches, cold-isostatic pressing (CIP) and

swaging, to densify the wires before heat treatment, increasing J_E(4.2 K, 5 T) of the VHFSMC wires to 810 A/mm^2.

Other VHFSMC achievements in 2010–2011 include:

- Identifying a new processing parameter and widening the heat treatment window.
- Characterizing stress-stress J_E of $Bi_2Sr_2CaCu_2O_x$ superconducting wires at 4.2 K in magnetic fields up to 16 T.
- Measuring the minimal quench energy and normal-zone propagation velocity of $Bi_2Sr_2CaCu_2O_x$ superconducting wires at 4.2 K up to 20 T.
- Testing a series of small-scale insert coils, one of which achieved 32 T (in a resistive background field of 31 T).

3.8.3 *Helical Cooling Channel Magnets*

The helical cooling channel requires a solenoid with superimposed helical dipole, quadrupole, and sextupole fields. A novel approach is to use a helical solenoid (HS) to generate the required field components. The basic concept employs short circular coils, equally spaced along the z-axis, with the center of each coil shifted in the transverse plane so as to follow the helical beam orbit. Because the orbit is tilted relative to the coils, they simultaneously generate longitudinal and transverse field components. In contrast to an earlier concept using a large bore magnet, where the longitudinal and transverse field components were controlled by independent windings, this small bore system has a fixed relation among all components for a given geometry. Thus, to obtain the necessary cooling effect, the coil must be optimized together with the beam parameters.

A series of helical solenoid magnets is being developed at Fermilab to demonstrate, in stages, the technology for muon cooling in a helical cooling channel. The first prototype magnet HSM01 was fabricated and tested in 2009 [6]. HSM01 had four coils wound from SSC NbTi cable onto stainless steel rings whose centers are offset on a helical path, and with continuous transition (no splices) between coil layers. Magnet size was limited to the largest diameter (about 25 in.) that fits in the helium vessel of the Fermilab Vertical Magnet Test Facility (VMTF). Based upon the HSM01 test results, a number of improvements were made in building the second model of very similar design, HSM02. Most notable were improved insulation and epoxy impregnation schemes, resizing of the rings and cable to pack 10 turns into each coil (37/40 turns total in HSM01/02), better lead support, protection heater placement and alignment features for magnetic field reference. Additionally, copper cooling tubes were installed around each coil to allow a test of conduction cooling. HSM02 fabrication was completed in June 2010, and the magnet was tested at the VMTF in two cold-test cycles in November and December 2010 [7-9]. To complete the test plan, magnetic field mapping at room temperature (for detailed comparison with the 3D model) is now under way.

HSM02 performance was generally improved over HSM01, and no problems occurred with coil insulation or due to inadequate superconducting lead support. The quench training profiles, however, were nearly the same, taking many quenches to reach[4] the expected maximum current. A third HSM prototype, having aluminum outer banding rings to provide pre-stress on the coils (to improve the quench training

---

[4] HSM01 reached 85% and HSM02 reached 100% of the predicted maximum current.

behavior), is considered the logical next step in this series. Future tests of the conduction-cooling scheme are contingent upon developing the appropriate cryogenic infrastructure, specifically a large vacuum vessel with the capability to supply helium to the cooling tubes, and high current power leads.
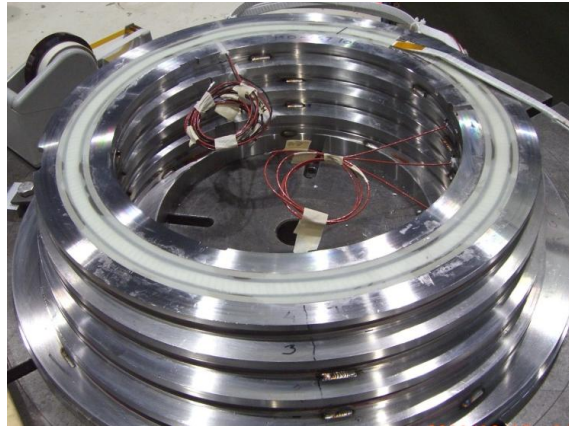
Figure 3: Helical Solenoid during fabrication.

3.8.4 Fast-Ramping Magnets

In one of the schemes for final acceleration, a pair of fast-ramping synchrotrons is employed. These require non-standard normal-conducting magnets made from grain-oriented silicon steel laminations. Several such magnets will be designed and fabricated to test the principle and to verify field quality. Two 6-mm-gap prototype dipoles will be built, the first 30 cm long and the second 6.3 m long. Thin grain-oriented silicon steel laminations are used in an EI transformer layout to minimize eddy current and hysteresis losses. OPERA-3D is being used to simulate eddy current and hysteresis losses of the EI layout, optimize magnet end shapes, and calculate sextupole fields from eddy currents.

A 400 Hz, 1.8 T test dipole with a 46 mm × 20 mm pole face and a 1.5 mm gap is currently being assembled.

3.8.5 *Collider Ring Magnets*

The collider ring will consist of arc dipoles, quadrupoles, correctors, and interaction region dipoles and quadrupoles. The arc dipoles must operate at high field in order to keep the ring circumference small, providing a larger number of crossings for a given number of stored muons. These magnets must also operate in a high-radiation and high-heat-load environment resulting from the muon decay electrons, which are preferentially swept into the magnet mid-plane. In order to avoid quenches, limit the cooling-power requirements, and maintain an acceptable magnet lifetime, the superconducting coils must be protected from excessive energy deposition due to the decay electrons. Similar considerations apply to the arc and IR quadrupoles.

A 'Mini-Workshop' on the Collider Ring Magnets was held at Fermilab in May 2011. More detailed simulations of energy deposition [10] in the arc dipoles indicated

that heat loads to the cryogenic system were far too high. Solutions presented included "open-mid-plane" designs with "block coil" configurations (Fig. 4), which created space for absorbers to intercept the decay electrons, as well as the familiar "cos θ" designs (Fig. 5), which featured an offset beam tube surrounded by an absorber to take advantage of the asymmetrical heat deposition from the decay electrons.
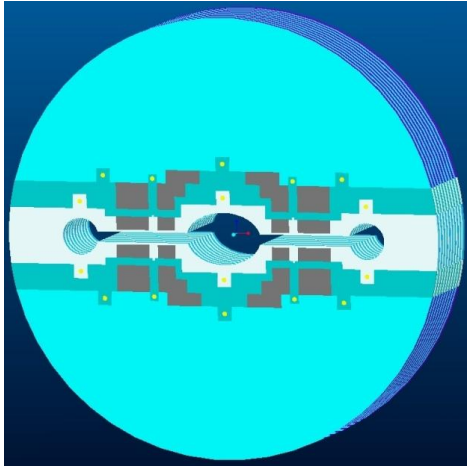
Figure 4: Open mid-plane dipole.   **Figure 5:** Cos θ dipole with offset beam tube.
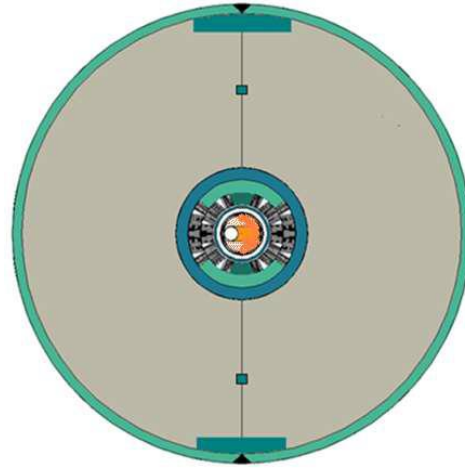
The total energy deposition in the magnets continues to be studied. An open mid-plane design with a 3 cm gap still has too high a high load from energy deposition; tracking studies indicate that a gap of at least 4 cm is needed. A novel design was suggested by Palmer that would utilize an elliptical coil cross section with a thick tungsten beam pipe and an offset aperture. No study of this option has yet been done.

3.8.6   References

1. M. Yu *et al.*, "Fabrication and Test of Helical Solenoid Short Model Based on YBCO Tape," in Proc. PAC11, New York, 2011, paper TUP153 (to be published).
2. Experimental Studies of Helical Solenoid Model based on YBCO Tape-Bridge Joints, in Proc. CEC-ICMC11, Spokane, Washington, 2011.
3. Shen T. 2010 *Ph.D. thesis* Florida State University.
4. Shen T, Jiang J, Kametani F, Trociewitz U P, Larbalestier D C, Schwartz J and Hellstrom E E 2010 *Supercond. Sci. and Technol.* **23** 025009.
5. Kametani F, Shen T, Jiang J, Scheuerlein C, Di Michiel M, Huang Y, Miao H, Parrell J A, Hellstrom E E, Larbalestier D C 2011 *Supercond. Sci. and Technol.* **24**, 075009.
6. M. Tartaglia *et al.*, "Test of Four Coil Helical Solenoid Magnet HSM01," TD-09-011, FNAL, April 2009.
7. M. Tartaglia *et al.*, "HSM02 Magnet Fabrication and Test Summary," TD note in preparation, July 2011.
8. V.S. Kashikhin *et al.*, "Four-Coil Superconducting Helical Solenoid Model for Muon Beam Cooling"; in Proc. EPAC08, Genoa, Italy.
9. M. Yu *et al.*, *"*Mechanical Analysis and Test Results of 4-Coil Superconducting Helical Solenoid Model", FERMILAB-CONF-10-568-TD.
10. N.V. Mokhov, Y.I. Alexahin, V.V. Kashikhin, S.I. Striganov, A.V. Zlobin, "Radiation Effects in a Muon Collider Ring and Dipole Magnet Protection,"Fermilab-Conf-11-095-APC-TD.

3.9   Project X R&D

Stephen D. Holmes, Fermilab, Batavia, IL 60510
Mail to: holmes@fnal.gov

3.9.1   Introduction

Project X is a high intensity proton facility being designed as the centerpiece of a world-leading U.S. Intensity Frontier program based at Fermilab. Project X is based on a 3 GeV continuous wave (CW) superconducting linac operating at an average current of 1 mA and a 3–8 GeV pulsed linac operating with a duty factor of 2–4%. The 3 GeV linac delivers a total beam power of 3 MW, the bulk of which is utilized to support a program of experimentation into the physics of rare processes. Between 2–4% of the 3 GeV beam is diverted into the 3–8 GeV linac for acceleration and injection into the Recycler/Main Injector complex in support of a long-baseline neutrino program driven by 2 MW beams from the Main Injector.

The high power linacs in Project X share many fundamental characteristics of the Proton Driver required as the front end of intense muon based facilities, e.g., a Neutrino Factory or Muon Collider. The requirements are approximately 4 MW of proton beam power at an energy in the range 5–15 GeV. However, requirements are for a very low duty factor beam, with very short, but intense, bunches. These requirements cannot be met by Project X alone, but will require some sort of beam reformatting after the linac. Self-consistent concepts for utilizing Project X as a platform for a muon facility are currently under development.

Project X is currently in the pre-conceptual design and development stage and an R&D program targeting the critical technical issues is under way.

3.9.2   Project X Mission Goals

Project X is a multi-MW proton facility being designed to support a multi-faceted Intensity Frontier program at Fermilab. Project X is an integral part of the long range strategic plan of the U.S. Department of Energy, consistent with the P5 report of May 2008 [1].

The primary mission elements assigned to Project X include:
1) Long baseline neutrinos: deliver 2 MW of proton beam power onto a neutrino production target at any energy between 60 – 120 GeV;
2) Rare processes: provide MW-class, multi-GeV proton beams supporting multiple kaon-, muon-, and neutrino-based precision experiments. Simultaneous operations of the rare processes and neutrino programs is required;
3) Muon facilities: provide a path toward a muon source for a possible future Neutrino Factory or Muon Collider;
4) Non-HEP applications: provide opportunities for implementing a program on Standard Model tests with nuclei and/or nuclear energy applications.

These mission elements establish the fundamental design criteria for Project X.

3.9.3 Project X Reference Design

The design concept for Project X has gone through several iterations, culminating in a concept designated the Project X Reference Design [2]. The Reference Design, shown schematically in Fig. 1, meets the high level design criteria listed above in an innovative and flexible manner. As already noted, the Reference Design is based on a 3 GeV CW superconducting linac, a 3–8 GeV superconducting pulsed linac, and modifications to the existing Main Injector/Recycler complex at Fermilab. The Reference Design represents a facility that will be unique in the world in its ability to deliver high power proton beams with flexible beam formats to multiple users.
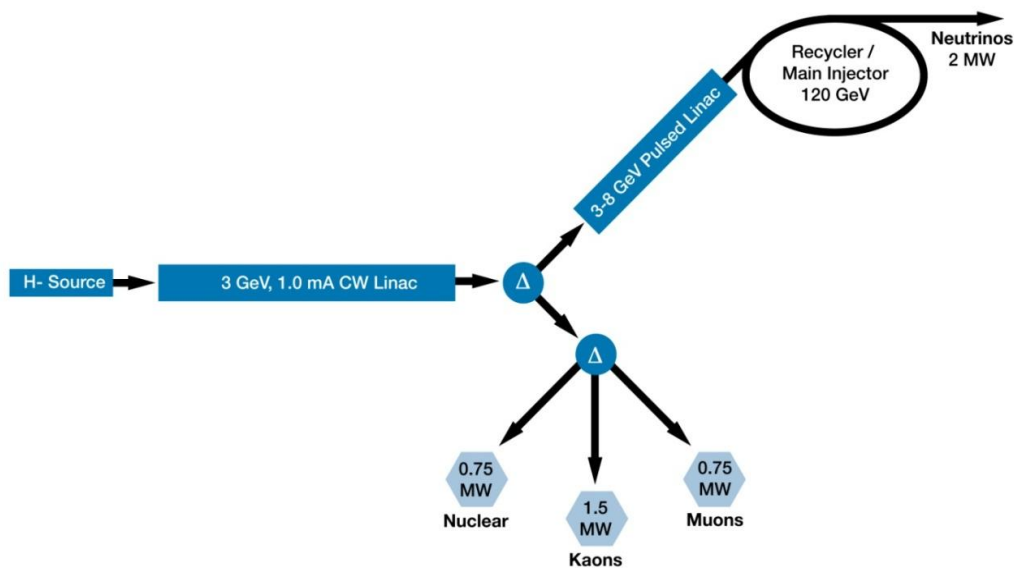
Figure 1: Project X Reference Design

The primary elements comprising the Reference Design are:
- An H⁻ source consisting of a CW ion source, 2.1 MeV RFQ, and Medium Energy Beam Transport (MEBT) line with an integrated wideband beam chopper capable of accepting or rejecting bunches in arbitrary patterns at 162.5 MHz.
- A 3 GeV superconducting linac operating in CW mode and capable of accelerating an average (averaged over >1 μs) H⁻ beam current of 1 mA, and a peak beam current (averaged over < 1 μs) of 10 mA.
- A 3 to 8 GeV pulsed linac capable of accelerating 1 mA of peak beam current at a duty factor of up to 4%.
- A pulsed dipole that can direct beam towards either the Main Injector/Recycler complex or the 3 GeV experimental areas.
- An RF beam splitter that can deliver the 3 GeV beam to multiple experimental areas.
- Modifications necessary to support 2 MW operations in the Main Injector/Recycler complex.
- All interconnecting beam lines.

3.9.4 Project X R&D Program

The Project X R&D program consists of facility design and systems optimization studies, and development of the critical underlying technologies of Project X. Foremost among the latter are the wideband chopper that provides the required bunch patterns, the system for providing multi-turn injection of H^- into the Recycler Ring, and superconducting RF development at three different frequencies. The Project X R&D program is being undertaken by a collaboration consisting of ten U.S. laboratories and universities, and four laboratories in India.

3.9.4.1   *Facility Layout*

The Project X front end consists of a CW H- source capable of delivering up to 5 mA of beam current at 30 keV, a 2.1 MeV RFQ operating at 162.5 MHz, and a wideband chopper integrated into the MEBT and capable of removing bunches in arbitrary patterns while maintaining an average current of 1 mA. The beam from the MEBT enters directly into the CW linac which is entirely superconducting. The technology layout of the linac is shown in Fig. 2. Six cavity types at three different frequencies are required to accelerate beam to 8 GeV. The details of this layout (beta functions, breakpoints, and technology) are still being optimized. However, at present, acceleration to 160 MeV is imagined to be provided by three families of spoke resonator cavities at 325 MHz, acceleration from 160 MeV to 3 GeV is via two families of elliptical cavities at 650 MHz, and acceleration from 3–8 GeV is via one family of 1300 MHz elliptical cavities. Approximately 500 superconducting cavities, contained in approximately 60 cryomodules, are required.
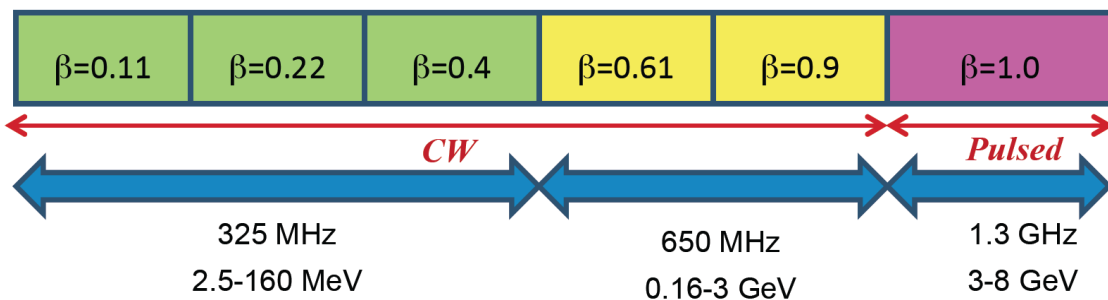
Figure 2: Project X Linac Technology Layout

3.9.4.2   *Wideband Chopper*

A key element of the Reference Design concept is the coordinated utilization of a wideband chopper at the linac front end and a transverse deflecting RF separator at the exit of the 3 GeV linac to provide different high duty factor bunch patterns to multiple users simultaneously. The transverse deflecting cavity operates at one fourth (or $n + 1/4$) of the fundamental 162.5 MHz bunch frequency of Project X. Bunches are deflected to three distinct experimental areas by the transverse cavity depending upon the phase of their arrival. By accelerating bunches in an appropriate pattern, as determined by the wideband chopper, the requisite bunch patterns can be delivered to three experiments simultaneously.

Development of the wideband chopper is a key element of the R&D program. The chopper consists of a set of four kickers, separated by 180 degrees of betatron phase in the MEBT, and a corresponding set of kicker drivers. The system is required to deliver a 1 ns rise and fall time, with a 1 ns flattop. Kicker voltages in excess of ±200 V are required and a repetition rate of 60 MHz must be supported. The criterion applied to bunch removal is that surviving H⁻ particles in a bunch that is disposed of should be less than 1×10^{-4} of the full bunch intensity. Helical transmission line structures have been developed that meet the kicker requirements, while MOSFET based wideband amplifiers are being investigated for the driver.

### 3.9.4.3 H⁻ Injection

Each 0.75 seconds, the pulsed linac is required to deliver 26 mA-ms of total beam charge to the Main Injector/Recycler complex to support 2 MW of beam power at 60–120 GeV. In the Reference Design this is supplied via six 4.4 ms pulses of 1 mA H⁻ current, repeating at 10 Hz. The H⁻ are stripped during a multi-turn injection into the Recycler. Simulations indicate that 400 turns is roughly the maximum number that can be tolerated when taking into account foil heating, emittance growth, and reasonable foil survival times. However, there would be advantages of injecting the full current directly into the Main Injector in a single 26 ms long, 1 mA, pulse – something that is not possible with standard foil techniques.

Alternative techniques under investigation include moving/rotating foils and laser assisted stripping – a technique currently under development at the Spallation Neutron Source at Oak Ridge National Laboratory.

3.9.4.4 Superconducting RF Development

A very significant superconducting RF development program has been under way for several years, utilizing resources both at Fermilab and partner laboratories [3, 4]. As noted above, six cavity shapes at three different frequencies are required for Project X. The emphasis within the program is on developing cavities with high Q_0 and modest gradients (typically 2×10^{10} and 15 MV/m) for the CW linac, and more modest Q_0 and higher gradients for the pulsed linac (typically 1×10^{10} and 25 MV/m). The pulsed linac development (1300 MHz) is most advanced at present, having strong overlap with the International Linear Collider (ILC) development program. A complete 1300 MHz cryomodule is currently under RF testing and a second cryomodule is under construction.

Development at 325 MHz is concentrated on the $\beta = 0.22$ single-spoke resonator. Figure 3 shows a cut-away view of the resonant structure (left) and the physical cavity (right). Two cavities have been built and tested, both achieving 15 MV/m with Q_0 of 1.5×10^{10} at 2 K.
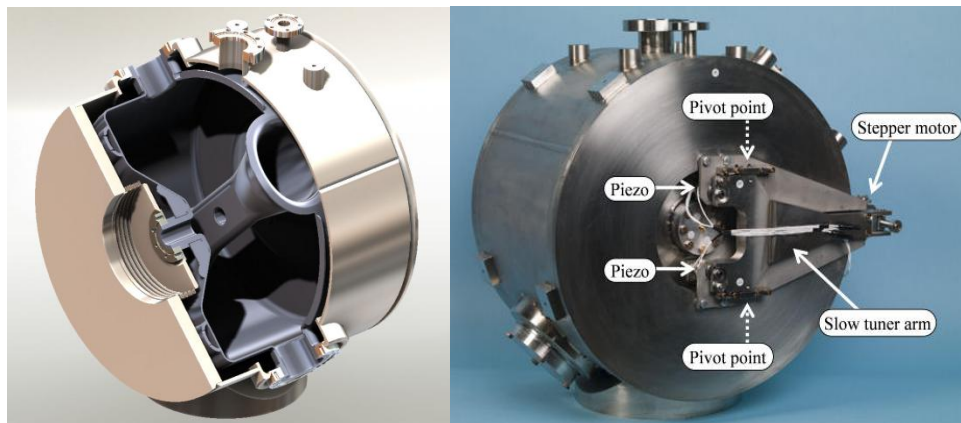
Figure 3: Single-spoke resonator at $\beta = 0.22$ and 325 MHz. Cut-away drawing (left), and physical prototype cavity (right).

The 650-MHz cavity development program is currently investigating a number of elliptical shapes, and is concentrating on single-cell tests. Preliminary indications are that Q_0 in excess of 2×10^{10} might be achievable.

In parallel significant effort is going into development of RF sources. In the CW linac, cavities will be driven by individual sources, with up to 30 kW per source required in the 650 MHz section. Solid-state sources have been identified as the preferred technology at 325 MHz, and both solid-state and inductive output tubes (IOTs) are being investigated at 650 MHz.

3.9.5   Project X as a Platform for a Muon Collider

The Muon Collider requires approximately 4 MW of beam power delivered onto a production target at an energy between 5 and 15 GeV. Furthermore, the beam should be delivered in a single bunch, with a bunch length of 2-3 nsec, at a 15 Hz repetition rate [5]. Requirements are modestly relaxed for a Neutrino Factory. It is highly desirable that the Project X Reference Design includes provisions for supporting such requirements in the longer term.

Providing the beam power and bunch structure requirements for a Muon Collider will require both an upgrade of the Project X 8 GeV beam power and additional facilities to reformat the high duty factor beam from Project X. A Task Force has been jointly sponsored by Project X and the U.S. Muon Accelerator Program (MAP) to develop a feasible concept and incorporate it into the Project X planning activities. This Task Force is asked to report by the end of 2011; however certain concepts are already being investigated.

3.9.5.1   *Beam Power at 8 GeV*

Project X naturally provides 350 kW of beam power at 8 GeV (8 GeV × 1 mA × 4.4 ms ×10 Hz). The strategy for providing 4 MW at 15 Hz, as required by the Muon Collider, is to increase the current to 5 mA, increase the pulse length to 6.7 ms, and increase the repetition rate to 15 Hz. The result is a 10% duty factor at 5 mA, or 4 MW of beam delivered from the pulsed linac at 8 GeV and 15 Hz repetition rate.

3.9.5.2 *Bunch Formatting at 8 GeV*

The beam delivered at 8 GeV must be reformatted to provide the very low duty factor required for muon facilities. It is believed that two rings will be required: 1) an accumulation ring that collects the 6.7 ms long H⁻ pulse and segregates it into roughly 4-8 bunches; and 2) a compressor ring that reduces the bunch to the required 2–3 ns. This would be followed by a "trombone" beam line that utilizes varying times of flight to deliver multiple bunches onto the production target simultaneously. This concept needs further development to establish viability. In particular, space charge effects and beam stability are very serious issues in both rings.

3.9.6 Summary

Project X is a multi-MW proton source being designed to support a world leading Intensity Frontier program at Fermilab. A Reference Design has been established that is unique in its ability to support multiple users with varying bunch pattern requirements simultaneously. An R&D program is under way, targeting the critical technical and cost issues. This program is being undertaken by a collaboration including both U.S. and Indian institutions. In the longer term, the U.S. community would like to see Project X designed in a manner that would provide a future platform for a Muon Collider or Neutrino Factory. A Task Force has been established, and concepts are being developed; however, a fully detailed concept does not yet exist. It is expected that such concepts will be developed and documented by the Task Force by the end of 2011.

3.9.7 References

1. "U.S. Particle Physics: Scientific Opportunities, A Strategic Plan for the Next Ten Years", May 2008, http://science.energy.gov/~/media/hep/pdf/files/pdfs/p5_report_06022008.pdf
2. Project X Reference Design Report, November 2010, http://projectx-docdb.fnal.gov/cgi-bin/ShowDocument?docid=776
3. T. Arkan, et al, "Superconducting RF Cryomodule Production & Testing at Fermilab", proceedings of the 2010 Linear Accelerator Conference, Tsukuba, Japan (2010). http://accelconf.web.cern.ch/AccelConf/LINAC2010/papers/tup081.pdf
4. C. Ginsburg, et al, "Superconducting RF Cavity Production Processing and Testing at Fermilab", proceedings of the 2010 Linear Accelerator Conference, Tsukuba, Japan (2010). http://accelconf.web.cern.ch/AccelConf/LINAC2010/papers/thp026.pdf
5. K. McDonald, "Target System Baseline", Muon Collider 2011, Telluride, CO https://indico.fnal.gov/getFile.py/access?contribId=69&sessionId=6&resId=0&materialId=slides&confId=4146

4   Activity Reports

4.1   Students Admitted to the Sixth International Accelerator School for Linear Colliders

Weiren Chou, Fermilab
Mail to: chou@fnal.gov

The student selection is complete for the Sixth International Accelerator School for Linear Colliders. This year's school will be held from 6 to 17 November 2011 in the Asilomar Conference Center, Pacific Grove, California, USA, continuing the tradition of cycling the school between Europe, Asia and the Americas. The focus of the school will be on accelerator science related to the next-generation TeV-scale colliders, including the International Linear Collider (ILC), the Compact Linear Collider (CLIC) and the muon collider.

This year we have again had a very large demand from many qualified applicants for the school. We selected 62 highly qualified students from a pool of 231 applicants from 51 countries. 67% were from countries that have high-energy physics programs. The country distribution of the accepted students includes 20 from Asia and Oceania, 25 from Europe and 17 from North and South America. These students will be divided among two curricula: Class A for accelerator physics and Class B for radiofrequency (RF) technology.

The organisation of the Linear Collider accelerator school is done jointly by the Global Design Effort (GDE), the Compact Linear Collider (CLIC) Study and the International Committee for Future Accelerators (ICFA) Beam Dynamics Panel. The continuing popularity and success of the school clearly indicates the important need for providing advanced training in accelerator science for the high-energy physics community. Particle physics has been responsible for much of the development of particle accelerator science because of our own need for new accelerators for our research and therefore our investment in advanced accelerator R&D.

The attendees at the LC school are graduate students, postdoctoral fellows and junior researchers from around the world, including physicists who are considering a career change from experimental physics to accelerator physics. The subjects from accelerator dynamics to superconducting RF are forward-looking in the field with many possible applications beyond the next-generation Terascale lepton colliders. The curriculum will contain an overview of the different future collider options, a lecture on linac basics and a lecture on beam instrumentation, followed by a choice of two in-depth tracks: one on electron and positron sources, damping rings, linacs and beam delivery system; and one on superconducting and warm radiofrequency technology, low-level RF and high-power RF.

We have excellent lecturers, well-qualified students, an in-depth curriculum and a beautiful site for the school. We are set to have another successful LC accelerator school this year.
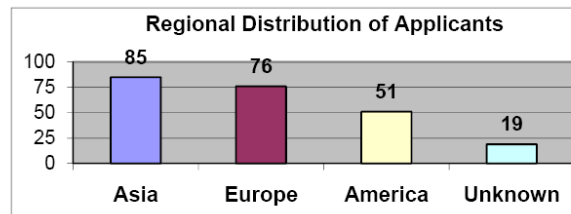
Lecturers of the 2011 LC Accelerator School

Lecture	Topic	Lecturer
I1	Introduction	Barry Barish (Caltech)
I2	ILC	Barry Barish (Caltech)
I3	CLIC	Frank Tecker (CERN)
I4	Muon collider	Robert Palmer (BNL)
A1	Linac	Daniel Schulte (CERN)
A2	Sources	John Sheppard (SLAC)
A3	Damping rings	Yunhai Cai (SLAC)
A4	Beam delivery & beam-beam	Andrei Seryi (John Adams Inst.)
B0	Beam instrumentation	Hermann Schmickler (CERN)
B1	Room temperature RF	Walter Wuensch (CERN)
B2	Superconducting RF	Shuichi Noguchi (KEK)
B3	LLRF & high power RF	Stefan Simrock (ITER)

2011 LC Accelerator School – Applicants Distribution

231 applicants from 51 countries

- 67% from 19 HEP countries
- 25% from 32 other countries
- 8% unknown

Regional Distribution of Applicants

Asia 85, Europe 76, America 51, Unknown 19

Distribution of Applicants in HEP Countries

China 16, India 35, Isreal 2, Japan 5, Korea 7, Belgium 2, Denamrk 1, France 2, Germany 5, Italy 1, Norway 1, Russia 12, South.. 4, Spain 2, Sweden 2, Switzerl.. 13, U.K. 2, Canada 1, U.S.A. 42
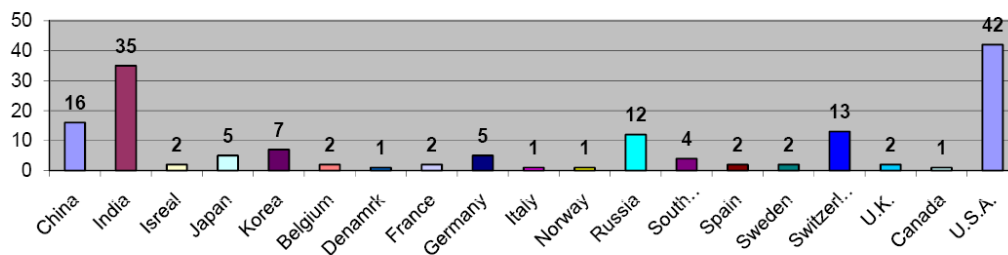
Distribution of Applicants in Other Countries

Armenia 1, Azerb.. 1, Bangl.. 2, Indon.. 1, Iran 2, Malaysia 1, Nepal 2, Pakistan 1, Saudi.. 2, Thailand 1, Turkey 3, Uzbek.. 1, Vietnam 4, Algeria 2, Belarus 2, Came.. 1, Cyprus 1, Egypt 2, Greece 1, Mada.. 1, Nigeria 3, Poland 3, Roma.. 3, Senegal 1, Slovenia 1, Ukraine 6, Brazil 2, Chile 1, Cuba 1, Ecuador 2, Mexico 1, Peru 1
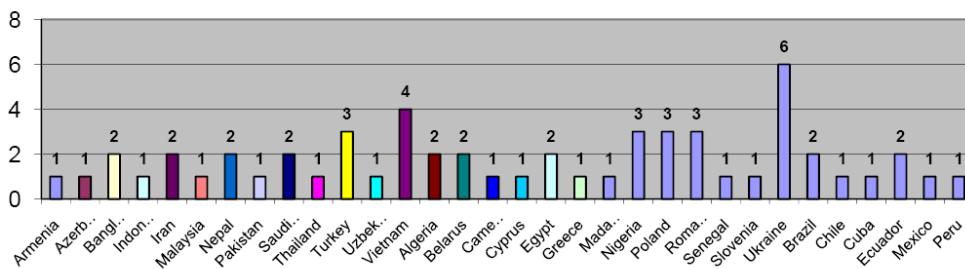
2011 LC Accelerator School – Students Distribution

• 62 students selected from 18 countries

• 92% from 14 HEP countries

• 8% from 4 other countries

Regional Distribution of Students

Asia 20, Europe 25, America 17

Country Distribution of Students

China 9, India 3, Isreal 1, Japan 2, Korea 3, Thailand 1, Turkey 1, France 1, Germany 3, Italy 1, Norway 1, Poland 2, Russia 3, Slovenia 1, Spain 2, Switzerland 9, UK 2, USA 17
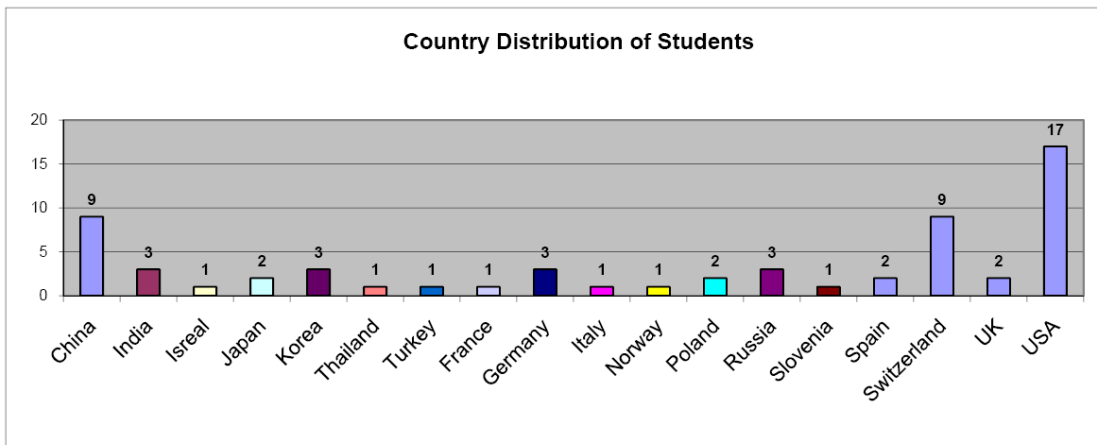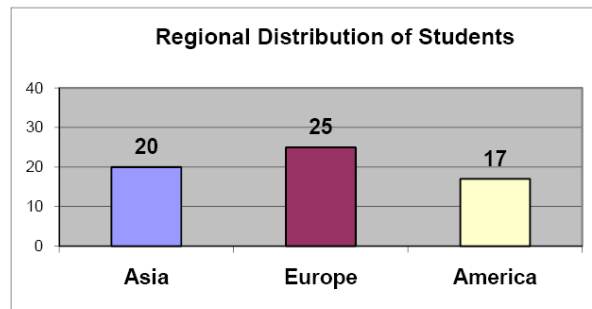
5   Workshop and Conference Reports

5.1   Update from the 15th International Conference on RF Superconductivity (SRF2011)

Bob Kephart, Fermilab
Mail to: Kephart@fnal.gov

Mike Kelly, Argonne National Laboratory
Mail to: kelly@phy.anl.gov

Nearly 400 scientists met July 25-29, 2011 in downtown Chicago for SRF2011, the 15th international conference on superconducting radio-frequency technology. SRF2011 was jointly hosted by Argonne and Fermilab with a local organizing team made up of staff from both labs. The conference continued the tradition of the 14 previous conferences and provided a lively forum for SRF scientists, engineers, students and industrial partners to present and discuss the latest developments in the science and technology of superconducting RF for particle accelerators.

The five-day meeting featured talks and poster sessions on the latest techniques for creating high performance superconducting radio-frequency systems. Contributions included topics such as cavity fabrication, testing, and repair; cavity processing; cryomodule design, and methods for controlling the radio-frequency power delivered to cavities. Scientists also discussed application of SRF technology in proposed and future projects such as the ILC, Project X, European Spallation Source, XFEL, Energy Recovery Linacs, and light sources.

The SRF2011 meeting was preceded by a three days of SRF tutorials sessions hosted by ANL and a one day meeting with international SRF industrial vendors organized by the ILC Global Design Effort.

At the conference banquet Hasan Padamsee of Cornell University gave a wonderful talk on progress in the field of RF superconductivity over the last 50 years.

The week concluded with tours of Argonne National Laboratory and of Fermilab.

"A wealth of new technical information was presented at SRF2011 underlining the vibrant and continued growth of this technology," said Fermilab's Bob Kephart who co-chaired the conference with Mike Kelly from ANL.

SRF2011 had the largest attendance of any SRF conference to date.

5.2 Update on Accelerator-Related Sessions at the Second International Conference on Technology and Instrumentation in Particle Physics (TIPP 2011)

Manfred Wendt, Fermilab
Mail to: manfred@fnal.gov

On June 9-14, 2011 the *Technology and Instrumentation in Particle Physics* (TIPP 2011) conference was held in downtown Chicago. About 480 participants discussed new technologies, trends and ideas, as well as upcoming challenges in the instrumentation of detectors for particle physics experiments, astro-particle physics and closely related fields. Beside the plenary talks and poster sessions, specialized talks were presented in 13 categorized parallel tracks. The *Machine Detector Interface and Beam Instrumentation* (MDI&BI) track had many links to accelerator technology and instrumentation. Within this track we had almost 30 presentations, which we grouped into three subcategories:

Machine Detector Interface and Background Diagnostics (14 talks)
Background and luminosity monitoring were discussed in detail during these sessions. The presentations span the instrumentation at present detectors, e.g. CDF and D0 (Tevatron), ATLAC and CMS (LHC), as well as the challenges for future machines, such as SuperKEKB and a Muon Collider. For the detection of beam losses with an excellent time resolution, an introductory talk on ionization chambers based on a diamond semiconductor technology was followed with great interest.

Primary Beam-line Diagnostics (7 talks)
This sub-session was focused on the diagnostics of proton beams in HE colliders and primary beam-lines, e.g. at LHC (CERN), NuMI and M-Test (Fermilab), and RHIC (BNL). Machine protection and beam loss monitoring (BLM) of high power

beams play a very critical role, as presented for the LHC and the NuMI beam-line. Two talks discussed new technologies for BLMs operating at cryogenic temperatures. Other topics were on the measurement of the spin polarization of proton beams, and the use of optical transition radiation (OTR) techniques to measure the transverse profile of high power proton beams.

Linear Collider Final Focus and IP Beam Diagnostics (8 talks)
Most talks in this sub-session were focused on the efforts on advanced beam diagnostics in frame of a future linear collider (LC), presenting results from the ATF2 test facility (KEK). The monitoring and control of beams with nano-meter size require new technologies, like high resolution cavity BPMs, laser interferometers, bunch-by-bunch feedback systems, etc. Also the Endstation-A at SLAC could again provide another test bed for advanced LC R&D experiments and beam diagnostics, but needs some rearrangements.

A little bit out of our MDI&BI track core mission, but very interesting, was a talk on the accurate measurements of velocity and acceleration of seismic vibrations, presenting new ideas to prevent accidents in nuclear power plants due to earth quakes.

These, as well as the all other TIPP 2011 presentations are found at: http://indico.cern.ch/conferenceTimeTable.py?confId=102998#20110608

5.3 Minutes of the Joint Meeting of the ICFA Beam Dynamics Panel and the Advanced and Novel Accelerators Panel

Weiren Chou, Fermilab, and Mitsuru Uesaka, Tokyo University
Mail to: chou@fnal.gov, uesaka@nuclear.jp

There was a joint meeting of the ICFA Beam Dynamics (BD) Panel and the Advanced and Novel Accelerators (ANA) Panel on September 7, 2011 from 18:00 to 20:30 in the Maria Cristina Room, Kursaal in San Sebastian, Spain during IPAC11. Twenty-four people attended, including 17 BD panel members or their representatives, and 7 ANA panel members or their representatives. The list of attendees is in Appendix 1 and the agenda in Appendix 2.

The meeting was chaired jointly by Weiren Chou, head of the Beam Dynamics Panel, and Mitsuru Uesaka, head of the Advanced and Novel Accelerators Panel. The format was a working dinner, kindly sponsored by the Fermi Research Alliance LLC. It was the second joint meeting between the two ICFA panels and proved to be stimulating, productive and mutually beneficial.

After a brief round-table introduction, the BD Panel welcomed four new members: Toshiyuki Okugi (KEK), George Neil (JLab), John Byrd (LBNL) and Elias Metral (CERN). The panel also expressed appreciation for the valuable service of four outgoing members: Junji Urakawa (KEK), Kwang-Je Kim (ANL), Miguel Furman (LBNL) and Alessandra Lombardi (CERN).

Weiren Chou gave a report on BD panel activities over the past two years. The Panel organized a number of ICFA Advanced Beam Dynamics Workshops (ABDWs) and mini-workshops. All ABDWs since 2006 have published proceedings via JACoW,

whereas formal proceedings are not required for the ICFA mini-workshops. The Panel published three newsletters in 2009 and three in 2010. All newsletters from no. 1 to no. 54 can be read and downloaded from the panel web site. The Panel has been organizing the annual *International Accelerator School for Linear Colliders* since 2006. The Panel together with the ANA Panel is involved in the newly formed collaboration between ICFA and ICUIL (the International Committee for Ultra Intense Lasers). A joint task force has been established between the two panels and the ICUIL.

Three working group leaders, Yoshiharu Mori (High Intensity Hadron Beams WG), Marica Biagini (High Luminosity e+e- Collider WG) and George Neil (Future Light Sources WG) presented reports on the activities of their working group and the ICFA workshops they are organizing (ERL2011, FLS2012, HB2012 and the Low Emittance Rings mini-workshop).

Ingo Hofmann reported on the ICFA-ICUIL Joint Task Force (JTF) and the first Joint Workshop last year held at GSI. The JTF presently has 16 members from the two committees and is chaired by Wim Leemans (LBNL). A JTF White Paper entitled "*High Power Laser Technology for Accelerators*," summarizing the discussions at the GSI workshop, is scheduled for publication this December. At this meeting the two panels unanimously approved a special edition of the *ICFA Beam Dynamics Newsletter* (no. 56, December 2011) for publishing the White Paper. The publication will be coordinated with the ICUIL for a synchronized announcement of the two committees. The second joint workshop will take place from September 20-22, 2011 at LBNL.

Mitsuru Uesaka gave a report on behalf of the ANA Panel. The Panel has 19 members. It organized the 68th Scottish Universities Summer School in Physics (SUSSP), which was also the 7th in the series of "*Laser-Plasma Interactions and Applications*," from August 15-27, 2011 at the University of Strathclyde. Mark Wiggins gave a detailed report on this school. The ANA Panel has started a newsletter, which is to be published once a year. Each newsletter has a theme. The next one is "*Compact accelerators for evaluation and analysis*." The editor is Chuanxiang Tang, who presented the table of contents, prospective authors and publication schedule. The ANA Panel organized a Laser and Plasma Accelerator Workshop (LPAW2011) last June in China. Patric Muggli reported on this workshop. Ryoichi Hajima discussed several new aspects in the development of advanced and novel accelerators.

Susumu Kamada, who has been in charge of the distribution and printing of the ICFA Beam Dynamics Newsletter in the Asia and Pacific region since 1988, will be retiring next year. Toshiyuki Okugi will take on this job starting January 2012.

At the meeting the ICFA BD Newsletter editors for the next two years were decided. They are:

No. 57 April 2012 – G. Neil (Jlab)
No. 58 August 2012 – E. Metral (CERN)
No. 59 December 2012 – J. Byrd (LBNL)
No. 60 April 2013 – Y. Cai (SLAC)
No. 61 August 2013 – T. Okugi (KEK)

There was a discussion about a request from the OECD Global Science Forum (GSF). It has a project for a case study of how one particular research infrastructure – CERN – generates impacts that go beyond its primary mission of advancing fundamental knowledge. In connection with this project, GSF asked the BD Panel for input on changes over the past 20-25 years in the numbers and locations of energy-

frontier HEP accelerators. GSF will also discuss current trends, possibly including intensity-frontier and cosmic-frontier projects. In order to provide accurate information to GSF, a small team including representatives from several HEP accelerator laboratories was formed at the meeting. It will prepare a table (names of HEP accelerators, locations, energies, operation periods, impact on the field, etc.) and send it to GSF.

The next panel meeting will be in May, 2013 in Shanghai, China during IPAC 2013.

Appendix 1: List of Participants

ICFA Beam Dynamics Panel
 Ralph Assmann (CERN, for Alessandra Lombardi and Elias Metral)
 Rick Baartman (TRIUMF)
 Marica Biagini (LNF-INFN)
 Mike Blaskiewicz (BNL, for Wolfram Fischer)
 Yunhai Cai (SLAC)
 Weiren Chou (Fermilab)
 Ingo Hofmann (GSI)
 Jiho Jang (KAERI, for In Soo Ko)
 Yoshiharu Mori (Kyoto U.)
 George Neil (Jlab)
 Toshiyuki Okugi (KEK)
 Chris Prior (RAL)
 Alex Ratti (LBNL, for Miguel Furman and John Byrd)
 Yuri Shatunov (BINP)
 Junji Urakawa (KEK)
 Rainer Wanzenberg (DESY)
 Chuang Zhang (IHEP, for Jiuqing Wang and Jie Gao)

ICFA Advanced and Novel Accelerators Panel
 Ryoichi Hajima (JAEA)
 Tom Luiten (TU Eindhoven)
 Patric Muggli (MPI)
 Louis Rinolfi (CERN)
 Chuanxiang Tang (Tsinghua U.)
 Mitsuru Uesaka (Tokyo Univ.)
 Mark Wiggins (Strathclyde U., for Dino Jaroszynski)

Appendix 2: Meeting Agenda

Round-table introduction
Welcome to new panel members: T. Okugi, G. Neil, (J. Byrd and E. Metral are absent)

Part I – Short presentations (5-10 minutes each):
 1. W. Chou (Fermilab): Report from the BD Panel
 2. Y. Mori (Kyoto U.): Report from the High Intensity Hadron Beams Working Group
 3. M. Biagini (INFN/Frascati): Report from the e+e- Collider Working Group

4. G. Neil (JLab): Report from the Future Light Sources Working Group
5. I. Hofmann (GSI): Report from the ICFA-ICUIL Joint Task Force (JTF) and Joint Workshop
6. M. Uesaka (Tokyo U.): Report from the ANA Panel
7. M. Wiggins (Strathclyde U.): Report on the International Summer School on Laser-Plasma Interactions and Applications
8. P. Muggli (MPI): Report on the Laser and Plasma Accelerator Workshop 2011
9. C. Tang (Tsinghua U.): Status of the Newsletter on Compact Accelerators for Evaluation and Analysis
10. R. Hajima (JAEA): New Aspects to Advanced and Novel Accelerators

Part II – Discussions (40 minutes):
1. ICFA BD Newsletter issue editors for 2012-2013
2. Newsletter distribution (R. Wanzenberg, T. Okugi, W. Chou)
3. Special edition of the December 2011 issue of the ICFA BD Newsletter for publication of the ICFA-ICUIL JTF White Paper
4. Request from the *OECD Global Science Forum* soliciting input from this panel on the changing landscape of high-energy accelerator laboratories over the past 20 years
5. Next panel meeting
6. Any other business

6   Forthcoming Beam Dynamics Events

6.1   Workshop on Beam Cooling and Related Topics (COOL`11)

The Program and Organizing Committees invite you to take part in the Workshop on Beam Cooling and Related Topics (COOL 11).

Date and location of the Workshop
The Workshop will be held from 12 to 16 September 2011 at the Pansionat "Dubna" (http://www.dubna-crimea.com/en/) in Alushta, Crimea, Ukraine.

Scope of the Conference

The workshop on beam cooling and related topics, COOL'11, will highlight the state of the art in physics and engineering of beam cooling systems and related techniques, including electron, stochastic, laser and muon (ionization) cooling. The program includes applications of beam cooling to traps, heavy ion and antiproton beams. Presentations of new developments and techniques as well as of the status of existing and future facilities are invited.

Workshop Layout

The workshop will highlight the following topics:

- Electron cooling
- Stochastic cooling
- Laser cooling
- Muon cooling
- Ionization cooling
- Storage and cooling of particles in antiproton and ion traps
- Other methods of phase space manipulation
- Cooled beam dynamics

Regulations

The Workshop will start on Monday morning, 12 September at 9 a.m. and finish on Friday, 16 September before 11 o'clock. Arrival of the participants in the Pansionat will be on 11 September 2011. The working language is English.

The Workshop will include invited presentations (30 min), oral contributions (20 min) and poster sessions (poster size will be specified in the next circular). It is planned to present as many as possible contributions in oral presentation. Those contributions, which will not be selected by the International Program Committee for oral presentation will be shifted to the poster sessions.

Registration

Applicants should pass the preliminary registration procedure filling in the attached form on the Conference web-site:

http://cool11.jinr.ru/

You should also register theses of your report on a site of JACoW:

http://oraweb.cern.ch/pls/cool2011/profile.html

You can find the instruction on registration on our site:

http://cool11.jinr.ru/abstracts.html

Abstracts and Proceedings

Abstracts must be submitted to the SPMS system developed by the JACoW collaboration. The authors should register at the JACOW system before submitting their abstracts.

The Proceedings will be published with JACoW.

Important Dates

Abstract submission 21 March – 10 July

Deadline for early registration fee – 10 July

Late registration 10 July – 31 August (if rooms are available)

Contacts

COOL secretariat	Ms. Ekaterina AKHMANOVA Joliot Curie, 6, Dubna, Moscow region, 141980 fax: +7 49621- 653-22 e-mail: cool11@jinr.ru
Visa information	Ms. Olga MATYUKHINA Joliot Curie, 6, Dubna, Moscow region, 141980 tel.: +7 49621- 655 -82 fax: +7 49621- 658-91 e-mail: omatyukhina@jinr.ru
JACoW's responsible person	Dr. Maksim V. KUZIN BINP SB RAS, Lavrentiev av. 11, Novosibirsk, RUSSIA, 630090 e-mail: M.V.Kuzin@inp.nsk.su

Workshop website: http://cool11.jinr.ru/

6.2 1st ICFA Mini-Workshop on Dielectric Laser Accelerators (DLA-2011)

We'd like to welcome you to attend Dielectric Laser Accelerators 2011, the first ICFA Mini-Workshop devoted entirely to laser-driven dielectric-structure based accelerators, to take place on September 15-16, 2011 at SLAC National Accelerator Laboratory.

DLA-2011 will present the tremendous technical progress in the fields of photonics, novel optical materials, and laser science, and the impact this progress has on developing laser-driven solid-state accelerators. Working groups will consider the applications of this technology, beam dynamics challenges, radiation production, material issues, laser developments, and fabrication techniques.

This workshop is held immediately following the Stanford Photonics Research Center Annual Symposium:

http://photonics.stanford.edu/events/sprc-2011-annual-symposium-0

Important Dates:
Last Day to book accommodations:
August 30th, 2011

Last Day to Register:
September 8th, 2011

Workshop Website:
http://www-conf.slac.stanford.edu/dla-2011/
Hosted by SLAC National Accelerator Laboratory.
Workshop chair: Eric Colby ecolby@slac.stanford.edu

6.3 Low Emittance Rings 2011 (LOWεRING 2011)

The organizers of the Low Emittance Rings 2011 workshop would like to invite you to attend the workshop in Heraklion on the island of Crete during the period 3-5 October 2011. The goal of the workshop is to bring together experts from the scientific communities working on low emittance lepton rings. This includes damping rings, test facilities for linear colliders, B-factories and electron storage rings. The theme will be common beam dynamics and technology challenges for producing and controlling ultra-low emittance beams and the participants will benefit from the experience of colleagues who have designed, commissioned and operated such rings. This is the second in a series of workshops initiated in 2010 (http://ler2010.web.cern.ch), by the joint CLIC/ILC working group on damping rings. During the 1st workshop and subsequent discussions, it was found that the state of the art in the design of accelerator systems in X-ray storage rings approaches the goals of linear collider damping rings and future e+/e- circular collider upgrade projects. This workshop specifically targets the strengthening of interactions within the low emittance ring community by forming a LOWεRING collaboration network.
Workshop sessions will include:
Low emittance optics design and tuning
- Low emittance cells design
- Non- linear optimization
- Minimization of vertical emittance
- Collective effects reduction through lattice design

Collective Effects and beam instabilities
- Electron cloud effect and fast ion instability
- Intrabeam Scattering

- Impedances
- Coherent Synchrotron Radiation

Low emittance Ring Technology
- Insertion devices, magnet design and alignment
- Fast kicker design
- RF systems
- Instrumentation for low emittance
- Feedback systems
- Vacuum technology

Proposals for contributions to the workshop should be addressed to one of the organizers or the chairman of the Scientific Program Committee, Dr. Hermann Schmickler (Hermann.Schmickler@cern.ch).

Web Site:
http://lowering2011.web.cern.ch/lowering2011/
Contact: Yannis Papaphilippou (CERN), ioannis.papaphilippou@cern.ch

The workshop is sponsored by ICFA Beam Dynamics Panel, the National Technical University of Athens, the John Adams Institute, CERN, Cornell University, the University of Crete, INFN-LNF, KEK, and the Joint Working Group on Damping Rings of the Compact Linear Collider (CLIC) Design Study and the International Linear Collider (ILC) Global Design Effort.

7   Announcements of the Beam Dynamics Panel

7.1   ICFA Beam Dynamics Newsletter

7.1.1   Aim of the Newsletter

The ICFA Beam Dynamics Newsletter is intended as a channel for describing unsolved problems and highlighting important ongoing works, and not as a substitute for journal articles and conference proceedings that usually describe completed work. It is published by the ICFA Beam Dynamics Panel, one of whose missions is to encourage international collaboration in beam dynamics.

Normally it is published every April, August and December. The deadlines are 15 March, 15 July and 15 November, respectively.

7.1.2   Categories of Articles

The categories of articles in the newsletter are the following:

1. Announcements from the panel.

2. Reports of beam dynamics activity of a group.

3. Reports on workshops, meetings and other events related to beam dynamics.

4. Announcements of future beam dynamics-related international workshops and meetings.

5. Those who want to use newsletter to announce their workshops are welcome to do so. Articles should typically fit within half a page and include descriptions of the subject, date, place, Web site and other contact information.

6. Review of beam dynamics problems: This is a place to bring attention to unsolved problems and should not be used to report completed work. Clear and short highlights on the problem are encouraged.

7. Letters to the editor: a forum open to everyone. Anybody can express his/her opinion on the beam dynamics and related activities, by sending it to one of the editors. The editors reserve the right to reject contributions they judge to be inappropriate, although they have rarely had cause to do so.

The editors may request an article following a recommendation by panel members. However anyone who wishes to submit an article is strongly encouraged to contact any Beam Dynamics Panel member before starting to write.

7.1.3   How to Prepare a Manuscript

Before starting to write, authors should download the template in Microsoft Word format from the Beam Dynamics Panel web site:

http://www-bd.fnal.gov/icfabd/news.html

It will be much easier to guarantee acceptance of the article if the template is used and the instructions included in it are respected. The template and instructions are expected to evolve with time so please make sure always to use the latest versions.

The final Microsoft Word file should be sent to one of the editors, preferably the issue editor, by email.

The editors regret that LaTeX files can no longer be accepted: a majority of contributors now prefer Word and we simply do not have the resources to make the conversions that would be needed. Contributions received in LaTeX will now be returned to the authors for re-formatting.

In cases where an article is composed entirely of straightforward prose (no equations, figures, tables, special symbols, etc.) contributions received in the form of plain text files may be accepted at the discretion of the issue editor.

Each article should include the title, authors' names, affiliations and e-mail addresses.

7.1.4   Distribution

A complete archive of issues of this newsletter from 1995 to the latest issue is available at

http://icfa-usa.jlab.org/archive/newsletter.shtml.

This is now intended as the primary method of distribution of the newsletter.

Readers are encouraged to sign-up for electronic mailing list to ensure that they will hear immediately when a new issue is published.

The Panel's Web site provides access to the Newsletters, information about future and past workshops, and other information useful to accelerator physicists. There are links to pages of information of local interest for each of the three ICFA areas.

Printed copies of the ICFA Beam Dynamics Newsletters are also distributed (generally some time after the Web edition appears) through the following distributors:

Weiren Chou	chou@fnal.gov	North and South Americas
Rainer Wanzenberg	rainer.wanzenberg@desy.de	Europe[++] and Africa
Susumu Kamada	Susumu.Kamada@kek.jp	Asia[**] and Pacific

[++] Including former Soviet Union.

[**] For Mainland China, Jiu-Qing Wang (wangjq@mail.ihep.ac.cn) takes care of the distribution with Ms. Su Ping, Secretariat of PASC, P.O. Box 918, Beijing 100039, China.

To keep costs down (remember that the Panel has no budget of its own) readers are encouraged to use the Web as much as possible. In particular, if you receive a paper copy that you no longer require, please inform the appropriate distributor.

7.1.5   Regular Correspondents

The Beam Dynamics Newsletter particularly encourages contributions from smaller institutions and countries where the accelerator physics community is small. Since it is impossible for the editors and panel members to survey all beam dynamics activity worldwide, we have some Regular Correspondents. They are expected to find interesting activities and appropriate persons to report them and/or report them by themselves. We hope that we will have a "compact and complete" list covering all over the world eventually. The present Regular Correspondents are as follows:

Liu Lin	Liu@ns.lnls.br	LNLS Brazil
Sameen Ahmed Khan	Rohelakan@yahoo.com	SCOT, Oman
Jacob Rodnizki	Jacob.Rodnizki@gmail.com	Soreq NRC, Israel
Rohan Dowd	Rohan.Dowd@synchrotron.org.au	Australian Synchrotron

We are calling for more volunteers as Regular Correspondents.

7.2   ICFA Beam Dynamics Panel Members

Name	eMail	Institution
Rick Baartman	baartman@lin12.triumf.ca	TRIUMF, 4004 Wesbrook Mall, Vancouver, BC, V6T 2A3, Canada
Marica Biagini	marica.biagini@lnf.infn.it	LNF-INFN, Via E. Fermi 40, C.P. 13, Frascati, Italy
John Byrd	jmbyrd@lbl.gov	Center for Beam Physics, LBL, 1 Cyclotron Road, Berkeley, CA 94720-8211, U.S.A.
Yunhai Cai	yunhai@slac.stanford.edu	SLAC, 2575 Sand Hill Road, MS 26 Menlo Park, CA 94025, U.S.A.
Swapan Chattopadhyay	swapan@cockroft.ac.uk	The Cockcroft Institute, Daresbury, Warrington WA4 4AD, U.K.
Weiren Chou (Chair)	chou@fnal.gov	Fermilab, MS 220, P.O. Box 500, Batavia, IL 60510, U.S.A.
Wolfram Fischer	wfischer@bnl.gov	Brookhaven National Laboratory, Bldg. 911B, Upton, NY 11973, U.S.A.
Yoshihiro Funakoshi	yoshihiro.funakoshi@kek.jp	KEK, 1-1 Oho, Tsukuba-shi, Ibaraki-ken, 305-0801, Japan
Jie Gao	gaoj@ihep.ac.cn	Institute for High Energy Physics, P.O. Box 918, Beijing 100039, China
Ajay Ghodke	ghodke@cat.ernet.in	RRCAT, ADL Bldg. Indore, Madhya Pradesh, 452 013, India
Ingo Hofmann	i.hofmann@gsi.de	High Current Beam Physics, GSI Darmstadt, Planckstr. 1, 64291 Darmstadt, Germany
Sergei Ivanov	sergey.ivanov@ihep.ru	Institute for High Energy Physics, Protvino, Moscow Region, 142281 Russia
In Soo Ko	isko@postech.ac.kr	Pohang Accelerator Lab, San 31, Hyoja-Dong, Pohang 790-784, South Korea
Elias Metral	elias.metral@cern.ch	CERN, CH-1211, Geneva 23, Switzerland
Yoshiharu Mori	mori@rri.kyoto-u.ac.jp	Research Reactor Inst., Kyoto Univ. Kumatori, Osaka, 590-0494, Japan
George Neil	neil@jlab.org	TJNAF, 12000 Jefferson Ave., Suite 21, Newport News, VA 23606, U.S.A.
Toshiyuki Okugi	toshiyuki.okugi@kek.jp	KEK, 1-1 Oho, Tsukuba-shi, Ibaraki-ken, 305-0801, Japan
Mark Palmer	mark.palmer@cornell.edu	Wilson Laboratory, Cornell University, Ithaca, NY 14853-8001, USA
Chris Prior	c.r.prior@rl.ac.uk	ASTeC Intense Beams Group, STFC RAL, Chilton, Didcot, Oxon OX11 0QX, U.K.
Yuri Shatunov	Yu.M.Shatunov@inp.nsk.su	Acad. Lavrentiev, Prospect 11, 630090 Novosibirsk, Russia
Jiu-Qing Wang	wangjq@ihep.ac.cn	Institute for High Energy Physics, P.O. Box 918, 9-1, Beijing 100039, China
Rainer Wanzenberg	rainer.wanzenberg@desy.de	DESY, Notkestrasse 85, 22603 Hamburg, Germany